Adaptation of Transactinide Handling Methods in Support of Gas-Phase Separations of Rare Earth Elements and Nuclear Forensic Analysis

A Dissertation Presented for the

Doctor of Philosophy

Degree

The University of Tennessee, Knoxville

David Paul Schappel

December 2023

This work is dedicated to my parents and family, to Jerry & Nancy Golsteyn, mentors, friends, and co-workers.

Acknowledgements

This work would not have been possible without the support of those around me. My advisors and professors have guided and corrected my efforts throughout my time at the University of Tennessee. I would like to thank my PhD Committee Chair, Howard Hall, for his advice, guidance, encouragement, and support. I want to thank Matthew Cook, Lawrence Heilbronn, and Robert Counce for serving on my advisory committee. They have graciously critiqued and guided the writing of this work, and in particular, Howard Hall and Mattew Cook have spent many hours helping to develop my communication skills. I would also like to thank Luke Breon for reviewing this work, along with Julie Harden and Abby Sherman at the Graduate School, for their amazing flexibility, patience, and dedication. I would also like to thank Scott Emert, Ashly Pearson, Dave & Laura Beaman, and the Breon family, for their creative perspectives, encouragement, and humor throughout my time at UT.

I want to thank my parents for sacrificially teaching my siblings and me, and for their patience, loving guidance, and amazing support. In addition, Jerry and Nancy Golsteyn provided exceptional educational therapy that allowed me to overcome various challenges and made this educational pursuit possible. I would like to thank Mike and Bekah and my brother Danny for their generosity, creative ideas, and practical support at critical moments during the development of this project. Many friends and extended family stood by me with their faithful prayers and encouragement. Most importantly, this has been a developmental process where Scriptures like 2 Corinthians 12:9 and Philippians 3:12-14 become a way of life.

Abstract

The intent of this work is to reduce the time needed for isotopic analysis of trace fission products following a large dispersal event. Trace fission products often have insufficient radiation signatures and overlapping atomic mass numbers, which requires time consuming separations of each element prior to isotopic analysis using well established methods. This work adapts transactinide characterization methods for the goal of continuously collecting and dissolving trace fission products immediately after their gas-phase separation by element, which will substantially reduce the time needed for characterization. Obstacles to widespread use were considered, resulting in a final prototype that demonstrates the feasibility of this endeavor using a minimalistic design and readily available components.

Conventional transactinide characterization designs of interest utilize gas-solid isothermal chromatography to separate chemical complexes based on their thermodynamic properties in conjunction with rapid transport methods that place the samples in proximity to appropriate characterization systems. These systems require an extensive laboratory setup to operate, so an alternative low-pressure spray system was designed using various drafting and modeling software suites. A prototype was constructed for feasibility demonstrations using readily available components. Each computational fluid dynamics (CFD) model was validated by constructing and testing an intermediate prototype, with the final prototype having no observable discrepancies compared to the CFD model.

Important to this work, the spray system incorporates a unique design that avoids cross contamination of separated elements, which would otherwise cause isobaric interferences. The spray system rinses aerosol samples into a collection chamber, where they are dissolved in dilute nitric acid and continuously withdrawn for analysis. To expedite the design process, less hazardous surrogates were used in the development process. Collection efficiencies up to 85 percent were observed in the final prototype. Sample collection efficiency and peak concentrations are strongly influenced by the spray rate and collection reservoir volume of the apparatus, respectively.

Keywords: Nuclear forensics; elemental separation; gas chromatography; capillary column; computational fluid dynamics

Table of Contents

Chapter 1: Introduction; Dissertation Overview and Motivation 1
1.1 Dissertation Overview 1
1.2 Motivation 2
Chapter 2: Context and Relevant Articles 4
2.1 Context 4
2.2 Relevant Articles 5
2.2.1 Gas Thermochromatography 5
2.2.1.1 Thermodynamics of Thermochromatography 6
2.3 Instruments for Super Heavy Element Characterization 8
2.3.1 OLGA I 8
2.3.2 OLGA II / ROMA 8
2.3.3 OLGA III 9
2.3.4 MANON 10
2.3.5 Super Heavy Element Instrumentation Summary 13
2.4 Gas Phase Separations 15
2.5 Final Development of Prior Efforts 15
2.6 Guiding Objectives 18
Chapter 3: Early Explorations of Candidate Collection Methodologies 20
3.1 Fabric Collection Surface 20
3.2 Metallic Collection Surface 20
Chapter 4: Conceptual Design of RESI Apparatus 27
4.1 Overall Design Concept 27
4.1.1 Gas-Phase Separations 27
4.1.2 Performance and Testing Criteria for The RESI Device 27
4.1.3 Introduction of RESI Design Logic 29
4.1.4 The RESI Device: Organometallic Collection and Dissolution Module 29
4.2 Substitution of Rare Earth Compounds with Less Reactive Aerosols 40
Chapter 5: Experimental Design, Prototyping, and Functional Testing of the RESI Collection Cylinder and Atomizer Nozzle 44
5.1 Nozzle and Collection Cylinder Design 44
5.2 Computer Aided Design Models of the Collection Columns 46

5.2.1 CFD Modeling 46
5.2.1.1 Physics Models 47
5.2.1.2 Model Convergence 47
5.2.1.3 CFD Boundary Conditions Derived from Direct Experimentation 48
5.2.2 Collection Cylinder 48
5.3 Induced Low Pressure Regions 49
5.4 Models of the Spray Nozzle and Rotating Air Currents 51
5.5 Buoyant Aerosols 62
5.6 Importance of Consistent Water Supply 62
5.7 Importance of Constant Air Pressure Supply 67
5.8 Mass Flow Rate Adjustments 70
5.9 Venturi Pumps 72
5.10 Reverse Flow Diverters 72
Chapter 6: Design of Balance of RESI Apparatus 77
6.1 Exhaust Gas Removal 77
6.2 Thermal Insulation 77
6.3 Practical Mass Flow Rate Measurements 79
6.4 Spray System Proof of Concept Using Sucrose and 0.75mL Reservoir 81
6.5 Spray System Proof of Concept Using Sucrose and 2.0mL Reservoir 81
Chapter 7: Functional Testing and Characterization of the RESI Apparatus 83
7.1 Mass Flow Rates for Specific System Configurations 83
7.2 Proof of Concept Results with Sucrose 85
7.3 Example of Undesirable Sample Retention 85
7.4 Example of Misaligned Spray Nozzle 85
7.5 RESI Repeatability 89
7.5.1 Results 89
Chapter 8: Research Summary and Next Steps 94
8.1 Research Summary 94
8.2 Device Summary 95
8.3 Next Steps 95
Bibliography 96
Appendices 100

Appendix A: Manifold Air Flow 100
Appendix B: Sucrose Solution Preparation 101
Appendix C: Liquid Phase Separations 103
C.1 Solvent Extraction 103
C.2 Liquid – Solid Ion Exchange 105
Appendix D: Introduction to Computational Fluid Dynamics (CFD 109
D.1 Governing Equations 109
D.2 Discretization Method 110
D.3 Mesh Refinement 112
D.4 Adiabatic Compressible Fluid Flow 112
D.5 Absolute, Total, Static and Dynamic Values 114
D.6 Laminar and Turbulent Fluid Flow 115
D.7 Boundary Layer Flow 115
D.8 Inviscid and Viscous Flow 115
D.9 Fluid Flow Description: Newtonian and Non-Newtonian Fluids 117
D.10 Heat Transfer: Conduction, Convection, and Radiation 117
D.11 Natural, Mixed, and Forced Convection 118
D.12 Practical Application 119
Vita 120

List of Tables

Table 1: Manifold volumetric air flow measurements..... 100

Table 2: Radiolytic yields (No. ion pairs per eV deposited) of CMPO degradation products in various solvents. Table reproduced from Mincher *et al.* [43]..... 106

List of Figures

Figure 1: TGA mass loss plot with new isotherms at 5-minute increments [14]. 7

Figure 2: Schematic of the OLGA III setup [18]. 11

Figure 3: Schematic of the MANON experimental setup [29]. 11

Figure 4: α particle spectra recorded from the top 7 detectors used by MANON for a 210 s live time and 30 s of aerosol collection [29]. 12

Figure 5: Percent relative yield of MoO_2Cl_2, WO_2Cl_2, and SgO_2Cl_2 as a function of isothermal temperature in a chromatography column [24]. 14

Figure 6: Chromatogram of ethyl ether containing 0.1g/mL of Sm, Tm, and Dy [Hfac] and generated using a thermal conductivity detector [1]. 16

Figure 7: Rotary wheel apparatus with exhaust snorkel duct fitting. 21

Figure 8: Rotary wheel apparatus used for aerosol deposition onto tape segments. 21

Figure 9: Conceptual deposition as a function of time onto electrically grounded metallic tape. 23

Figure 10: Powder Injection Straw (L) and Wheel Apparatus Exterior View (R). 23

Figure 11: Powder Paint Deposits: Through Truncated Pipet (L), and Interior View (R). 24

Figure 12: High Voltage Emitter (L) and Electrical Grounding Spring (R). 24

Figure 13: Wheel Apparatus Interior view (L) and Sample Collection Wheel (R). 25

Figure 14: Stepper Motor (L) and Rotary Wheel Housing Box (R). 25

Figure 15: Exhaust Side of Wheel (L); Vacuum Adapter to the Snorkel Exhaust System (R). ... 26

Figure 16: Spring driven infusion pump 31

Figure 17: RESI teststand overview. 32

Figure 18: Stainless-Steel collection cylinder. Front view on left and back view on right. 33

Figure 19: Relationship between REE injection nozzle, atomizer nozzle, and colleciton cylinder. 34

Figure 20: Exhaust channel and collections reservoir. Exhaust channel (upper left), collection reservoir (upper right), sample port and collection reservoir (lower left), and drip guide (lower right). 36

Figure 21: Sample port with mock extraction device. 37

Figure 22: Atomizing spray nozzle 38

Figure 23: Modified nozzle tip 39

Figure 24: Thermal testing of Rare Earth Separtions Instrument. Note the 90 degree deflection of the propane flame after entering the collection cylinder. 41

Figure 25: Powder paint deposits on the collection cylinder; back surface (left) and front surface (right). 43

Figure 26: Process overview. 45

Figure 27: CAD models of the sequence preserving collection column (R) and higher efficiency aerosol collection column (L). Note that both columns are the same diameter but different lengths. 50

Figure 28: Depiction of air currents within the incomplete collection cylinder when using a flat fan spray nozzle. 50

Figure 29: Velocity profile viewed from the front of the spray nozzle. Total length of the scale is approximately 22.5 mm and the velocity range is from 5 mm/s (dark blue) to 9,300 cm/s (red). 52

Figure 30: Cross-sectional side view of high velocity air exiting flat fan spray nozzle. 53

Figure 31: Cross-sectional side view of the low static pressure regions shown in cyan that are generated by the high velocity air in Figure 30. 54

Figure 32: Depiction of air currents within the modified collection cylinder when using a flat fan spray nozzle. Note the ambient air being drawn into the cylinder at 'E' in the third frame. 55

Figure 33: Flame test of the modified collection cylinder using compressed air at 25 psig and discharging into the ambient environment at 0 psig. 56

Figure 34: 3D vector flow field showing the rotating air currents produced by the modified spray nozzle in an open ambient environment. Note that velocity magnitude is indicated by color only and not the length of each vector. 58

Figure 35: 3D vector flow field located 1.9 mm downstream of the modified spray nozzle tip. Velocity magnitude indicated by color, not the length of each vector. 59

Figure 36: 2D vector flow field 2 mm downstream of modified spray nozzle tip. The red line marks the location of the velocity magnitude data points ploted in the following figure while the white origin indicates the midline of the spray nozzle tip. Note that the velocity magnitude is indicated by color, not the length of each vector. 59

Figure 37: Velocity magnitude along the red line in Figure 36. Note, the origin is at the midpoint of nozzle tip. 60

Figure 38: Horizontal vector flow field showing two contra rotating vortices in the collection cylinder that constantly wash the interior surfaces. Velocity scale is 0 (dark blue) to 2,700 cm/s (red). 61

Figure 39: Side view of modified flat fan spray nozzle. 63

Figure 40: Section view of indentations machined into spray nozzle tip. 63

Figure 41: Side and back view of the modeled spray nozzle, collection column, and thermal air deflector. 64

Figure 42: Buoyant aerosols from heated mixture of glycerin and water. 65

Figure 43: Special effects smoke being drawn into the stainless-steel collection tube. Note the column of smoke being expelled in the background. 65

Figure 44: Buoyant smoke aerosols being drawn into the stainless-steel collection column via the low-pressure zone facilitated by the atomizer spray nozzle. 66

Figure 45: Dilute nitric acid supply bottle with virtually constant pressure head. Note that the hose bracket keeps the feed hose in a fixed position relative to the large storage bottle. 68

Figure 46: Changing fluid levels in the dilute nitric acid supply system. Panels A through D show how the buoyancy of the small 95 mL generates a nearly constant pressure head on the feed hose. Panel E shows how an experiment running past the intended limits will result in a high variation flow rate and then air ingestion into the feed hose. 68

Figure 47: Schematic of the compressed air supply manifold. 69

Figure 48: Manifold for Rare Earth Separations Instrument. 71

Figure 49: 3D printed base plate with fine grooves to assist with reproducible D.I. water flow control. 73

Figure 50: Valve position control for the flat fan spray system. 73

Figure 51: General layout of pneumatically driven flow diverter sampling system[33]. 74

Figure 52: Reverse flow diverter [34]. 74

Figure 53: Simplified schematic of a pneumaticly powered reverse flow diverter [36]. 75

Figure 54: General schematic of a reverse flow diverter [36]. 75

Figure 55: Snorkel exhaust adapter connected to RESI. 78

Figure 56: Adapted shop vacuum and snorkel exhaust. 78

Figure 57: Thermal test of the PVC adapter. 80

Figure 58: Thermal test of the PVC adapter and spray nozzle. 80

Figure 59: Sample collection apparatus (L), with high contrast surrogate liquid (R). Liquid enters the back of the reservoir and samples are continuously withdrawn via the side port. Reservoir retention capability is slightly more than 0.5 mL of liquid. 82

Figure 60: Mass flow rate variations and features. 84

Figure 61: Sucrose concentration in 2 mL reservoir following cessation of injection at Time = 0 seconds. 86

Figure 62: Sucrose injection with reduced output from injection pump beginning at T = 294 seconds with cessation at T = 339 seconds, resulting in the plot being left skewed. 87

Figure 63: Sucrose injection with misaligned spray nozzle producing ineffective rinsing coverage of the back half of the collection cylinder, resulting in a left skewed plot of concentration versus time. 88

Figure 64: Sucrose injection using 43.5 °Brix solution and 5 mL / minute water spray. Sucrose injection ended at Time = 0. 90

Figure 65: Repeated sucrose injections using 42.9 °Brix solution and 8 mL / minute water spray. Sucrose injection ended at Time = 0 91

Figure 66: Repeated sucrose injections using 42.9 °Brix solution and variable DI water spray rates. Constant flow of 32 mL / minute DI water spray compared to 8 mL / minute DI water spray during sucrose injection followed by 32 mL / minute rinse rate. Sucrose injection ended at Time = 0 .. 93

Figure 67: Thermolyne Stir-Light, model SL-7225. 102
Figure 68: Multistage counter-current flow diagram[32]. 104
Figure 69: Separation of decay products via ion exchange chromatography [45]. 108
Figure 70: Summary of the Energy Equation. 111
Figure 71: Conceptual example of a one-dimensional mesh and linear shape function [47]. 113
Figure 72: Mesh autosizing applied to crossectional view of a compressed air line, backlit in yellow with ambient air backlit in blue. 113
Figure 73: Turbulent flow profile with laminar boundary layers [49]..... 116

Nomenclature

CFD: Computational fluid dynamics

CMPO: n-octyl(phenyl)-N,N-di-isobutyl carbamoyl methyl phosphinoxide

DMDOHEMA: N,N′-Dimethyl, N, N′-dioctyl-hexylethoxymalonamide

EGA: Evolved gas analyzer

ER: Evaporation residues

FLNR: Flerov Laboratory of Nuclear Reactions

GC: Gas chromatography

HDEHP:Di-2-ethyl-hexyl phosphoric acid

Hfac: Hexafluoroacetylacetone

MANON: Measurement system for alpha-particle and spontaneous fission events on-line

MS: Mass spectrometer

NFAA: Nuclear forensics and attribution act

OLGA: On-line gas chromatography apparatus

PIPS: Passivated ion implanted planar silicon

PSI: Paul Scherrer Institute

REE: Rare Earth Elements

RESI-I: Rare earth separations instrument

SHE: Super heavy element

$t_{1/2}$: Halftime

TALSPEAK: Trivalent Actinide Lanthanide Separation with Phosphorus-reagent Extraction from Aqueous Komplexes

TCE: Trichloroethylene

TGA: Thermogravimetric analysis

TNF: Technical nuclear forensics

TODGA: Tetraoctyl Diglycolamide

TRUEX: Trans uranium extraction

ROMA: Rotating wheel multidetector apparatus

Chapter 1: Introduction; Dissertation Overview and Motivation

This dissertation documents the design, prototype fabrication, and feasibility testing of an innovative device that demonstrates the ability to condition a continuous gaseous stream of rare earth elements separated in time by element into a format that can be characterized by a mass spectrometer. As demonstrated throughout this dissertation, this device represents a key component of a system that can substantially reduce the time and effort required to analyze the content of rare earth elements in a field-collected sample. The anticipated benefits of this new device are important, as will be discussed in the motivation section at the end of this chapter.

Chapter 1 of this document is divided into two parts. The first part is an overview of this dissertation and outlines the content discussed throughout the remainder of the dissertation. The second part describes the motivation of this work and highlights the significance of the results.

1.1 Dissertation Overview

A concise outline for the remainder of this dissertation is given in this section. Chapter 1 develops the motivation for this work. The motivation is discussed in high-level and includes further introductions to the work in addition to important background topics. The motivation section also includes a mapping of important prior efforts that are included in the literature review along with discussions on traditional processing methods.

Chapter 2 contains further context for this work and gives a review of pertinent prior efforts as well as important aspects of conventional methodologies and recent developments. The review begins with recent innovations in the field of nuclear forensics and tracks those developments as they demonstrate the potential for substantially faster and more efficient methods of performing forensics tasks. Those improvements ultimately motivate the development of this research work. Chapter 2 finishes with a discussion of the foundation for this work and an outline of the most important objectives of this dissertation.

Chapter 3 documents early efforts in the research and development pathways taken. Those efforts were important stages of early work but did not ultimately become integrated aspects of the engineering solutions. The efforts are included in the dissertation because they offer starting positions for future research and development that should be undertaken to address potential improvements in addition to the device demonstrated in this work. Such potential improvements include reduced losses of separated rare earth elements and less expensive processing options.

Chapter 4 introduces the Rare Earth Separation Instrument (RESI), the device invented by the R&D that supports this dissertation. Chapter 4 states the design objectives and performance metrics used to functionally test the final RESI prototype. A logical design overview of the RESI is given in Chapter 4 followed by a detailed description of the RESI and comments about surrogates and substitutions used to make this work feasible for laboratory execution.

Chapter 5 describes the development of the collection cylinder and accompanying atomizing spray nozzle that constitute the most important innovations of this work. As these aspects of the designs represented the more challenging accomplishments of the invention, substantial effort was directed

to the design, prototype indexing, testing, and characterization of these components. The balance of the RESI design aspects and surrounding comments are presented in Chapter 6.

Chapter 7 describes the overall functional testing and characterization of the RESI along with the many lessons learned throughout the development process. The overall summarization of this R&D is given in Chapter 8 along with concluding remarks. Chapter 8 also outlines future work that will be worth investing into further transitioning the RESI to a field-deployable system.

Background information considered relevant to the context and development of this work but of lesser importance for understanding the accomplishments of this research are given in the appendices. Also included in the various appendices are collections of the more tedious testing results and experimental procedures.

Appendix A documents flow rate measurements that supported the testing and development of the atomizer spray nozzle, Appendix B contains detailed data resulting from the various characterization tests of the RESI prototypes. Appendix C provides background on liquid-liquid chemical separation methodologies, and Appendix D is a primer on the CFD support used to assist the design of the collection cylinder. Given next is a development of the motivation for this work.

1.2 Motivation

Performing isotopic analysis of sample material is one of many important capabilities used during the process of attributing events involving the dispersal of nuclear material. Mass spectrometer (MS) systems are often used for isotopic analysis but are vulnerable to isobaric interferences, where overlapping charge to mass ratios obscure or can confound measurements of the isotopic composition of a sample.

To prevent isobaric interferences, collected samples are subject to a separations process that prevents different isotopes having the same mass from entering a MS at the same time. Often, the separations process is accomplished using an elaborate chemical process while the sample is in the liquid phase, which can be time consuming.

The time-consuming facet of conventional methods for separating rare earth elements presents an important problem, as rapid characterization of dispersal events of nuclear material such as detonation events is of high importance. The ability to reduce the time needed to complete such an elemental separations process and the subsequent analysis by MS from weeks to a timeframe of less than half a day is of substantial value.

Accomplishments by Hanson *et al.*[1] demonstrated that it can be possible to separate a collected sample of various, mixed, rare earth elements quickly using innovations that will be further described in Chapter 2. However, the output format of that separations process is not of a type that is immediately compatible for uptake and analysis by a MS.

In particular, the output of the new process provides a stream of separated rare earth elements suspended in a helium or other carrier gas. The elements supplied are separated in the time domain but belong to a continuous stream of gaseous flow. To be acceptable for analysis by an MS, the

separated gaseous stream needs to be reformatted into a liquid, or dissolved form. An example of an acceptable format for consumption by an MS is rare earth elements dissolved in dilute nitric acid.

The conditioning of such a gas stream into a solute presents an interesting technical challenge in that all the separated gaseous rare earth metals need to be accommodated by the conversion process without admitting contamination on any part of the conversion device.

Such contamination could lead to the remixing of the separated rare earth elements at some point during the characterization process and corrupt the analysis provided by the MS due to the introduction of isobaric interferences. Further technical complexity stems from the need to accommodate separation of dissolved solutes and inert carrier gases inside the device without causing isobaric interferences.

This research and development is in response to the need for a practical conversion device as identified in this motivation section. Fortunately, a successful practical prototype was designed, fabricated, and demonstrated, as will be discussed throughout this dissertation. The next chapter provides background context that serves as a foundation for the work done herein.

Chapter 2: Context and Relevant Articles

This chapter presents some additional context for this work and provides a review of relevant literature and recent developments that both support and require the R&D published in this dissertation.

2.1 Context

Public Law 111-140, also known as the Nuclear Forensics and Attribution Act (NFAA), which was enacted to, "Strengthen efforts in the Department of Homeland Security to develop nuclear forensics capabilities to permit attribution of the source of nuclear material, and for other purposes" [2]. This law is part of the impetus for this work.

Technical nuclear forensics (TNF) is a specialized field of study that, because of this law, has made substantial recent improvements to traditional techniques and analytical methods. Further reducing the time needed to obtain high quality forensic data is prudent provided accuracy and precision are not compromised. The implications of TNF data are significant and must be obtained from legally defensible forensic methods if they are used to support attribution claims at the international level and legal prosecution of malevolent actors. What is known as the Daubert standard applies to Rule 702, Article 7, of the Federal Rules of Evidence[3][4]. From the Daubert standard, judges are provided the means to assess the testimony of a scientific expert on the reasoning or methods employed. Five factors are considered when assessing validity[3]:

- The method or theory has been tested
- It has been peer reviewed and published
- Its error rate is known
- Standards controlling its operation are maintained
- It is widely accepted within a scientific community

Future attribution conclusions developed by the United States, along with supporting evidence, will be examined with a certain degree of skepticism. Thus, certified reference materials and other TNF data must be obtained with great care to ensure international acceptance of attribution claims [5].

Several super heavy element separation systems have been developed and the results subject to rigorous review. These methods have high potential for adaptation to separate lanthanide series elements and satisfy the five judicial assessment factors previously mentioned. Of these potential methods, two such separation systems are of continued interest. They are the On-Line Gas chromatography Apparatus (OLGA) III and the Measurement system for Alpha-particle and spontaneous fissioN events ON-line (MANON).

These designs use gas-solid thermochromatography to separate complex samples based on their thermodynamic properties along with rapid transport methods to place the analytes into appropriate characterization systems and are discussed in Section 2.3. Given that the samples processed by the adapted system are rare earth elements, this new apparatus is referred to in this dissertation as the Rare Earth Separations Instrument (RESI).

The use of microwave bombs has been successfully explored as a method to increase reaction rates and yields. However, this process is difficult to scale beyond laboratory level, and is not ideal for samples containing analytes at or below tracer scale concentrations [6].

2.2 Relevant Articles

This work began with an exploration of relevant previous efforts and built upon those efforts in the development of designs, prototypes, and feasibility testing of the new apparatus. The exploration of prior studies begins with efforts by Garrison *et al.* [1] and Hanson *et al.* [2]. These authors identified evidence that fission products present in debris could be separated while in the gas phase and experimentally investigated using thermochromatography. Thermochromatography systems have been used extensively to assist with the identification of new transactinide isotopes[7][8]. Gas phase separations are also of practical interest because conventional radiochemical methodology typically involves liquid phase chemical separation methods, which have some important limitations.

Chemistry in the liquid phase offers many valuable benefits but is also known for several disadvantages that become important in the context of the attribution process. Chief among these are the non-trivial, lengthy steps inherent to separations in the liquid phase.

In addition, the difference between theoretical and observable yields for liquid separations are substantial and can vary considerably between elements. This requires extensive use of expensive certified reference materials to identify changes in element ratios caused by sample preparation. Developing other means of separating rare earth elements is essential for nuclear forensics, and once successful, can potentially be adapted to benefit other industries that use rare earth elements such as renewable energy systems, hybrid transportation, electronics, and other consumer products. The rare earth elements used by these other industries are frequently found in various mine tailings. However, rare earths are often present at concentrations below 1%, where their recovery is financially prohibitive using current methods.

Separation of rare earth elements in the gas phase can constitute improvements in time and effort versus the conventional methodologies of using liquid-liquid or liquid-solid chromatographic separation techniques. While chemical separation methods are important to the background of this effort, they are not essential to the innovations of this work other than providing motivation for the developments described here. As such, discussion of some of the most important methods of liquid phase separations are provided in this dissertation and are in Appendix C to allow the discussion in Chapter 2 to focus on recent innovations.

2.2.1 Gas Thermochromatography

Thermochromatography causes sample material to separate based on differences in thermodynamic properties and polarity of the sample constituents while traversing a capillary column. The thermodynamic properties of interest are the enthalpy and entropy of adsorption and will be discussed in greater detail in Section 2.2.1.1. The time needed for a sample to traverse a thermochromatography column is known as the retention or elution time.

The length of the column is selected based on the expected similarity of the sample constituents and desired time between each constituent eluting from the column. Columns are often formed from quartz and often have exterior and interior coatings. Often, the exterior coating is made from Kapton, a temperature resistant protective film that gives the column an amber color. Interior coatings are nuanced in composition and thickness, and available in many variations. The interior coating prevents the loss of sample material via diffusion into the column wall and must remain stable while subjected to inorganic and organic compounds, and substantial changes in temperature. Optimizing the operating conditions for thermochromatography requires a thorough understanding of the thermodynamic properties of sample constituents.

2.2.1.1 Thermodynamics of Thermochromatography

Sublimation enthalpy is one of the indicators of a compound's volatility and is often measured by thermogravimetric analysis (TGA) [9]. During TGA, a small sample is heated and consequential changes in weight are recorded. Variations of this general process include isobaric and isothermal conditions, numerous purge gas options, and pressures reaching as low as 6.7×10^{-3} Pa[10]. Gases released by heated samples can be discarded or investigated using an evolved gas analyzer (EGA). EGAs often use mass spectroscopy or Fourier transform infrared spectroscopy to identify the vapor products[11]. Langmuir introduced the use of isothermal conditions for TGA when generating mass loss plots and observed that sublimation has zeroth order kinetics. The mass loss rate from sublimation is described by Equation 2.1, where Δt and Δm denote change in time and mass, respectively[12]. For steady state temperatures, the mass loss rate is constant.

$$\dot{m}_{sub} = \frac{\Delta m}{\Delta t}$$

Equation 2.1

The recording of TGA data is continuous and can capture non-constant sublimation mass loss rates during temperature changes. An example of this is shown in Figure 1, where the slope transitions at the five- and ten-minute marks are different from the others, likely because the temperatures are isothermal and above 100 °C, and because the organic compound is a hydrate. This effect contrasts with later temperature transitions where all water molecules had been driven off, resulting in somewhat abrupt changes in slope.

In his work, Langmuir expressed the vapor pressure of a solid, p, as a function of sublimation rate, $\dot{m}_{sub}$, temperature, T, ideal gas constant, R, molecular weight of the compound, M_w, and vaporization coefficient, α, which is often presumed to be unity in a vacuum [12]. This is shown below in Equation 2.2. It should be noted that the vaporization coefficient must be identified when TGA is performed in non-vacuum conditions [13].

$$p = \sqrt{\dot{m}_{sub} \frac{2\pi RT}{\alpha^2 M_w}}$$

Equation 2.2

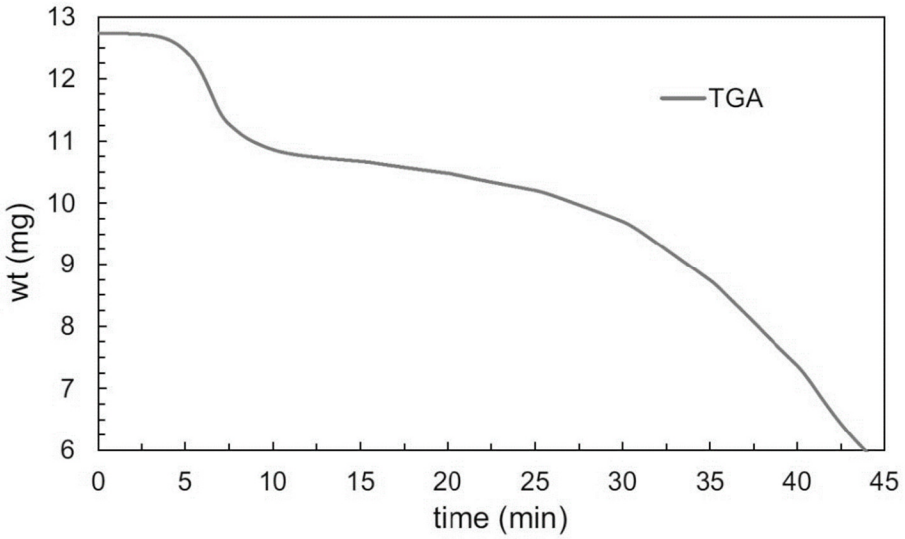

Figure 1: TGA mass loss plot with new isotherms at 5-minute increments [14].

What is known as the Clausius–Clapeyron relation equates change in vapor pressure with change in sublimation enthalpy, H_{sub}, and is shown below in Equation 2.3.

$$\frac{d[ln(p)]}{dT} = \frac{\Delta H_{sub}}{RT^2}$$

Equation 2.3

Combining and integrating Equations 2.2 and 2.3 produces a relation between enthalpy of sublimation and sample mass loss rate at isothermal temperatures. The resulting equation is shown below in Equation 2.4.

$$ln\left(\dot{m}_{sub}\sqrt{\frac{T}{M_w}}\right) = \frac{-\Delta H_{sub}}{RT} + \left[\frac{\Delta H_{sub}}{RT_{sub}} - ln\left(\sqrt{\frac{2\pi R}{\alpha^2}}\right)\right]$$

Equation 2.4

Correlations between adsorption enthalpy and sublimation enthalpy for certain organic complexes presently appear to have significant potential for use in gas-phase separations of rare earth elements. This topic will hopefully be further investigated in the near future given that similar correlations exist for heavy metal compounds on uncoated quartz capillary columns [15][16].

2.3 Instruments for Super Heavy Element Characterization

Gas-phase transactinide chemistry studies have frequently used continuous isothermal chromatography. Originally developed for investigating elements with atomic numbers greater than 111, continuous isothermal chromatography provides the option to use both continuous separation of volatiles and in-situ detection. This necessitates single atom counting techniques and meticulous efforts to address inherently poor counting statistics. To this end, new devices were developed like OLGA.

2.3.1 OLGA I

OLGA I and its more recent variants have proved to be highly successful applications using inert carrier gases in the search for volatile atoms. For OLGA I, the target recoil products are expeditiously transported down a narrow capillary tube to the high-temperature chromatograph setup via aerosol gas-jet. The transport method typically uses He flow rate between 1 to 2 L min^{-1}, a capillary inner diameter of 1.5 to 2 mm, and a length of about 10 m. The resulting retention times are typically less than 10 s. Initial studies involving p-elements At, Pb, Bi, and Po indicated good separations were possible from d and f elements at temperatures up to 1000 °C. Gäggeler *et al.* first used OLGA I in 1985 to investigate ^{211m}Po [17]. However, this first version is vulnerable to corrosive compounds and only effective with volatile elements, oxides, and hydroxides [18].

2.3.2 OLGA II / ROMA

The use of increasingly volatile substances in gas-phase transactinide chemistry studies resulted in improved separations but was often detrimental to the detection equipment. The first efforts by

von Dincklage *et al.* to investigate ^{261}Rf (65 s) were unsuccessful when using $RfCl_4$ because the surface barrier detectors were rendered inoperable due to the extended presence of the chlorinating agents. To remedy this problem, OLGA II was developed by Gäggeler *et al.* to investigate ^{261}Rf (65 s),^{262}Db (34 s), and ^{263}Db (27 s), which primarily decay via alpha emission or spontaneous fission. For ^{261}Rf, alpha decay leads to ^{257}No (25 s) and thence to ^{253}Fm (3 d).

The target recoil molecules were condensed onto KCl aerosols and transported to a high-temperature Gas Chromatography (GC) device where the aerosols were deposited onto a quartz wool filter and subject to heated HBr and HCl gases until the target recoil molecules and KCl aerosols vaporized. The transactinide bromides and chlorides, along with other halide compounds and byproducts, were then separated in a thermochromatography column and the recoil molecules condensed onto new KCl aerosols and directed down a second capillary column to the counting system. There, the laden aerosols were deposited onto thin 40 μg cm^{-2} polypropylene foils for counting with Passivated Ion-Implanted Planar Silicon (PIPS) detectors.

This transport process was termed "reclustering" and proved to be effective despite the time required to achieve reasonable separations [19]. These foils were located on a large wheel, allowing for the foils to be rotated under solid-state detectors via a ROtating wheel Multidetector Apparatus (ROMA) for counting of spontaneous fission and decay events [20][21]. Other configurations deposited the KCl aerosols onto a tape system first developed at the Paul Scherrer Institute (PSI). The tape method allows for a nearly 4π detection geometry by moving each processed sample between pairs of α detectors.

2.3.3 OLGA III

OLGA III was developed during the late 1990s to increase the chromatographic resolution and decrease the time needed for separations. The initial application was the synthesis of ^{261}Rf and ^{165}Hf using a cyclotron located at the Flerov Laboratory of Nucleactions (FLNR) Dubna, Russia. The recoil particles were thermalized in He carrier gas containing carbon aerosols and transported to a gas chromatograph. In the first stage of the GC (5 m, 2 mm I.D.), a wool plug made of quartz and heated to 900 – 1000 ºC was used to detain the aerosols while reactive gases were added. To study tetrachlorides, HCl, graphite strips coated in thionyl chloride, $SOCl_2$, and activated charcoal were introduced in the first stage of the GC to react with the recoil products.

Alternatively, Cl_2, $SOCl_2$, and O_2 were added to study the effects of oxygen on the recoil products. The second stage of the GC (1.9 m, 1 mm I.D.), functioned as an isothermal chromatography section and operated at a minimum of 300 ºC. This allowed group 6 oxychlorides to promptly traverse the column while less volatile compounds eluted much later.

At the end of the second section a reclustering unit combined the eluted constituents with CsCl aerosols for transport to the detection system. The result from using this system was a substantial reduction in separation times while realizing vastly improved chromatographic resolution. OLGA III has been used with MANON/ROMA and separately with variants of the PSI tape system [18][22]. These characteristics have resulted in OLGA III being used to study oxyhalides and volatile halides of Db, Rf, Bh, and Sg [8][23][24][25]. A schematic of a typical OLGA III setup is shown in Figure 2 [26].

2.3.4 MANON

High-intensity ion beams used in the production of transactinides frequently result in plasma degrading the efficiency of gas-jet transport. Pre-separation of the super heavy atoms has been proposed with promising results reported due to separation of unwanted plasma from the aerosols. Future production of transactinides with longer half-lives for experimentation will be based on hot fusion reactions using targets like ^{244}Pu and ^{248}Cm. However, the evaporation residues (ER) produced have low recoil velocities which cause significant complications in the operation of gas-jet transport systems. Separator transport efficiency decreases substantially with lower recoil velocity due to chains of small angle scatter events that dominate in the fill gas. The solution involves the use of a thin window made of MYLAR approximately 0.5 µm thick. The setup is shown in Figure 3.

In Figure 3, a beam of 95.5 MeV $^{18}O^{5+}$ ions are directed into a target of $^{248}Cm_2O_3$ having a thickness of approximately 280 µg cm^{-2} and reinforced by a 0.9 mg cm^{-2} Ti foil. The target chamber operates with He gas at 33 Pa and drives the reaction ^{248}Cm(^{18}O, 5n) ^{261}Rf. The reaction ions are then sent into a gas-jet chamber cylindrical in shape and having interior dimensions of 100 mm diameter x 20 mm in depth. To enter the gas-jet chamber, the reaction ions enter through a 0.5 µm MYLAR window that is supported by a grid due to the nearly 49 kPa He pressure differential.

The MYLAR window thickness and gas pressure is optimized to prevent lower energy ions from traversing the barrier and ensure that ^{261}Rf ions de-excite and adsorb onto the KCL aerosols within the chamber. A Teflon capillary column of 2 mm I.D. and 10 m length is used to transport the coated KCL aerosols to the spectroscopy station using 2 L min^{-1} He carrier gas. This station, the MANON, is a stainless-steel wheel 420 mm in diameter having 200 MYLAR foils, each 0.5 mm thick, located on the peripheral of the disk. The disk is noved at 30 s intervals to rotate each foil under 7 pairs of Si PIN photodiodes operated in event-by-event mode, having an energy resolution of 60 KeV full width half maximum (FWHM) and α particle counting efficiency of 38% [27][28][29].

Figure 4 shows α particle spectra recorded from the upper 7 detectors used by MANON with a 210 s live time and 30 s of aerosol collection [29]. Peaks from ^{261}Rf(68 s, 8.323 MeV) can be clearly seen in the low radiation background. A peak at 7.687 MeV is from the decay of ^{214}Po which is a daughter isotope of naturally occurring ^{222}Rn in the air. The beam target contains lead impurities which contribute to the production of unwanted isotopes from the elements Po, Rn, Fr, At, Ra, Ac, and Th. The absence of large peaks from these isotopes indicates that the system is effective at preventing unwanted isotopes from reaching the MANON apparatus. 168 decays from ^{261}Rf and ^{257}No were recorded for a mean ^{261}Rf production rate of 0.5 atoms min^{-1}. Comparing the recorded spectrum with results from a Si detector used in a different experiment, a gas-jet transportation efficiency for ^{261}Rf of 52% ± 12% was calculated.

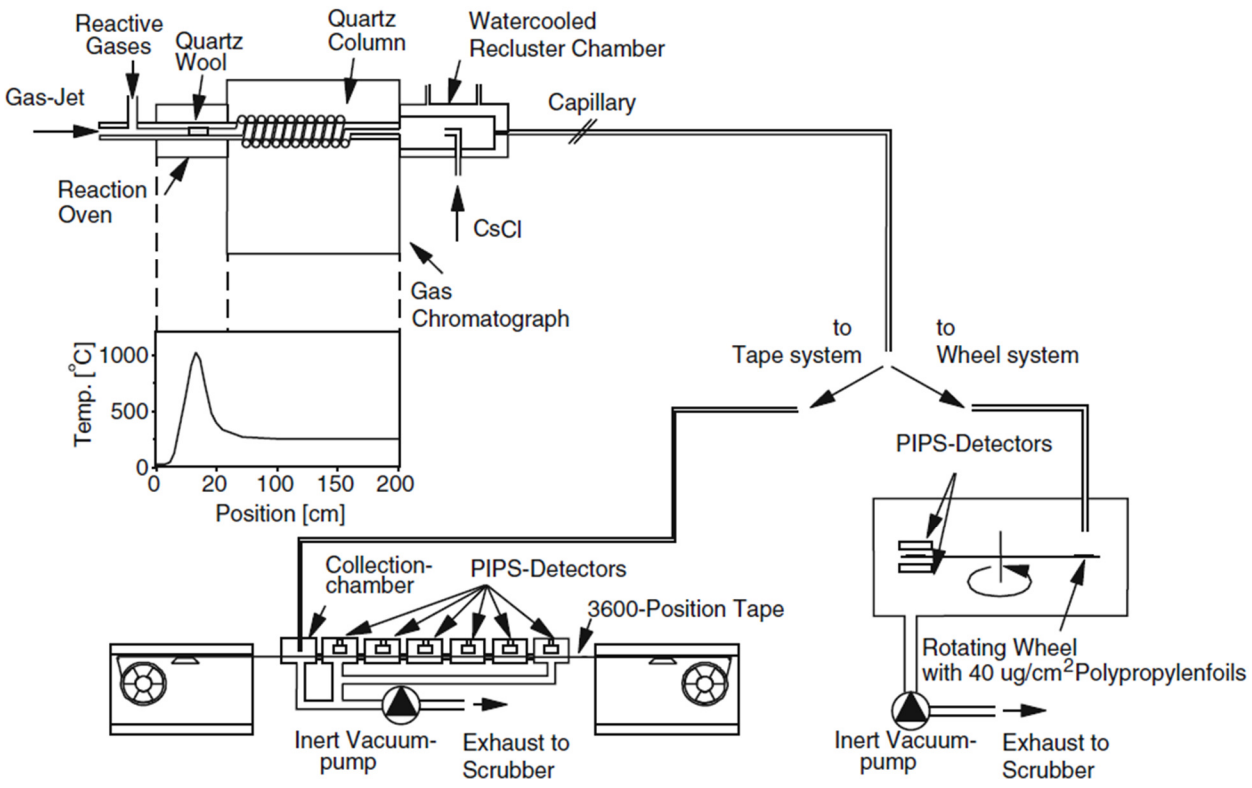

Figure 2: Schematic of the OLGA III setup [18].

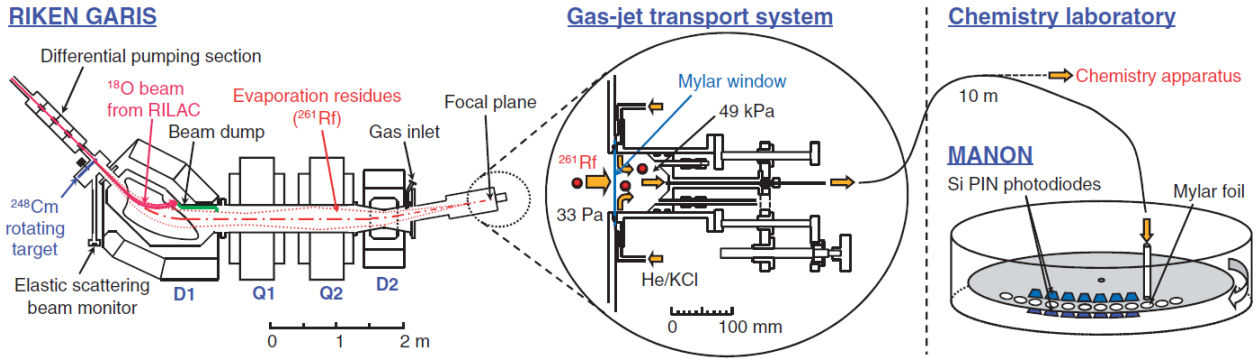

Figure 3: Schematic of the MANON experimental setup [29].

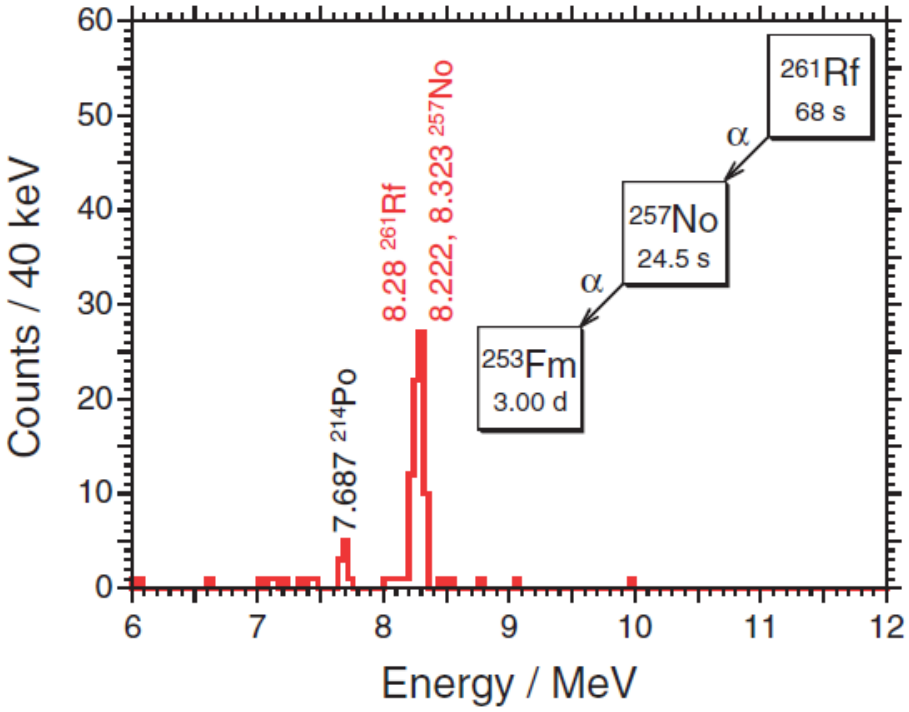

Figure 4: α particle spectra recorded from the top 7 detectors used by MANON for a 210 s live time and 30 s of aerosol collection [29].

A. Türler *et al.* used a 10 m, 2 mm I.D., quartz capillary tube to transport compounds between the beam target and GC and had a mean velocity of about 5 m s^{-1}. A reaction oven was positioned at the entrance to the GC and 150 mL min^{-1} Cl_2, saturated with $SOCl_2$, and 2 mL min^{-1} O_2 were added to the stream of laden aerosols. The capillary tube diameter was reduced to 1.3 mm, and a quartz wool plug within the tube was heated to 1000 ºC. The capillary tube retained the carbon aerosols long enough for the formation of CO_2, SgO_2Cl_2, and gaseous sulfur compounds.

The isothermal column following the capillary tube was maintained between 300 ºC and 400 ºC, which allowed the group 6 oxychlorides to elute unimpeded while retaining actinides and other products due to their lower volatilities. The total time spent in the GC was about 3 seconds and the column was 2.5 m in length. After eluting from the GC, CsCl aerosols were reclustered with the SgO_2Cl_2, and the laden aerosols were ducted to the ROMA alpha spectroscopy station. The setup used capillary column lengths and diameters that differ from the general OLGA III description due to specific experimental needs.

In a second experimental campaign, A. Türler *et al.* confirmed their initial ^{265}Sg results and expanded upon that by varying the isothermal column temperature between 130 and 400 ºC. During the campaign, they generated ^{168}W, which produces a 178.5 keV gamma-ray with 100% yield. This was accomplished by adding ^{152}Gd to the ^{248}Cm beam target and was used to monitor the system. The elution yields are a function of temperature and are shown in Figure 5 [24]. It should be noted that relative yields for ^{265}Sg at lower temperatures were somewhat reduced due to the approximately 8 s half-life and resulting appreciable material loss due to decay. Monte Carlo simulations of molecular migration in an isothermal column were conducted and matched to the experimental data [30].

2.3.5 Super Heavy Element Instrumentation Summary

The OLGA series instruments address concerns shared with isotopic nuclear forensic analysis and appear well suited for adaptation. Sample transport and accounting methods are of particular interest. Concerns exist regarding the time needed for sample preparation, sample adherence to applicable films, and ability to satisfy the Daubert standard. Super heavy element (SHE) instruments were designed for short-lived isotopes and are characterized by rapid gas-phase reaction rates and continuous physical transport systems.

Additionally, SHE instruments operate with exceptionally low analyte concentrations, whereas most TNF work is accomplished at or above such levels. The increase in analyte concentration is expected to assist with material accounting and changes to elemental ratios during sample preparation. One of the other benefits of SHE instruments is the opportunity to analyze the separation efficiency of thermochromatography columns by recording column output as a function of time. Sample deposition onto films utilizes physical or chemical reactions with the film, or differences in electrostatic charge. These reactions are essential to ensure each sample is efficiently collected. The early effort presented in Chapter 3 emphasizes an electrostatic wheel apparatus based on the MANON design. Separations in the gas phase is a central feature of SHE instruments and is described in further detail in Section 2.4.

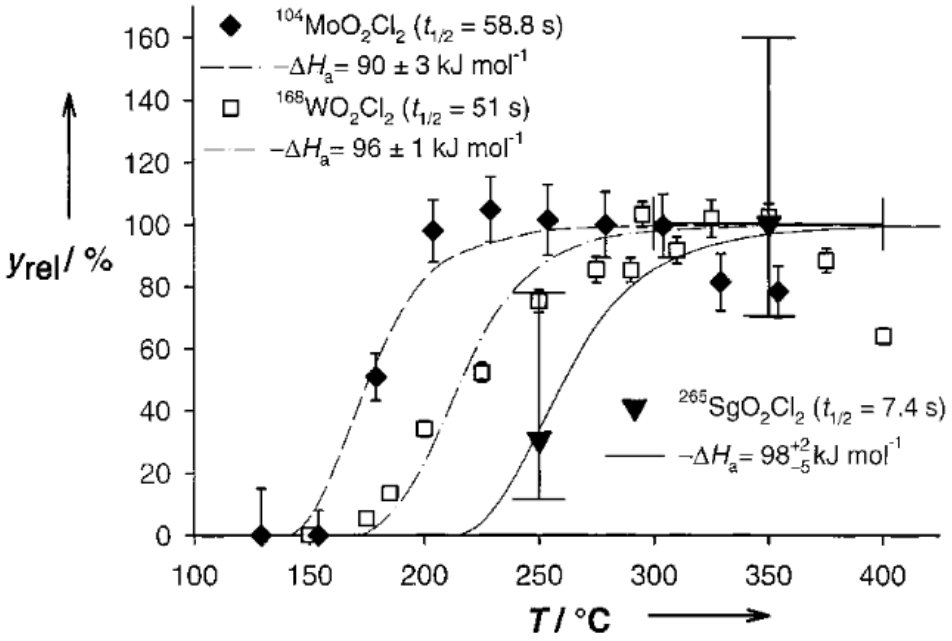

Figure 5: Percent relative yield of MoO_2Cl_2, WO_2Cl_2, and SgO_2Cl_2 as a function of isothermal temperature in a chromatography column [24].

2.4 Gas Phase Separations

Super heavy element investigations have made extensive use of gas phase separations via kinematic separators and thermochromatography. A kinematic separator, essential to conventional SHE investigations, uses a window made of MYLAR or similar material to prevent low energy beam target recoil products from entering the thermochromatography column while allowing higher velocity transactinide elements to traverse the barrier. The kinematic separators used for the OLGA I-III and MANON systems greatly reduce the throughput and other demands placed on a thermochromatography column. Kinematic separators are not a topic of study in this dissertation. However, the need for selective ionization dependent on atomic mass is an important topic for future TNF work.

Most thermochromatographic applications use an inert carrier gas flowing down a narrow quartz capillary column to move sample material as it adsorbs and de-adsorbs from the column surface. These columns are typically between 0.1 and 1.0 mm inside diameter, and when used for SHE investigations, often have an isothermal temperature profile that helps retain low volatility compounds while allowing the more volatile ones to rapidly elute. Ideally, each analyte has thermodynamic properties that result in a unique mean time spent in the adsorbed state and frequency of adsorption and desorption from the column surface.

In some cases, a linearly decreasing column temperature profile is used, which results in the species exponentially spending more time adsorbed to the column surface and is helpful when separating analytes having nearly identical enthalpies at commonly selected temperatures. The difficulty with this approach is the precise temperature control needed over the entire column length. Samples can be introduced or injected into the column flow continuously, resulting in slightly reduced resolution, or in pulses, which often result in chromatograms having improved resolution. One of the notable features of SHE investigations in the early 2000s is the complexing of transactinide atoms with heated reactive gases. This allowed for rapid chemical reaction rates at temperatures approaching 1000 °C, which avoided the slower reaction rates and kinematics of liquid phase chemistry used in prior investigations.

2.5 Final Development of Prior Efforts

Previous work by Hanson *et al.* demonstrated gas-phase separations using thermochromatography and the rare earth elements Sm, Dy, and Tm complexed with volatile organic compounds like 1,1,1,5,5,5-hexafluoro-2,4-pentadione (Hfac). The experimental setup included a GC oven that facilitated sample injections of rare earth complexes, dissolved in ethyl ether, into an interior lined quartz capillary column maintained under isothermal conditions near 130 degrees C. The thermochromatography column was approximately 30 m in length and used an inert carrier gas that without samples present would nominally exit the column after approximately 93 seconds. Sm, Dy, and Tm were complexed with Hfac, mixed and injected into the column. These complexes exited the column at 3.5 minutes, 4.15 minutes, and 4.9 minutes post injection, respectively, with reasonable resolution evident in the chromatogram, as shown in Figure 6 [1].

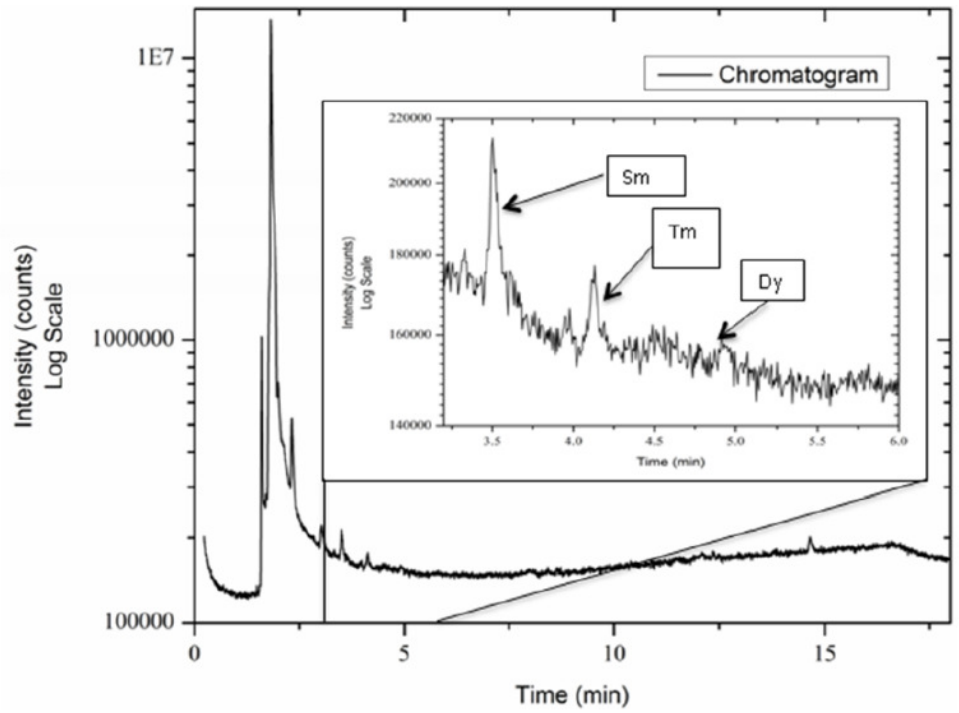

Figure 6: Chromatogram of ethyl ether containing 0.1g/mL of Sm, Tm, and Dy [Hfac] and generated using a thermal conductivity detector [1].

Rare earth elements are often the focus of TNF investigations and are frequently obtained in chemical forms that require lengthy sample preparation work. One of the important forms is glassy debris from a nuclear detonation. Gill *et al*. explored four methods of preparing glassy debris for isotopic analysis using Inductively Coupled Plasma-Time of Flight-Mass Spectrometer ICP-TOF-MS. These methods were an adapted form of the Maxwell Method (sodium hydroxide fusion), the Larivière Method (lithium fusion), the Eppich Method (acidic digestion), and the Hall-Auxier Method (modified rapid acidic digestion) [6].

The Maxwell Method was originally developed to separate U, Pu, Am, and Cm from asphalt samples that contain diverse hydrocarbon and organic compounds. After separation, samples were analyzed using alpha spectroscopy. Gill *et al.* sought to address concerns about adapting the method to include additional elements, and ideally, any heavier than oxygen. Given the broad inclusion of elements it was necessary to use ICP-TOF-MS for analysis.

The general goal was to convert samples into water soluble forms prior to ICP-TOF-MS analysis. The Maxwell Method reacts samples with NaOH at 600 ˚C for 20 minutes, then with concentrated HCl and HNO_3 solutions. The supernatant is afterwards drawn off and evaporated, and samples are diluted with deionized water to meet the maximum concentrations ICP-TOF-MS can accept. Gill *et al.* found that this method generates high yields for some transition metals like Ni but remarkably low yields for other metals like Ba. It was found that the concentrations of U and Ba could not be detected meaningfully, and as such, this method was deemed ill-suited for adaptation to advanced gas-phase separations work [6].

The Larivière Method combines powdered samples with ultra-pure LiBr and lithium metaborate, $LiMBO_2$, and briefly heated multiple times to 1000 °C in a platinum-gold alloy crucible. After the heating, the samples were cooled and placed in a HNO_3 / HF acid bath, evaporated for 24 hours, and then analyzed using ICP-TOF-MS. The yields from this method were slight improvements over the Maxwell Method but involved a much longer process and required the use of an expensive crucible. The substantial financial costs of this method were deemed excessive considering the slightly improved analysis results, and therefore excluded from future adaptation to advanced gas-phase separations work.

The Eppich Method combines and reacts powdered samples with concentrated HNO_3 and HF over 24 hours to form fluoride precipitates. These precipitates are then combined with concentrated $HClO_4$ solution and evaporated to remove the fluorine. The new precipitates are then added to concentrated HCl and supernatant is drawn off and evaporated. Finally, the remainder is dissolved again in a less concentrated HCl solution, evaporated again and diluted with deionized water for ICP-TOF-MS analysis. The yields from this method were substantial improvements over the Larivière and Maxwell methods but still required well over 24 hours to accomplish.

The Hall-Auxier Method [6] is a modified version of the Eppich Method that substantially reduces processing time while achieving yields that are a minimum five-fold improvement. The Hall-Auxier Method uses a Parr microwave bomb to elevate the temperatures and pressures exerted on the samples while reacting with concentrated HNO_3 and HF solutions. The acid digestion requires approximately 90 minutes to accomplish compared to more than a day for the Eppich Method.

Therefore, the preferred process for sample preparation currently is the Hall-Auxier Method for applications involving samples obtained from a nuclear detonation event. Variations of the Hall-Auxier Method might be adapted for specific scenarios, but difficulty remains in the form of isobaric interferences when using ICP-TOF-MS for isotopic analysis.

To address isobaric interferences, Stratz *et al.* investigated the potential adaptation of isothermal chromatography for gas-phase separations of rare earth elements [31]. One adaptation effort investigated the potential for direct injection of powdered samples into an isothermal chromatography column. The experimental work demonstrated the feasibility of injecting volatile organic rare earth compounds. However, the high throughput caused substantial erosion of the MS interface chamber cones.

One of the challenges with adapting chromatography-based separation systems for use with rare earth compounds is identifying the effectiveness of design changes and the retention times of sample constituents within the column. Depositing the separated sample constituents onto a moving film or foil will allow for rapid assessment of separation efficiency and effectiveness by examining the deposition concentration as a function of time.

After depositing onto a film, the samples can then be dissolved in HNO_3 and diluted to meet the concentration requirements for ICP-TOF-MS. Of course, the benefits from effective sample preparation and element separation methods are negated if isobaric interferences occur during the final analysis. Instrumentation that can accept samples prepared according to the Hall-Auxier method and condition them for analysis by a MS while precluding the possibility of isobaric interferences is needed as a follow-on effort to the impacts provided by the Hall-Auxier method.

This progression of ideas and technical developments serve as the foundational starting point of the RESI device. Initial efforts at addressing the gaps presented in this subsection are discussed in Chapter 3. However, those efforts were not fully developed in this work. Instead, the R&D ultimately took the form of developing the RESI system. That system is discussed in Chapter 4 and the remaining chapters. However, the initial work done provides a platform for useful future work and is worthy of documentation here. A general list of guiding objectives for this work are given in Section 2.6. These objectives respond to the gaps presented by the recent developments discussed in this section.

2.6 Guiding Objectives

The remainder of this dissertation focuses on work done to develop and demonstrate a practical device capable of formatting a continuous stream of gaseous rare earth elements into an acceptable form that can be sampled and analyzed by a mass spectrometer. Important, guiding objectives for this development are as follows:

- The device must accept a continuous stream of separated rare earth elements separated one from another in time
- The device must convert the gaseous stream of rare earth elements into a solute of appropriate concentrations for analysis by a mass spectrometer

- The device must handle all gas-borne particles in real time without allowing remixing of separated elements
- The device must retain substantial percentages of the rare earth particles supplied to it for ultimate analysis
- The device must be tolerant of temperatures up to 250 ˚C

Additional objectives of this work considered desirable but less important to the success of the device include:

- The device should accommodate ultimate collection of all injected rare earth elements to avoid uncontrolled release of hazardous materials to the environment
- The device should be designed and tested using a design and testing philosophy of inexpensive prototyping and fail-fast experimentation.

Chapter 3: Early Explorations of Candidate Collection Methodologies

Preserving the chronological order of gas-phase separated samples, and formatting those samples for uptake and analysis by a mass spectrometer is an important gap identified by the recent developments discussed in Section 2.5. This chapter discusses early attempts at two different candidate methods for collecting a stream of gas-phase particles and supporting the processing of the collected particles for consumption by a mass spectrometer.

Both methods use a rotating wheel design that collects gas particles that impinge on the wheel at different angular locations around the wheel. The wheel is rotated, or indexed, periodically to present different surface areas on the wheel at different times to maintain the chronological order of the impinged gaseous stream. The essential differences between the two implementations are that one implementation used a fabric collection surface, and one used a metallic collection surface. These are discussed further in the following two sections.

3.1 Fabric Collection Surface

For the tests with the fabric collection drum, the drum was connected to a chemical fume snorkel to draw the carrier gas and aerosols of actual rare earth elements through the fabric pieces and over the various tape segments. A picture of this drum, a fabric piece, and exhaust snorkel is shown in Figure 7.

Figure 8 shows an early version used for testing the deposition of aerosols onto tape segments. It was also discovered that a UV pen light and yellow tinted safety glasses from a R134A leak detection kit provide a quick means to identify large surface deposits of rare earth compounds. Unfortunately, these overall efforts were ultimately unsuccessful due to the aerosolized samples not adhering to the intended surfaces under a wide range of experimental conditions.

3.2 Metallic Collection Surface

Because aerosols are often prone to the impartation of static charges it is worthwhile to consider an approach involving pre-charging the particles for achieving depositions onto tape segments in future work. As such, an apparatus was built to test the theory of electrostatic collection of rare earth aerosols.

The apparatus built uses the high voltage generated by a powder coating paint system to induce a static charge on particulates, which generally adhere to the surface of aluminized tape segments placed on a rotary wheel.

Rather than using actual rare earth elements in the testing of this device, various powdered surrogate materials were used. The testing involved several different powdered materials with mean diameters ranging from 15 µm to 125 µm. These particulates were larger in diameter than what were expected with gas-phase separated aerosols, but visual inspection of the aluminized tape segments suggests that this collection method has significant potential and should be further investigated.

Figure 7: Rotary wheel apparatus with exhaust snorkel duct fitting.

Figure 8: Rotary wheel apparatus used for aerosol deposition onto tape segments.

During normal conceptual operations of the rotary wheel apparatus, rare earth compounds exit a gas-phase separations column and rapidly condense into aerosols, which then pass near a high voltage emitter and enter an electric field strong enough to induce a static charge on the aerosols while they travel to the nearest electrically grounded metal tape segment in the apparatus. This produces a concentration distribution resembling what is shown in Figure 9. The output from a separations column is continuous under normal operating conditions, but the intermission while rotating the wheel for sequential tape segments would produce a stepwise collection pattern.

The apparatus is connected to a chemical fume snorkel that creates a steady air flow into the apparatus and compliments the electric field forces. Upon entering the apparatus, the aerosol laden air passes directly over an electrically grounded metal tape segment before entering the exhaust snorkel. Only one metal tape segment is grounded at a time and foam separators guide the air flow away from the other tape segments to help prevent cross-contamination.

Electrical grounding of each tape segment is accomplished from a spring-loaded grounding wire that touches only one metal tape segment at a time as the wheel rotates, resulting in a simple, automatic process. Testing the apparatus with powder paint demonstrated that cross contamination was prevented during normal operations, and that deposits on the metal tape were significant and in the expected locations.

Work remains to position a high voltage emitter near the gas-phase separations column exit without electrically grounding to the coupling oven while maintaining a sufficient temperature for the column to avoid clogging by condensed compounds. Figure 10 through Figure 15 show the wheel apparatus.

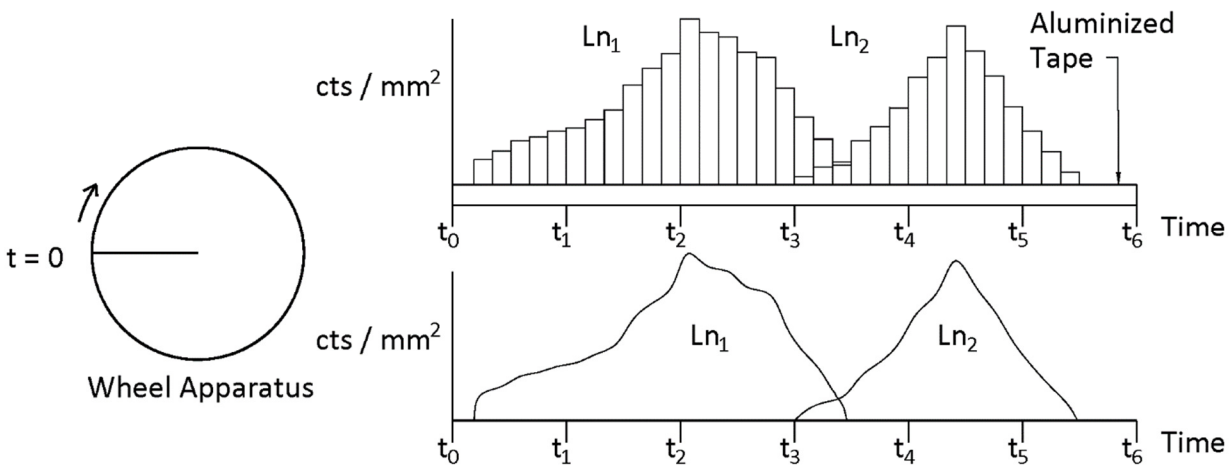

Figure 9: Conceptual deposition as a function of time onto electrically grounded metallic tape.

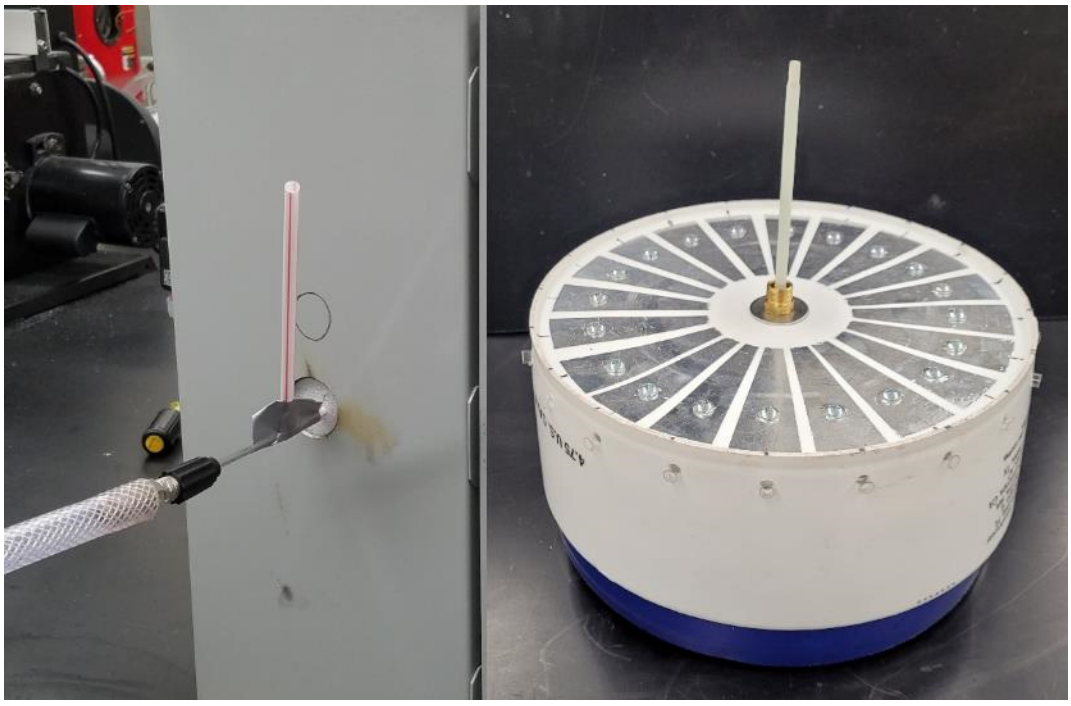

Figure 10: Powder Injection Straw (L) and Wheel Apparatus Exterior View (R).

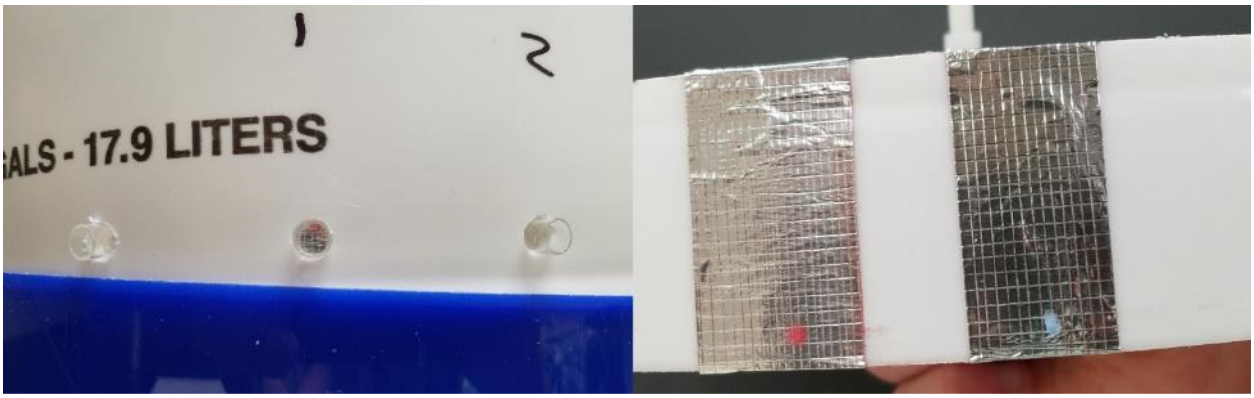

Figure 11: Powder Paint Deposits: Through Truncated Pipet (L), and Interior View (R).

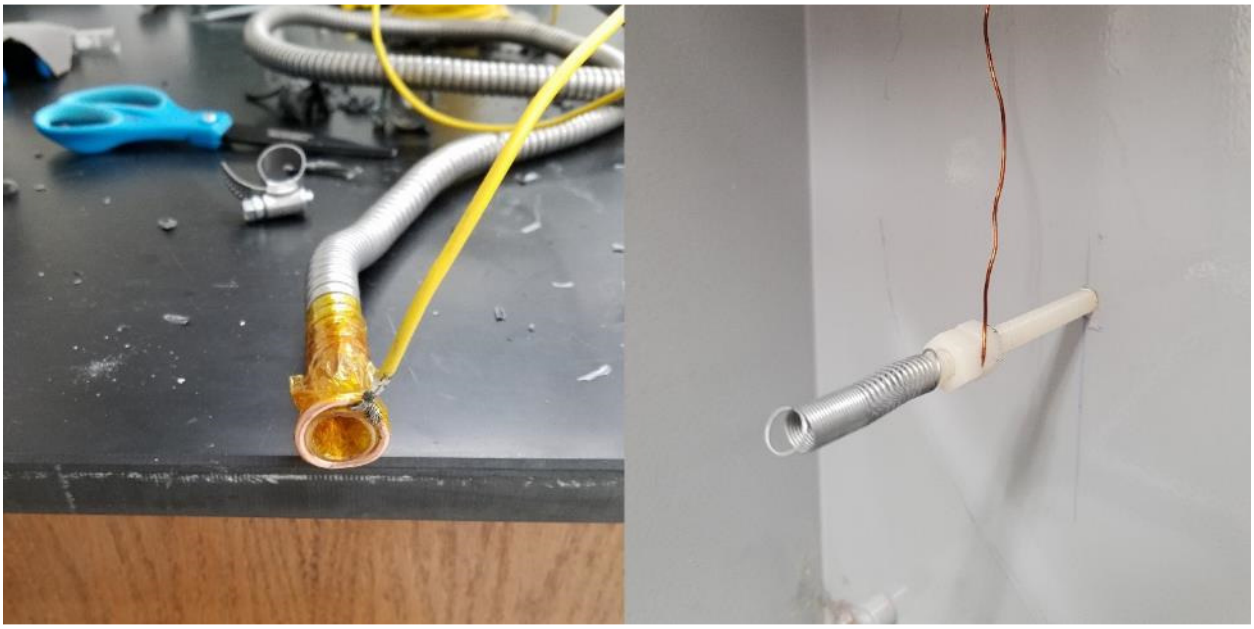

Figure 12: High Voltage Emitter (L) and Electrical Grounding Spring (R).

Figure 13: Wheel Apparatus Interior view (L) and Sample Collection Wheel (R).

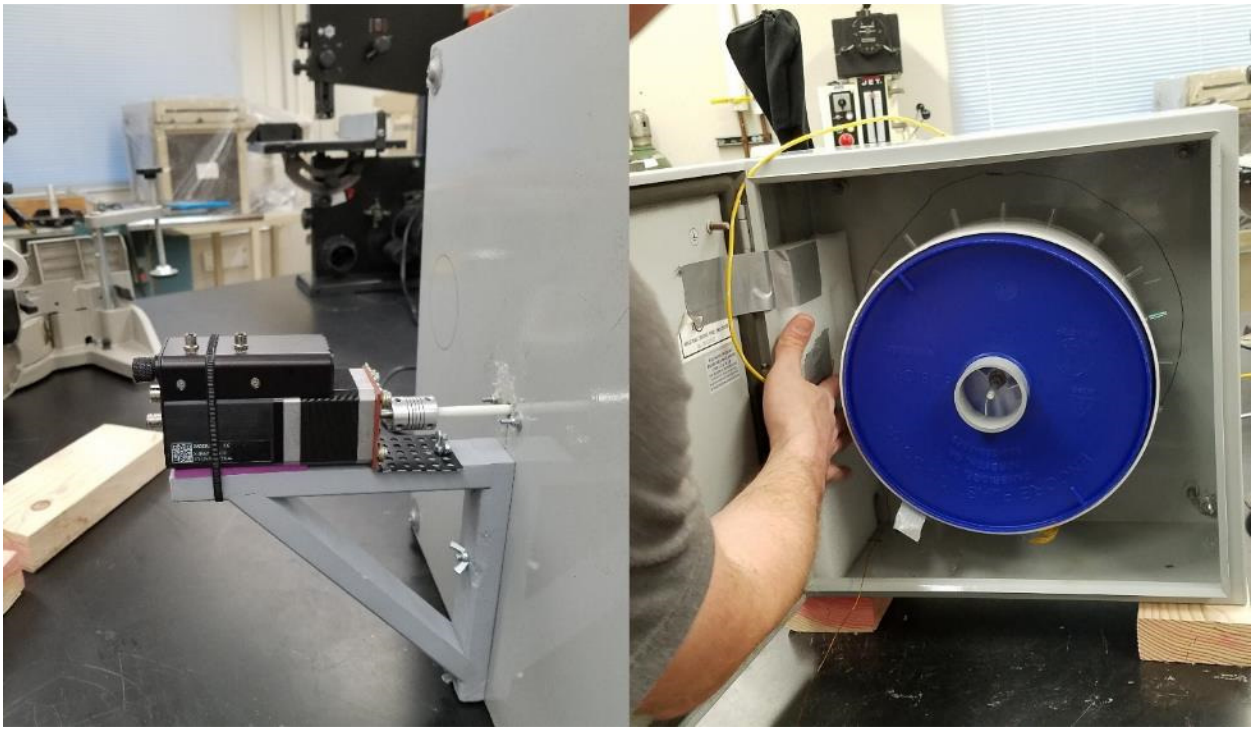

Figure 14: Stepper Motor (L) and Rotary Wheel Housing Box (R).

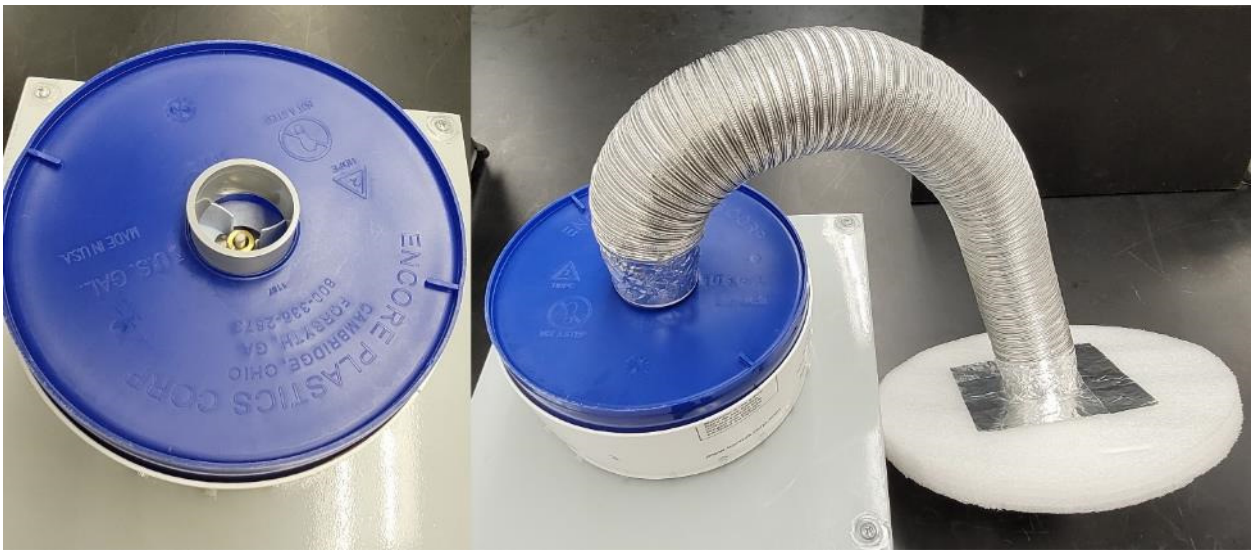

Figure 15: Exhaust Side of Wheel (L); Vacuum Adapter to the Snorkel Exhaust System (R).

Chapter 4: Conceptual Design of RESI Apparatus

Following the early explorations with the wheel type collection apparatus described in Chapter 3, a fresh and innovative idea was pursued as discussed in this chapter. This new idea was thought to be potentially able to incorporate the benefits of maintaining the separation of rare earth compounds shown in the apparatuses in Chapter 3 while also providing dissolution of the rare earth compounds in preparation for sampling by the mass spectrometer. A conceptual overview of this idea, eventually named the Rare Earth Separation Instrument (RESI), and thoughts toward prototyping a practical implementation of the design, are given in the following subsections.

4.1 Overall Design Concept

The practical device accepts a gaseous stream of rare earth compounds delivered to it by a heated coated capillary separations column [32]. A detailed introduction to gas-phase separations is given in Section 2.2, but a functional introduction is given next in Section 4.1.1. The RESI device accepts a flow of rare earth compounds delivered by gas-phase separations column. The device then converts the rare earth elements to a form that can be sampled by a mass spectrometer. The following sections discuss these items further.

4.1.1 Gas-Phase Separations

This separations column produces a flow of rare earth elements separated such that batches of unique rare earth elements exit the column at different points in time. Essentially, one element species will exit the column, then there will be an intermission of inert carrier gas, followed by the next species of rare earth elements.

Rare earth elements exiting the column are bound to volatile organic compounds, like Hexafluoroacetylacetone (Hfac), and transported via carrier gas, often helium or argon. These compounds leave the separations column in gaseous form. Prior work has shown that this gas condenses immediately upon exiting the column [1], [31]. Carrier gases separate from the rare earth elements and the volatile compounds they are bound to upon leaving the separations column.

Further details about this column are given in Chapter 2, but the flow stream this column provides is the input the RESI device is intended to accommodate. Next is a list of performance objectives the RESI needs to satisfy for the intended operating conditions. A summary of the test objectives are as follows:

4.1.2 Performance and Testing Criteria for The RESI Device

A summary of the test objectives for the RESI as used in this work are given here in summarized format:

- Thermal tolerance
  Gas-phase separation columns are frequently used with a coupling oven. Coupling ovens keep the column contents at elevated temperatures near 250 ˚C while they leave the separations column and enter the downstream process. For this work, the downstream process is the RESI, so the RESI must be able to tolerate such temperatures.

- Capture and handling of carrier gases

  Carrier gases could be a source of contamination inside the RESI if they are not effectively handled and captured. This is because tiny particulates of REEs that avoid mixing with dilute nitric acid could be carried along with the flow of escaping carrier gases. It is important that all carrier gases are drawn into the RESI device.

- Sample collection efficiency

  Due to the small quantities of REEs processed in a typical analysis sequence, it is important that REEs entering the RESI ultimately make their way to the mass spectrometer. As a result, one of the performance metrics is the ratio of REEs ultimately harvested to those delivered by the separations column. A ratio close to one is ideal.

  This performance metric can be measured two different ways. One, is to measure and integrate the real-time concentration of solution provided to the mass spectrometer. The second method, which is more practical for laboratory testing, is to collect all the solutes pertaining to a particular separated rare earth element that flows through the RESI and calculate the aggregate quantity of said rare earth element as compared to the quantity known to enter the RESI. The aggregate quantity harvested divided by the quantity delivered is the effective ratio of interest.

- Gaseous waste processing

  Carrier gases and any entrained particulates are not delivered to the mass spectrometer. If not accounted for, these could lead to contamination, both of the RESI and of the external environment. The RESI must accommodate an incoming flow of carrier gases and REE compounds but must also allow for the ultimate separation of the carrier gases from successfully dissolved REEs, again, without admitting the remixing of separated REEs. Combined with other requirements of the RESI, this requirement represents a substantial engineering challenge.

- Continuous sample processing

  Due to the constant stream nature of the gas-phase separations apparatus that feeds the RESI it is important that the RESI functions continuously and does not need intermissions for cleaning during operation. Essentially, the RESI is required to provide continuous sample collection, dissolution, and distribution to a mass spectrometer.

- Demonstration of clean rinsing action(development testing)

  Because the RESI cannot stop for cleaning, it is important that the RESI maintain good cleaning action between separated REEs supplied by the separations column. Therefore, special attention is needed in testing of the self-cleaning action of the RESI device. It is imperative that all active surfaces of the RESI do not retain particles of REEs flowing through, as such retention would result in remixing.

- Performance metrics and their minimum acceptable thresholds

  Thermal tolerance to at least 250 ˚C and satisfactory demonstration of carrier gas capture. Sample collection efficiency must be 70% or greater. Satisfactory

demonstration of carrier gas separation from aerosol stream and suitable capture of the aerosols for processing. Intermission in system operation for cleaning must be kept too a minimum. Measurement of the concentration of REEs that persist in the collection reservoir between batches of separated REEs must be kept to a minimum.

4.1.3 Introduction of RESI Design Logic

The RESI device captures the flow leaving the separations column and dissolves the rare earth compounds with a solvent suitable for isotopic analysis by a mass spectrometer. The RESI is designed to capture both the rare earth constituents and heated carrier gas in a continuous stream as is provided by the separations column.

Once pulled into the RESI device, the rare earth elements that have since condensed into aerosols and started separating from the carrier gas are mixed with a solvent. Rare earth elements complexed with Hfac are well known to readily dissolve in water. Hfac complexes are sometimes known to break down into large fragments while flowing through a separations column. These fragments and their associated rare earth elements do not readily dissolve in water.

Because the RESI device needs to accommodate both Hfac complexes and associated fragments, dilute nitric acid is used instead of water as the solvent. Both Hfac, and any broken Hfac fragments, readily dissolve in dilute nitric acid. Furthermore, in the event that organometallic compounds, like Hfac, decompose during the separations process, the resulting chemical compound fragments that enter the RESI readily dissolve in the dilute nitric acid.

Rare earth elements and chemical complexes dissolved in dilute nitric acid are suitable for isotopic analysis using a device such as a mass spectrometer. The goal of the RESI device is to ensure that all separated REEs entering the device are dissolved and can get to the mass spectrometer without remixing. Remixing of REEs can occur from unhelpful circulation patterns of carrier gas that could transport REEs to unwanted locations within the RESI, essentially forming surface contamination that could later combine with dissolved REEs from another batch.

Within RESI is a reservoir that briefly retains the dissolved complexes and fragments. The reservoir is designed to retain dissolved REEs long enough for a mass spectrometer to withdraw enough dissolved REEs to generate statistically significant results. A peristaltic or other pump withdraws small quantities of dissolved REEs from the reservoir through a small feed line and into the mass spectrometer for isotopic analysis. Surplus REE solutions continuously flow out of the reservoir while dilute nitric acid continuously feeds into the reservoir. These continuous flows produce a natural rinsing action between REE samples that allows for continuous operation, thereby removing the need for complete disassembly for cleaning between every sample. The next section describes the final RESI design in more detail.

4.1.4 The RESI Device: Organometallic Collection and Dissolution Module

Section 4.1.3 introduces the design logic for the RESI. This section introduces the as-built system in detail and in a narrative format. Like Section 4.1.3, this section develops the RESI in a logical progression and important concepts are reiterated and further built out.

As discussed in Section 4.1.3, separated rare earth complexes, decomposition fragments, and carrier gas exit the separations column and enter the mixing module, where they are combined with dilute nitric acid and compressed air. The mixing module must tolerate carrier gases up to 300 °C without undergoing appreciable chemical reactions or structural deformation. In addition, the module is designed to separate liquids from gaseous products without the use of moving parts in contact with the REEs. For this work, the separations column is simulated by a spring driven infusion pump that supplies mock REEs to the RESI through a capillary tube.

In keeping with the fail-fast design philosophy of this work, the major components within the mixing module include a 316 stainless-steel collection cylinder, a Polyvinyl Chloride (PVC) frame to hold the collection cylinder, a low-pressure spray system to introduce dilute nitric acid, and a waste removal system. This design facilitates rapid modifications and adjustments as needed while providing chemical resistance to the anticipated streams.

Figure 16 shows the medical grade constant rate infusion pump used to inject sucrose solutions into the RESI device.
Figure 17 shows an overview of the RESI device including atomizer nozzle, simulated separations column, collection cylinder, collection reservoir, compressed air supply line, and dilute nitric acid supply line. Figure 18 shows close-up images of the stainless-steel collection cylinder, with the REE sample injection orifice visible in the front view. Figure 19 shows the assembled REE simulated injection nozzle, the atomizing spray nozzle, and the collection cylinder.

The collection cylinder accepts the stream of rare earth compounds, organometallic fragments, and carrier gases, and combines them with a continuous spray of dilute nitric acid and compressed air. Discharge from the collection cylinder includes a liquid stream and gaseous products. Extensive modifications to the spray nozzle ensure continuous rinsing of the collection cylinder, thereby ensuring the REEs are flushed into the collection reservoir or ducted into the gaseous waste removal system.

The airborne products and gases exiting the collection cylinder are principally carrier gases mixed with air, water vapor, and dilute nitric acid droplets. The PVC frame ducts the gases and airborne constituents into a waste removal system. This waste collection system also provides thermal insulation to a collection reservoir for the liquid and suspended constituents.

The liquid stream from the collection cylinder contains dissolved REEs and mixtures of rapidly dissolving organometallic fragments. This liquid is directed into a small collection reservoir where it is temporarily retained. While in the collection reservoir, small quantities are removed by a peristaltic pump system connected to a mass spectrometer. The reservoir is designed to retain the dissolved rare earth complexes and to be self-cleaning from continuous rinsing with dilute nitric acid.

Figure 20 shows the exhaust channel, collection reservoir, and sample extraction port. The upper left figure panel shows the overall device with the top of the anti-contamination drip guide. The drip guide transfers dissolved REEs leaving the collection cylinder to the collection reservoir. The drip guide is designed to keep the flow from splashing into the collection reservoir and to ensure a steady flushing of the solvent within the reservoir.

Figure 16: Spring driven infusion pump.

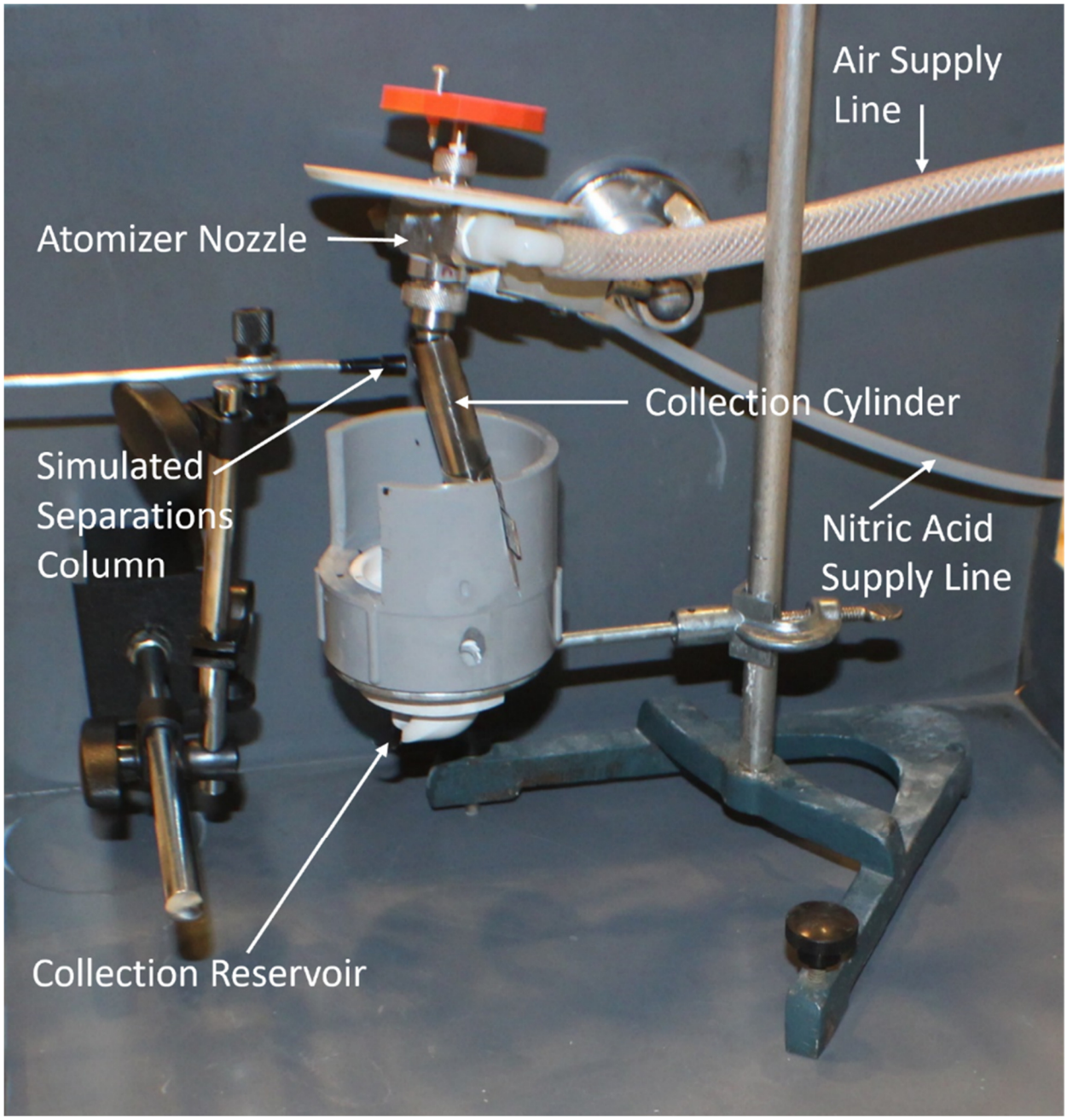

Figure 17: RESI teststand overview.

Figure 18: Stainless-Steel collection cylinder. Front view on left and back view on right.

Figure 19: Relationship between REE injection nozzle, atomizer nozzle, and colleciton cylinder.

The upper right panel of Figure 20 shows the collection reservoir and the bottom tip of the drip guide. The lower left figure panel shows the dissolved REE sampling port that provides access for the mass spectrometer to draw solvents out of the collection reservoir as they flow through the RESI. The lower right image shows a perspective of the bottom portion of the drip guide as seen through the collection reservoir.

The mass spectrometer sample port is shown in Figure 21 with a pipet inserted through the port to demonstrate how the mass spectrometer would harvest samples from the bulk passing through the collection reservoir.

The motive forces for system operation are directly provided by the spray nozzle used to distribute the dilute nitric acid, along with moderate contributions from the vacuum operated waste removal system. The carrier gas exiting the gas-phase separations column contributes limited motive forces that are immediately overshadowed by ambient airflow entering the collection cylinder.

Spray nozzles naturally create low pressure regions within their respective spray fields and pressure gradients in the peripheral volume. As a result, it is a theoretically viable matter to orient any spray nozzle at the entrance to a suitably sized cylinder, thereby creating conditions where ambient air is sucked into the cylinder along with the liquid and compressed gases emitted from the spray nozzle.

The spray nozzle used in this work is oriented into the top of the stainless-steel collection cylinder. When in operation, the nozzle injects compressed air and water droplets into the cylinder while creating a low-pressure region around the top of the stainless-steel collection cylinder. Any vapors, aerosols, and ambient air in the vicinity are sucked into the collection cylinder.

The original spray nozzle design produced a flat fan spray pattern and was modified to add a conical spray pattern to one side of the flat fan shape. This modification was needed to prevent water droplets from scattering onto any part of the heated separations column and connection fittings while ensuring continuous rinsing of the collection cylinder. The separated REEs and organometallic complexes are highly temperature sensitive and prone to forming deposits if the environmental conditions are not carefully maintained.

Figure 22 shows a close-up photograph of an atomizing spray nozzle. Compressed air is fed into the nozzle while liquid is drawn into the other side by the venturi effect facilitated by the compressed air flowing through the nozzle head. Figure 23 shows one of the modified nozzle tips tested as part of this work. This nozzle tip was originally manufactured to produce a flat fan spray pattern, and the modifications are meant to convert this nozzle to generate a half-cone spray pattern.

Testing with various sources of open flame demonstrates the thermal stability of the RESI under anticipated thermal conditions generated by a capillary separations column. Ambient air drawn into the collection cylinder as part of normal operation, in conjunction with the waste removal vacuum, provides cooling of the stainless-steel collection cylinder and all PVC components.

Figure 20: Exhaust channel and collections reservoir. Exhaust channel (upper left), collection reservoir (upper right), sample port and collection reservoir (lower left), and drip guide (lower right).

Figure 21: Sample port with mock extraction device.

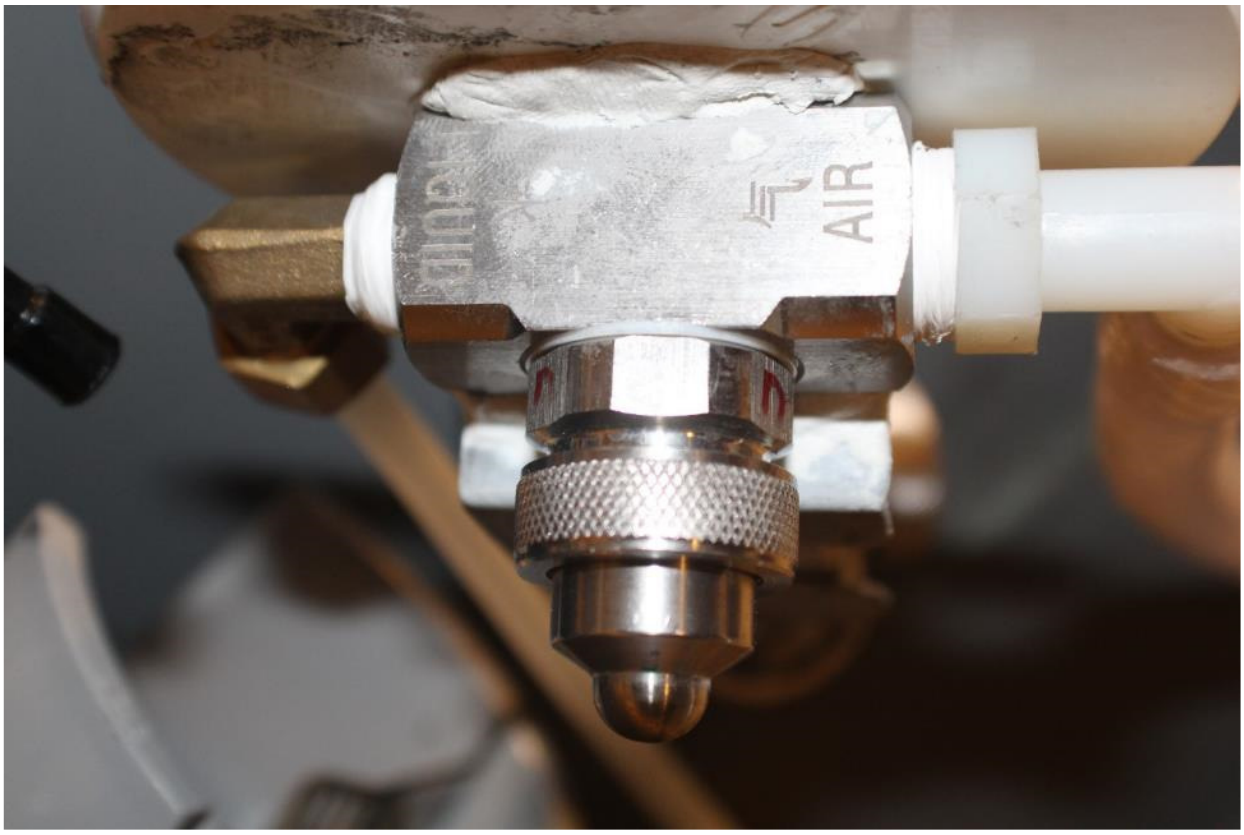

Figure 22: Atomizing spray nozzle

Figure 23: Modified nozzle tip

Open flame testing was also used as a visual indicator of the air currents generated by normal operation of the RESI apparatus as well as to test thermal stability. Particular combustion scenarios include flames generated by a butane lighter, a table candle, and a propane torch. The propane torch was used with a low flame setting for the visualization tests, and a high flame setting was used for the thermal tests. The RESI apparatus can accommodate the smaller, visualization, flames used, but some components such as the PVC frame need to be insulated for the larger, thermal, flame testing. Future versions of the RESI could replace low temperature tolerate components with metals or ceramics.

Figure 24 shows one of the flame tests. A propane torch flame is set to impinge directly onto the REE injection port of the collection cylinder while the atomizer nozzle is active. The atomizer nozzle is successfully establishing a low-pressure zone as desired. The photograph shown illustrates the drawing action of the low-pressure zone by showing that the flame bends at about 90 degrees to travel axially down the collection cylinder. This result demonstrates that carrier gases traveling towards the injection port will indeed be drawn into the collection cylinder. Figure 24 shows that the carrier gases will be contained in the collection cylinder and directed properly down the axis of the tube with the dissolved REEs. These gases are allowed to separate from the dissolved REEs after leaving the bottom of the collection cylinder, where they are captured by the exhaust gas removal system.

4.2 Substitution of Rare Earth Compounds with Less Reactive Aerosols

To accelerate the adaptation process, non-toxic aerosols were substituted for rare earth compounds. Substituted aerosols were used for two basic purposes in this work. One of these purposes is to test the ability of the RESI to ensure proper rinsing of the collection cylinder between batches of separated rare earth element. This was an important aspect of informing the effectiveness of the intermediate designs of the various RESI components and for providing insights regarding how to index the designs.

The other purpose of using the surrogate aerosols is to collect performance data on the ability of the RESI to process injected aerosols, dissolve them with the dilute nitric acid, and deliver them to the mass spectrometer in an appropriate format. This purpose was primarily used to demonstrate the functionality of the final RESI design. For these purposes, sucrose was considered an acceptable surrogate because of its readiness to dissolve in water or dilute nitric acid and its similarity in molecular size to the organometallic compounds ultimately meant to be used with the RESI.

The identity of the substitutions used to test the gaseous uptake and rinsing action of the collection cylinder and to inform the designs of the RESI, in order of decreasing mean particulate diameter, are:

- polyester powder paint
- corn starch
- confectionery sugar
- talcum powder
- partially oxidized glycerin vapor

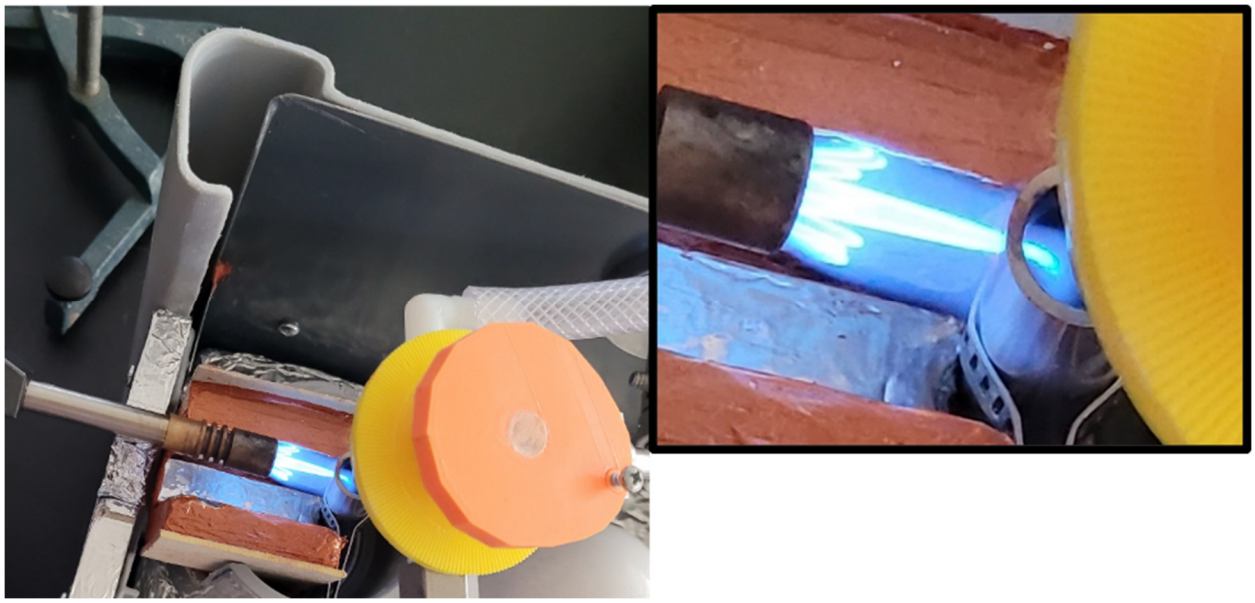

Figure 24: Thermal testing of Rare Earth Separtions Instrument. Note the 90 degree deflection of the propane flame after entering the collection cylinder.

The powder paint was particularly helpful in identifying areas where aerosols were likely to fall out of suspension and prematurely collect on the interior surfaces of the waste stream plumbing fittings. For example, Figure 25 shows how powder paint was used to identify contamination occurring on an early collection cylinder design. This result led to the understanding that the flat fan spray pattern was insufficient for keeping a reliable rinsing action. Consideration of this problem inspired the endeavor to modify the spray nozzle to produce a half-cone spray pattern. Subsequent powder paint testing revealed that the half-cone spray pattern was successful at facilitating a reliable rinsing action.

The corn starch was effective at identifying regions that would be coated with excess aerosols in the event of unsteady system operation. This material was also useful in validating the self-cleaning design of the sample collection pool. Red food coloring and confectioners' sugar were used to estimate the time needed for the collection pool to clear itself during normal operation

The heated glycerin vapors were used as a very effective demonstration for the final RESI design that carrier gases and condensates did not collect on up-stream surfaces inside the collection column or on the spray nozzle. Ensuring that aerosols do not collect in these areas is particularly important due to the consequent potential for remixing and isobaric interference. Use of the heated glycerin showed that such collection becomes possible if the nozzle becomes mispositioned within the collection column or if the spray angle is not consistent.

The smallest aerosols investigated were those involving talcum powder, which ranged from approximately 0.5 μm to 25 μm in diameter. Smaller aerosols, such as aluminum powder, with a mean diameter below 1 μm were also considered but were ultimately not used due to potential for exothermic reactions and possible damage to nearby power tools and laboratory equipment.

Figure 25: Powder paint deposits on the collection cylinder; back surface (left) and front surface (right).

Chapter 5: Experimental Design, Prototyping, and Functional Testing of the RESI Collection Cylinder and Atomizer Nozzle

The design process presented in this chapter highlights the most important design features and the associated CFD models. Experimental laboratory testing was used extensively along with the CFD modeling in the design and refinement stages of developing the spray mixing system. Generally, important design objectives of the spray mixing system were tested to regions beyond the intended operating conditions of the instrument in the most extensive of the laboratory experiments.

The design progression begins with unmodified hardware used to validate the CFD modeling methods and continues through distinct design changes that are essential for the performance of the apparatus. A plethora of additional intermediate designs were also developed and tested in this work, but detailed documentation of these designs and their respective performance documentation is not captured in this dissertation.

This experimental design is intended to continuously collect, dissolve, and discharge rare-earth compounds for analysis. The designed instrumentation is intended to accept rare-earth compounds separated in advanced gas-phase separations instruments such as those making use of the Hall-Auxier method. Rare-earth compounds are transported within the gas-phase separations instrument via helium or argon carrier gas and are known from the prior referenced work to exit the separations instrument as aerosols or gaseous compounds that immediately condense [31].

These aerosols are rinsed out of the carrier gas and ambient air in the instrumentation designed in this work via a dilute nitric acid spray system, dissolved, collected in a small reservoir, and continuously sampled via ICP-MS induction line. Surplus liquid in the reservoir is continuously discharged as waste and the dilute nitric acid spray cleans the relevant device surfaces to prevent different rare-earth elements from remixing and causing isobaric interference in the ICP-MS. A brief depiction of the designed process is shown in Figure 26.

5.1 Nozzle and Collection Cylinder Design

Turbulent air emitted from a nozzle will produce regions of low pressure immediately downstream of the nozzle tip as described by Bernoulli's principle. One device capable of facilitating such a flow condition is the reverse flow diverter pump system described at the end of this chapter. A second example device capable of creating the subject flow is a low-pressure misting nozzle. Design iterations of the instrumentation that led up to the final prototype used this type of nozzle and are presented later in this chapter.

The shape of a turbulent boundary layer between a jet of air and the ambient environment determines where regions of lower pressure will form. Most pneumatic spray nozzles eject air in the shape of narrow stream, a fan shape, or as a cone. In all these cases the low-pressure region is symmetrical around the centerline of the spray nozzle.

Low pressure spray nozzles use the venturi effect to draw water or other liquid into the turbulent air stream, where the water is dispersed into small droplets that form a mist upon exiting the nozzle. For simplicity of design, siphon fed spray nozzles were selected in the development of the spray

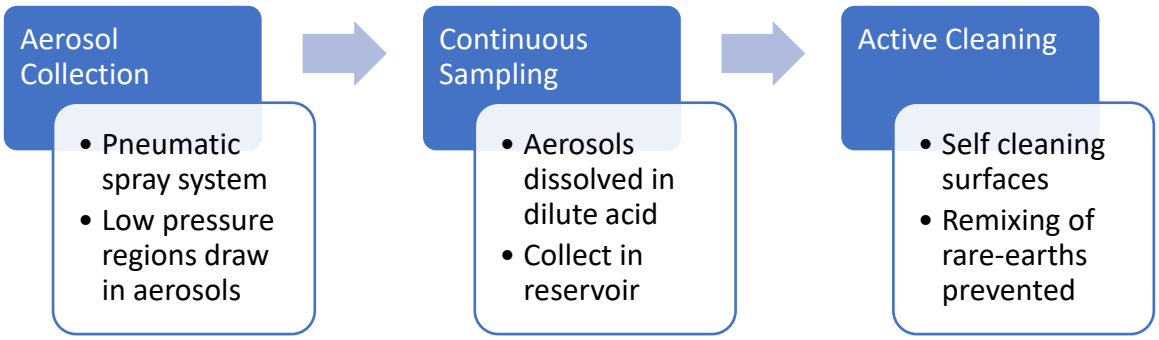

Figure 26: Process overview.

mixing system over gravity or pressure fed systems. Placing a spray nozzle near the entrance of a pipe section produces flow not unsimilar to the flow produced by reverse flow diverters. Key differences between the two scenarios include fluid viscosity, mass flow rate, entrance angle and diameter of the diffuser, and length of pipe downstream of the diffuser.

Early spray system and collection cylinder designs used a cone shape spray to evenly coat the interior of the collection cylinder while using the venturi effect to draw sample surrogate material into the cylinder. Functional testing consistently showed that cone shaped spray systems would frequently eject water droplets outside the spray cone region. These ejected droplets were sufficient to cause obstructions at the sample injection orifice, resulting in the rejection of cone shaped spray patterns. Alternative spray patterns were explored, with the most promising being a half-cone shape that was implemented by modifying a flat fan spray nozzle. The resulting spray pattern is conical on one side while retaining the flat fan spray pattern on the other side. Further discussion of this functionally modified spray nozzle is given in the next sections along with CFD computations that supported the design of the nozzle.

5.2 Computer Aided Design Models of the Collection Columns

As mentioned, the Rare Earth Separations Instrument (RESI) system ultimately implemented a modified flat fan spray to draw buoyant aerosols into a stainless-steel collection column where the spray droplets collide with the particulates and remove them from the air flow. The motivation for selecting the nozzle system was to take advantage of the low-pressure gas region provided at the exit of the nozzle. The modified fan spray type was investigated to provide clean rinsing by the nozzle in addition to the low-pressure zone.

A hole placed in the side of the gas mixing tube was used as a gas inlet port to accept the aerosolized rare earth elements and the carrier gases. The placement of this port was designed to admit the aerosolized mixture into the region of low pressure following the nozzle so that the gases entering the mixing tube are drawn into the flow of atomized dilute nitric acid facilitated by the fan nozzle.

5.2.1 CFD Modeling

Autodesk CFD uses imported geometry files to create a two, or three, dimensional wireframe mesh that divides the geometry into small elements. The appropriate governing equations, described in Appendix D, are iteratively solved at each point and surface of these elements, thereby creating a mathematical fluid model based on the original geometry and operating conditions. The smaller each mesh element, the better the mathematical description and capability to show applicable gradients and fluid movement.

However, fine meshes are computationally intensive and can easily exceed available resources. CFD programs sometimes offer automatic sizing and distribution of mesh elements to help optimize the use of computational resources. Common areas that require finer meshes include regions of sudden changes in geometry and surface curvature, along with regions likely to experience significant changes in fluid properties, including velocity, turbulence, and other flow characteristics.

5.2.1.1 Physics Models

This work involves the use of compressed air to operate a flat fan spray nozzle. Therefore, the basic relevant fluids involve turbulent subsonic compressible gas flow with heat transfer and buoyancy effects.

Velocity of air at Mach 0.3, or 0.3 times the speed of sound, is the commonly accepted lower limit where compressibility effects become significant. Below Mach 0.3, compressibility effects are still present, but cause changes to density and viscosity of 5 percent or less. Multiple sensitivity studies conducted as part of this work examined the differences between subsonic compressible and subsonic incompressible air flow, with the subsonic compressible models producing results that were in much better agreement with preliminary experimental results.

Through preliminary experimental testing, it was discovered that flow separation and resulting adverse pressure gradients are easy to generate when a spray nozzle is operating in proximity to a cylindrical pipe. Flow separation occurs when the curvature of a surface changes at a faster rate than what a moving fluid can follow. The resulting adverse pressure gradient can produce a recirculation of suspended aerosols, which is an important consideration.

It was also postulated that free stream turbulence would play a role in the movement of fine dust and aerosols within the RESI apparatus. Given the likely importance of flow separation and free stream turbulence, it was decided to use the shear stress transport (SST) $k - \omega$ turbulence model because it effectively addresses both types of fluid movement, whereas other physics models are not optimized to simultaneously address both flow regimes.

5.2.1.2 Model Convergence

Once the imported geometry has been discretized and the appropriate physics model selected, the next step is to set the convergence criteria used by the CFD solver when iterating to a mathematical solution. Convergence criteria is generally satisfied when subsequent iterations by the CFD solver produce results that vary from the mean value by less than a specified limit. For preliminary models, these limits are set to large tolerances that produce crude estimates. As model development progresses, the convergence criteria are reduced to match the need for greater precision in the results. Due to computational resource limitations, convergence criteria are only made stringent near the end of the design process.

Convergence criteria are based on residual values produced when solving the governing equations in matrix form. A matrix will have the general form $AX = b$ with a residual vector of $r = b - Ax$. The residual value of each matrix is ideally zero and the CFD solver will iterate towards this goal. However, solving all matrices such that their residuals are all precisely zero is often virtually impossible.

Instead, Autodesk CFD uses the square root of the sum of squares to measure the solver progress. The resulting value gives an excellent indicator of how close the CFD model is to the ideal mathematical solution where each residual value is zero. This general process is applied to each variable the CFD model is solving for, such as velocity, pressure, temperature, etc. Plots of the

residual values, also known as convergence plots, can be used to visually verify the solver is making steady progress and that the model is relatively free of fluctuations and instabilities.

5.2.1.3 CFD Boundary Conditions Derived from Direct Experimentation

The CFD solver requires a set of initial conditions applied to the simulated objects within the model. These initial conditions are specific to the respective objects and can include temperature, pressure, velocity, viscosity, density, thermal conductivity, heat generation rates, diffusion coefficients, and other properties. Most CFD suites, including Autodesk CFD, include common material libraries that automatically interpolate for dependent variables, such as thermal conductivity, which is dependent on temperature, etc.

Best practices for CFD modeling include selecting initial conditions that are both measurable and minimize the use of computational resources. One example, described in detail later in this work, is the use of pressurized air flowing through a nozzle. Static and dynamic air pressures are relatively easy to measure or use as a boundary condition, but this incurs an unjustifiable consumption of computational resources to correctly account for pressure losses within the nozzle before the air enters the ambient environment. Volumetric air flow rates were experimentally measured and then converted into mass air flow rate boundary conditions within various CFD models. Similar examples involving heat generation and waste air filtration systems are also discussed later in this work.

5.2.2 Collection Cylinder

Collection cylinders of widely varying diameters were investigated, with the strongest venturi effects being produced in pipes ranging from 3 inches inside diameter down to 0.5 inch. A propane torch was used to test whether the venture effect can cool a heated gas stream to temperatures tolerable of polyvinylchloride (PVC) materials intended to be used downstream of the mixing nozzle. The torch was also used to heat the stream entering the venturi and a PVC elbow set downstream of the venture was observed for signs of softening. Experimentation verified that the venturi effect could provide sufficient cooling to protect downstream materials made of PVC.

The design concept driving this arrangement is that gases introduced into the low-pressure zone following the atomizer nozzle will be efficiently mixed into the dilute nitric acid solvent without any tendency to spatter onto any surfaces of the mixing tube that are not constantly rinsed clean by the atomized nitric acid solution spray. This effectively facilitates the combination of a gaseous flow into a liquid stream in a way that provides for dissolution of the gas, mixing of the combined quantities, and avoidance of debris that would later contribute to isobaric interferences.

Because the bottom end of the mixing tube is open to adjacent air mass that is held under a slight vacuum, quantities of gases that do not dissolve into the nitric acid stream can be ejected without causing unacceptable pressure buildups in the mixing tube or other detrimental effects on the low-pressure combination area following the atomizer nozzle.

The aerosols and carrier gas enter through a small hole on the side of the column while the flat fan spray enters at an angle between 10 and 20 degrees from parallel to the column. The liquid then

collects on the lower interior side of the column and drips off the narrow tip, carrying a percentage of the former aerosols with it.

To facilitate dissolved aerosols exiting the column at a predictable point on the column rather than everywhere around the circumference of the column, a “V” shaped notch (essentially two conical sections) was cut at the bottom end of the cylinder. The resulting geometry is shown in Figure 27 (right). Cutting the bottom end in this fashion encourages the dissolved solution to culminate on either of the two resulting tips and exit the column at predetermined, discrete locations. Any aerosols that reach the bottom end of the collection cylinder are automatically discarded into the waste stream and collected into the vacuum system.

Iterations of the design of the collection column eventually led to a cylinder edge resulting from a single conical section as shown on the left side of Figure 27. The reason for this will be discussed later. The sharp tip and square lip at the bottom of the cylinder facilitate the use of surface tension to ensure water droplets collect and drip off the cylinder at a single point, rather than along the entire circumferential edge of the cylinder.

The inverted split-v design preserves the chronological sequence during collection but has a drawback in that this design only recovers a fraction of the initial sample mass. To address a means of capturing a greater percentage of the input aerosol quantities, a second column was built and modeled that prioritizes collection efficiency by channeling all surface droplets into the receptacle. A new problem was introduced with this design, however, because laboratory experiments showed that this column did not maintain the chronological elution sequence of the injected aerosols and carrier gases. Maintenance of the chronological order is important in avoiding isobaric interferences when sampling with the downstream mass spectrometer, and further work was needed to implement a design that allowed both a separation of elements and a strong rate of claimed solvents.

5.3 Induced Low Pressure Regions

As previously mentioned, high velocity air emitted from a nozzle produces regions of low pressure as described by Bernoulli's principle. Accordingly, the flat fan spray nozzle produces two regions of low-pressure immediately adjacent to the high velocity turbulent air flow. These two low-pressure regions occur along the front and back side of the flat fan and generate suction forces that draw aerosols into the collection cylinder.

In addition to drawing in aerosols, these low-pressure regions can also cause unhelpful vertical recirculation, as depicted in Figure 28. This figure shows schematic descriptions of the progression of air within the collection cylinder in the left frame, the resulting flow divergence in center frame, and the unhelpful recirculation in the right frame. The so-called unhelpful recirculation occurs near the location marked as ‘E’ on the right frame and can allow remixing of the separated rare earth elements. The high velocity air from the flat fan spray nozzle contains a significant quantity of water droplets, which collect on the cylinder surface and drip off the lip at ‘C’ and ‘D.’

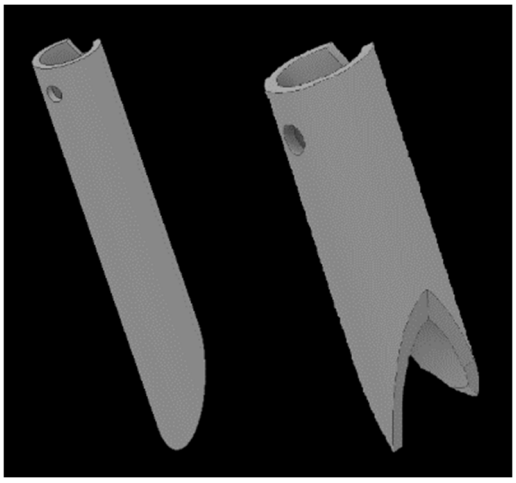

Figure 27: CAD models of the sequence preserving collection column (R) and higher efficiency aerosol collection column (L). Note that both columns are the same diameter but different lengths.

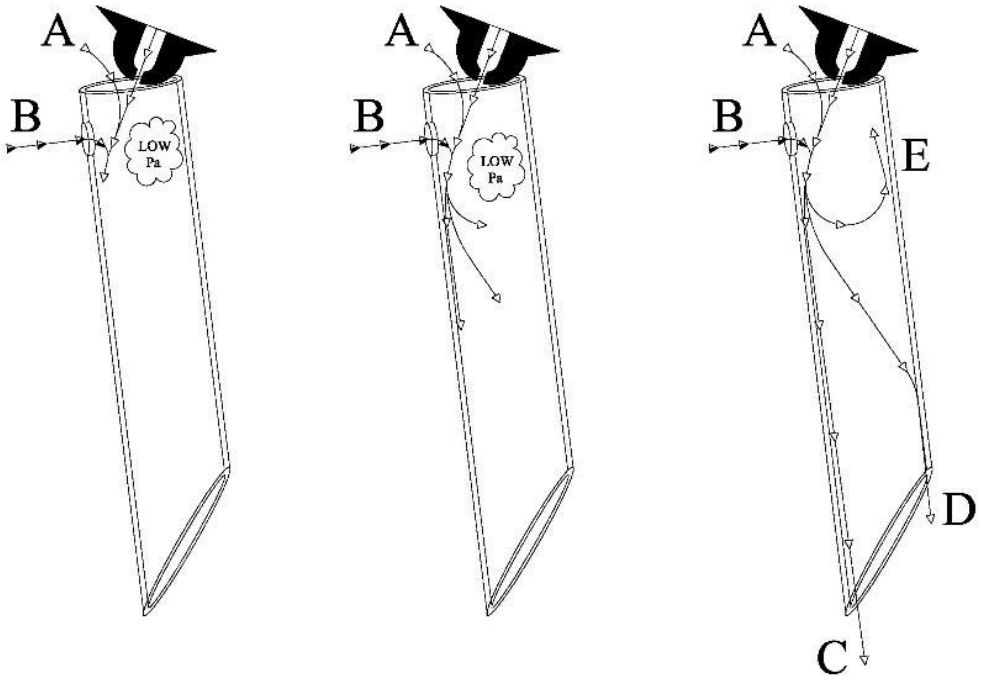

Figure 28: Depiction of air currents within the incomplete collection cylinder when using a flat fan spray nozzle.

The spray nozzle depicted in Figure 29 shows the design that was used as a basis for many permutations of CFD models used to study turbulent airflow relevant to this work. These CFD models were also compared to experimental airflow results generated by matching nozzles in a machine shop. These comparisons were instrumental in validating the basic model results.

Figure 29 shows a velocity profile model of turbulent air emitted from an unmodified flat fan spray nozzle. The legend is not shown, but ranges from 93 m/s in red to 5 mm/s in dark blue. Cross-sectional side views of the high velocity air and the resulting effects on downstream static pressures are shown in Figure 30 and Figure 31, respectively.

It was found that cutting an opening, or channel, into the side of the collection cylinder greatly reduces the impact from the low-pressure region originally shown in Figure 28. Discussion of the development of this opening are given in section 5.4, but as demonstrated in that section, it was shown that the additional airflow from this cut was found to greatly reduce the flow divergence and create a much more uniform exit flow, as shown conceptually in Figure 32. An image of the modified collection cylinder is shown in Figure 41.

The channel cut into the collection cylinder reduced the drawing strength of the injection port on the front side of the cylinder but eliminated the recirculation flow introduced in Figure 28. As such, the opening opposite the injection port was deemed an important design modification for the mixing tube. A simple laboratory test using the visible combustion artifacts of a candle flame as the combustion gases are drawn into the modified cylinder is shown in Figure 33. For this experiment, the candle wick was held at the same elevation as the 4.5 mm diameter opening. A jacket of cool air that insulates the flame as it enters the cylinder can be noticed around the flame. This experiment demonstrates a satisfying visual confirmation of the drawing effect that the low-pressure region exerts on gases injected into the mixing cylinder.

5.4 Models of the Spray Nozzle and Rotating Air Currents

One of the disadvantages of using high velocity air to drive fluid movement within the collection cylinder is the circulation of air up and down the length of the collection cylinder. Even with the spray nozzle set at an angle relative to the axis of the collection cylinder, vertical recirculation is still a potential way separated rare earth elements could remix between dissolving in the dilute nitric acid and being taken up by the mass spectrometer.

Angling the spray nozzle, coupled with leaving a large space between the cylinder top and spray system, allows enough ambient air into the top of the cylinder to prevent recirculation on the front, or sample inlet side, of the collection cylinder. However, this produces an especially strong recirculating air current along the back side of the cylinder. To alleviate this, various sized axial cuts in the collection cylinder were modeled and the most promising design, as per the CFD results was selected.

Modeling revealed that the highest efficiency introduced by the cut occurs when the axial cut is long enough for the counter-rotating air currents introduced by the atomizer nozzle spray to combine just below the backside lip. A beveled lip was added to this simulated cut to reduce the turbulent energy. Some of the modeled cut permutations were too wide or long to be helpful.

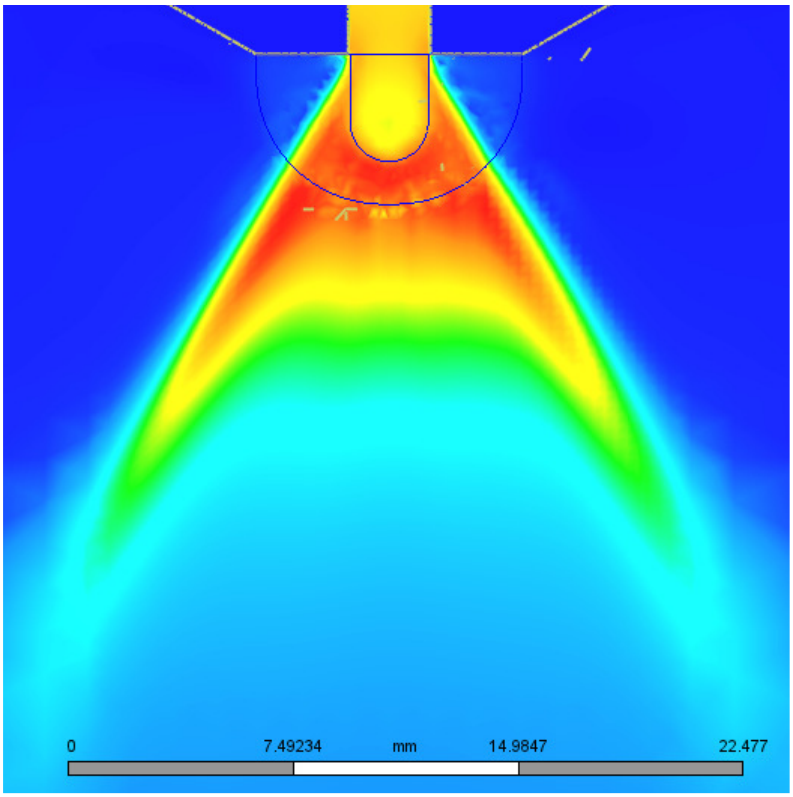

Figure 29: Velocity profile viewed from the front of the spray nozzle. Total length of the scale is approximately 22.5 mm and the velocity range is from 5 mm/s (dark blue) to 9,300 cm/s (red).

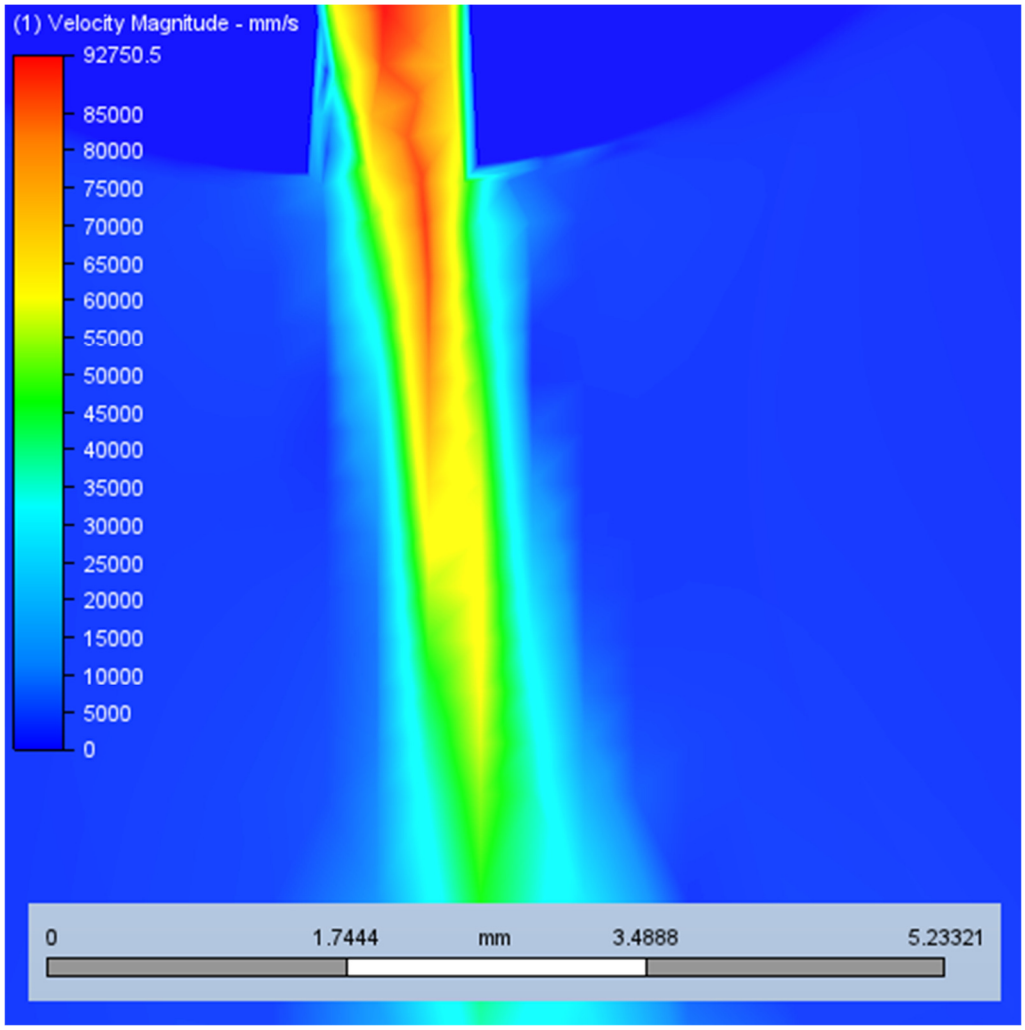

Figure 30: Cross-sectional side view of high velocity air exiting flat fan spray nozzle.

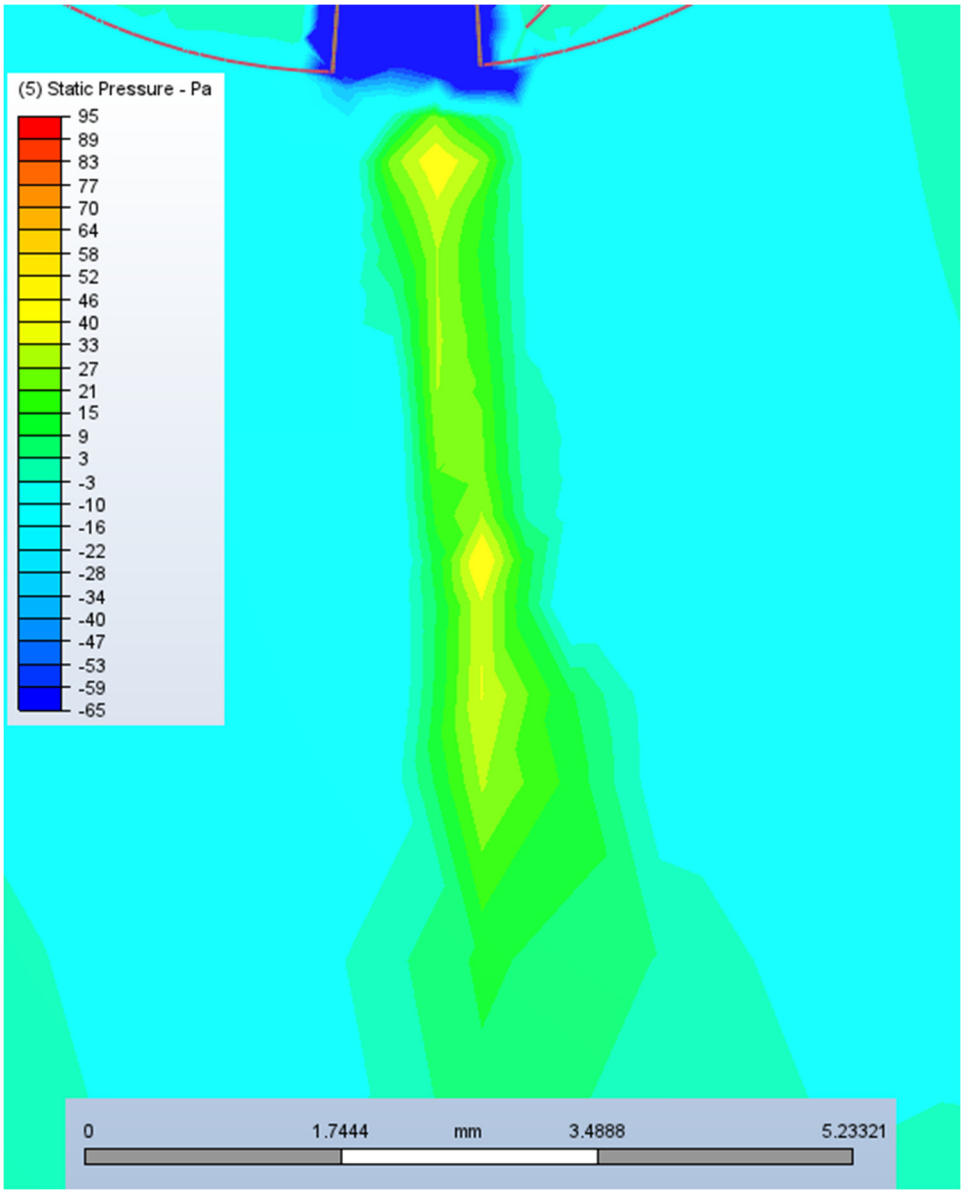

Figure 31: Cross-sectional side view of the low static pressure regions shown in cyan that are generated by the high velocity air in Figure 30.

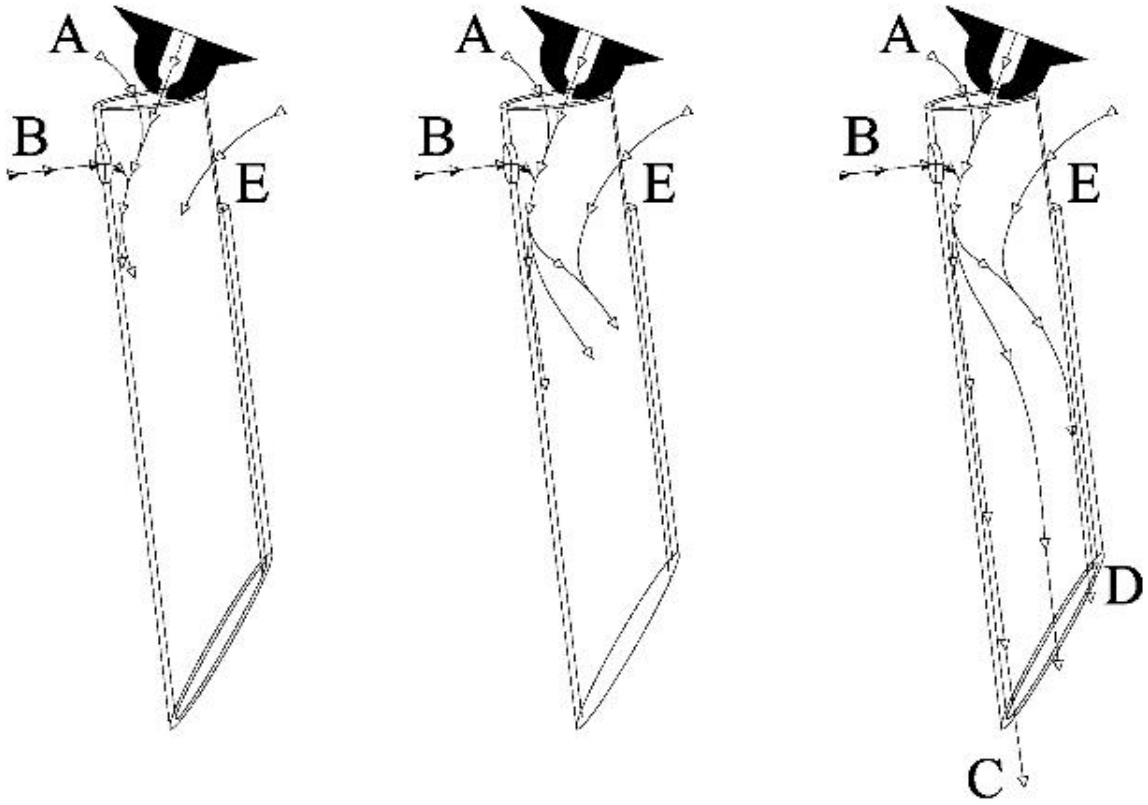

Figure 32: Depiction of air currents within the modified collection cylinder when using a flat fan spray nozzle. Note the ambient air being drawn into the cylinder at 'E' in the third frame.

Figure 33: Flame test of the modified collection cylinder using compressed air at 25 psig and discharging into the ambient environment at 0 psig.

Those tended to reduce the suction intensity near the sample inlet. There are undoubtedly different shapes and sizes of cuts that can alleviate the detrimental axial recirculation while maintaining sufficient suction force on the sample inlet. However, the modeling eventually described one candidate vent option that proved sufficient.

To further address the tendency of axial recirculation to allow remixing of the dissolved rare earth elements, it was decided to try modifying the flat fan profile of the spray nozzle into a half-cone spray pattern. The idealized concept was to try a nozzle that develops a flat fan spray pattern on one side of the nozzle, and a full cone pattern on the other half.

Numerous experimental modifications to a nozzle tip originally manufactured to produce a flat fan spray pattern gradually led to the ability to generate the desired half-cone spray pattern. This modified nozzle developed counter rotating air currents on only one side of the flat fan airflow.

Figure 34 shows CFD computational results of the velocity field established by the modified spray nozzle tip when set to discharge into an open ambient environment. Superimposed on the vector field are thin blue lines depicting selected features of the spray nozzle geometry. These include the modified nozzle tip shape (both the modified and unmodified sides) and the nozzle outer diameter. Also shown is the nozzle base, which is not important for the fluid dynamic results. These features of the nozzle are denoted in the figure.

Figure 35 shows a zoomed in image of the left side of the velocity field shown in Figure 34. In this figure, the arrows demonstrate the three-dimensional vector velocity field. As can be seen in the figure, a vortex is generated at the outer edge of the spray pattern. Examination of this result also shows the upward component of the velocity produced in the vortex region.

The data in Figure 36 are very similar to those given in Figure 35, but the vectors are two-dimensional. Also, a red line representing a sample section of the velocity field is shown. The two-dimensional velocity magnitude plot across the red line is given in Figure 37. The data given in Figure 37 using an origin that starts with the midline (plane of symmetry of the nozzle).

It was shown that the rotational energy developed in the collection cylinder could be further increased by angling the spray nozzle tip relative to the collection cylinder to direct the atomized dilute nitric acid onto the curved interior surface of the cylinder rather than parallel to it.

These modifications resulted in reduced pressure losses on the back side (opposite the injection side) of the flat fan air flow. Figure 38 shows CFD predictions of these counter rotating air currents as a vector field. The results shown in Figure 38 represent the fluid flow in the collection cylinder over a cross-section of the cylinder. The axial location of the vector field shown in the figure is located approximately 2 cm downstream of the spray nozzle tip.

Figure 38 demonstrates that the turbulent air flow wraps completely around the interior cylinder surface and then forms two miniature vortices near the back side of the cylinder. Two other miniature vortices help mix the collected aerosols with the water droplets within the spray.

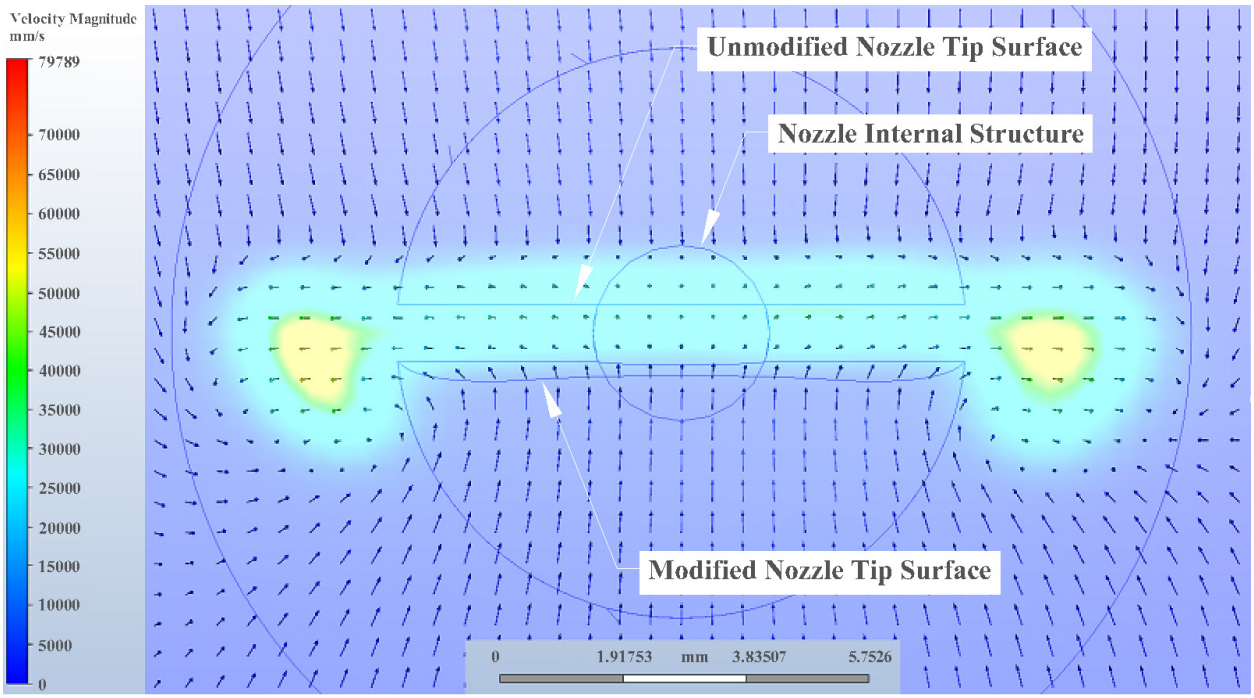

Figure 34: 3D vector flow field showing the rotating air currents produced by the modified spray nozzle in an open ambient environment. Note that velocity magnitude is indicated by color only and not the length of each vector.

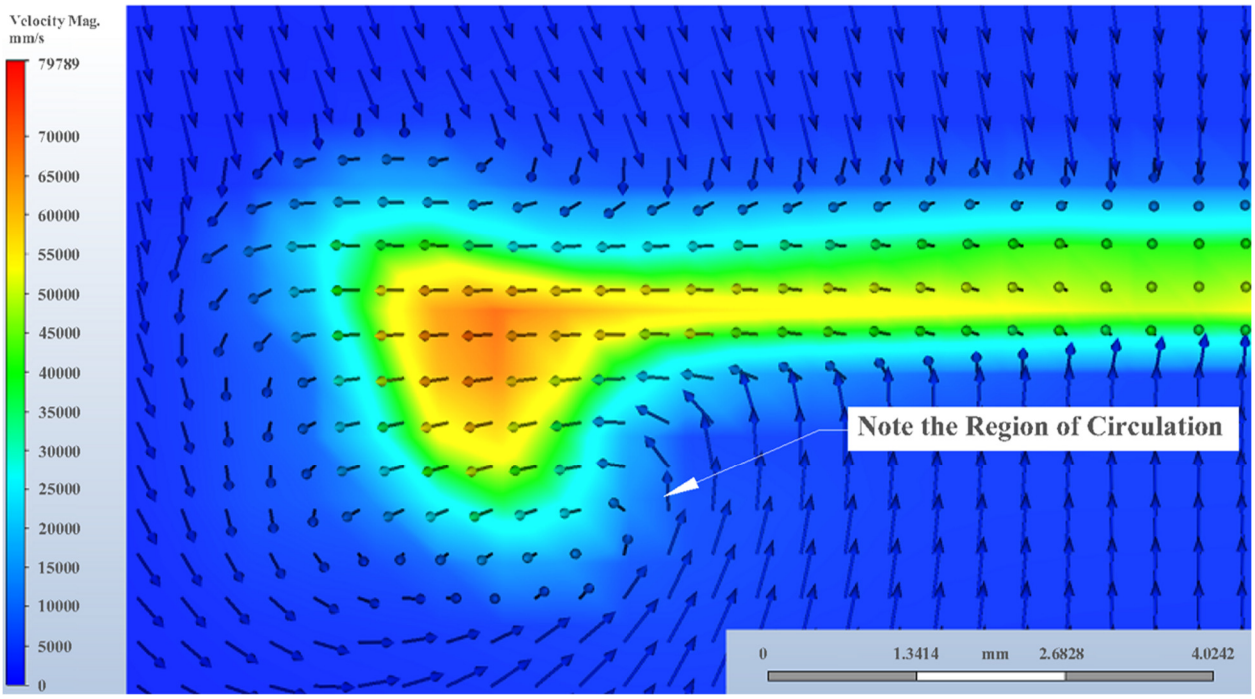

Figure 35: 3D vector flow field located 1.9 mm downstream of the modified spray nozzle tip. Velocity magnitude indicated by color, not the length of each vector.

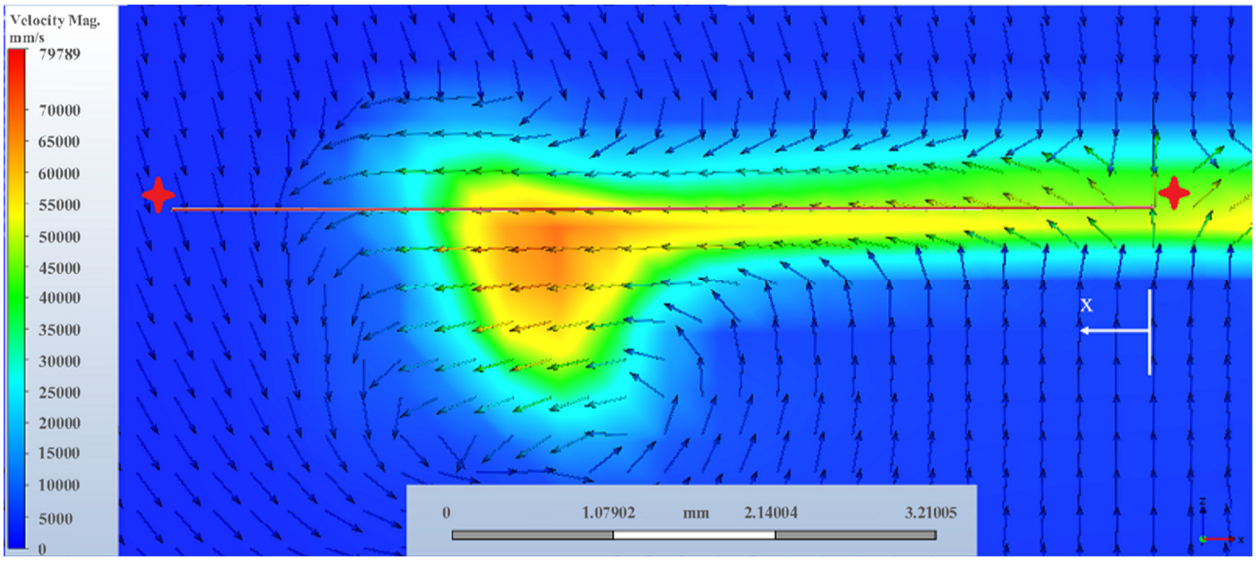

Figure 36: 2D vector flow field 2 mm downstream of modified spray nozzle tip. The red line marks the location of the velocity magnitude data points ploted in the following figure while the white origin indicates the midline of the spray nozzle tip. Note that the velocity magnitude is indicated by color, not the length of each vector.

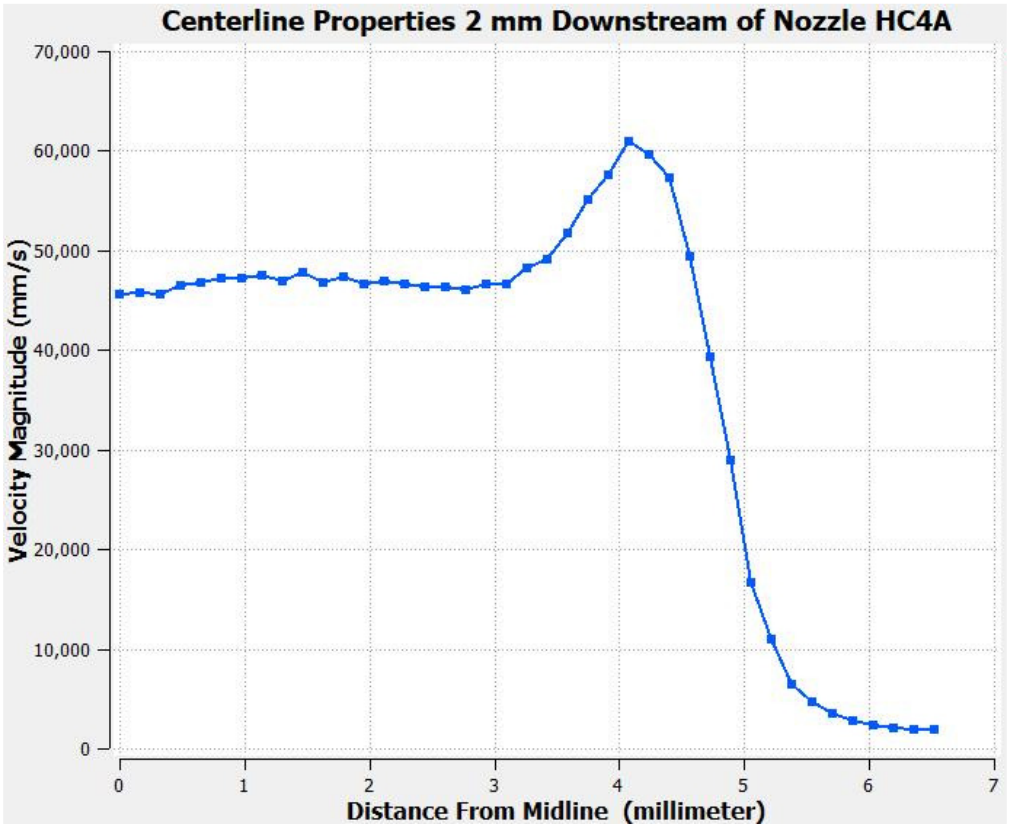

Figure 37: Velocity magnitude along the red line in Figure 36. Note, the origin is at the midpoint of nozzle tip.

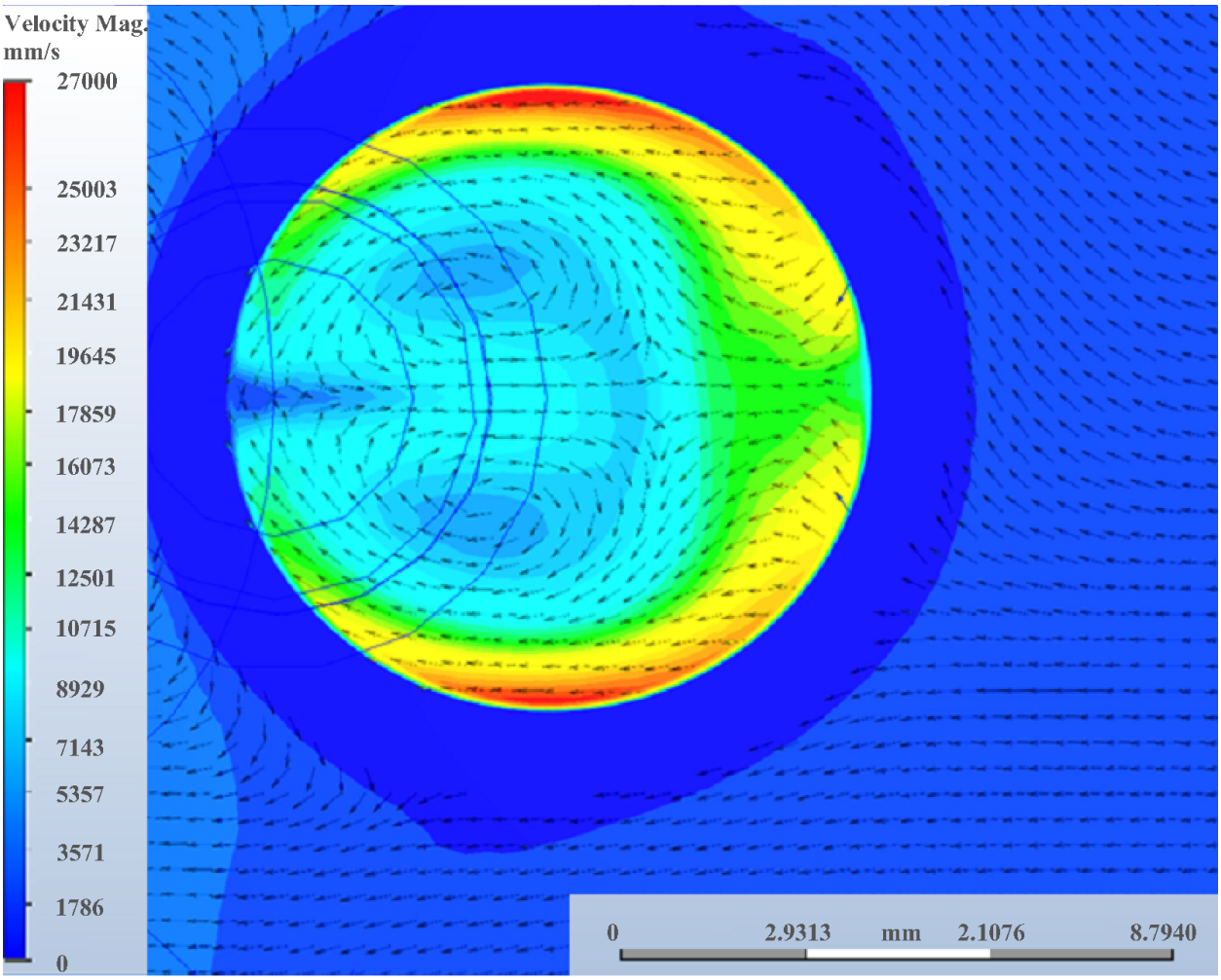

Figure 38: Horizontal vector flow field showing two contra rotating vortices in the collection cylinder that constantly wash the interior surfaces. Velocity scale is 0 (dark blue) to 2,700 cm/s (red).

Rotating jets of air also collide under the sample inlet port and produce a small but important upwards motion. This upward motion keeps the lower inlet lip free of aerosols that might otherwise collect on the surface and cause subsequent isobaric interferences. An added benefit from the modified flat fan spray nozzle tip is that the rotating columns of air continuously wash the interior surface of the collection column. The moving air forces the water droplets into a circular motion as they descend inside the collection cylinder.

The nozzle modifications used to change the flat fan spray pattern into a half cone pattern were accomplished by machining irregularities into the surface of the flat fan spray nozzle. These are depicted in Figure 39 and Figure 40. Figure 41 shows the spray nozzle and collection column.

5.5 Buoyant Aerosols

A mixture of water and glycerin, when heated, produce a non-toxic buoyant aerosol, commonly used to generate smoke for special effects. In this testing, a propane torch was used to provide the heat in making the subject aerosols buoyant. Approximately 1 mL of glycerin was mixed with 1 mL of tap water in a small steel tin and vigorously heated.

A small opening near the edge of the tin allowed the aerosols to escape in a controlled manner, as shown in Figure 42. The flat fan spray nozzle was then magnetically attached to a steel box and charged with 20 PSIG air. To provide better visibility, a stainless-steel collection tube was held under the nozzle with a pair of pliers rather than with the PVC holder. The heated tin was then placed in proximity to the collection tube. Figure 43 and Figure 44 show this process with a small tin and then with a larger tin for better visualization.

5.6 Importance of Consistent Water Supply

During normal operations, deionized water or a dilute nitric acid solution of a few percent is withdrawn from a storage container and fed into the spray nozzle. The spray nozzle creates a suction effect proportional in strength to the air flow rate passing through the nozzle. This suction can typically raise water several vertical feet inside a 1/4 inch inside diameter polyethylene hose.

However, the placement of the hose and any changes to the liquid level in the feed water container cause statistically significant changes to the mass flow rate collected by the rare earth separations instrument. These changes are not linear, and if not kept under control might potentially cause the concentration of dissolved rare earth compounds to reach damaging levels for the mass spectrometer.

To ensure that varying head pressures in the feed water source do not adversely affect the resulting concentrations of dissolved aerosols, some work was done to explore prototypic means of controlling those variations in head pressure in experimental tests. After numerous attempts, a design was ultimately found that reduces the change in flow rate to within approximately 3% by holding the feed hose in a constant position relative to the liquid level.

In a basic feed water container, water withdrawn out of a bottle causes a direct drop in liquid level and a corresponding drop in the pressure head at the spray nozzle. A modification following the

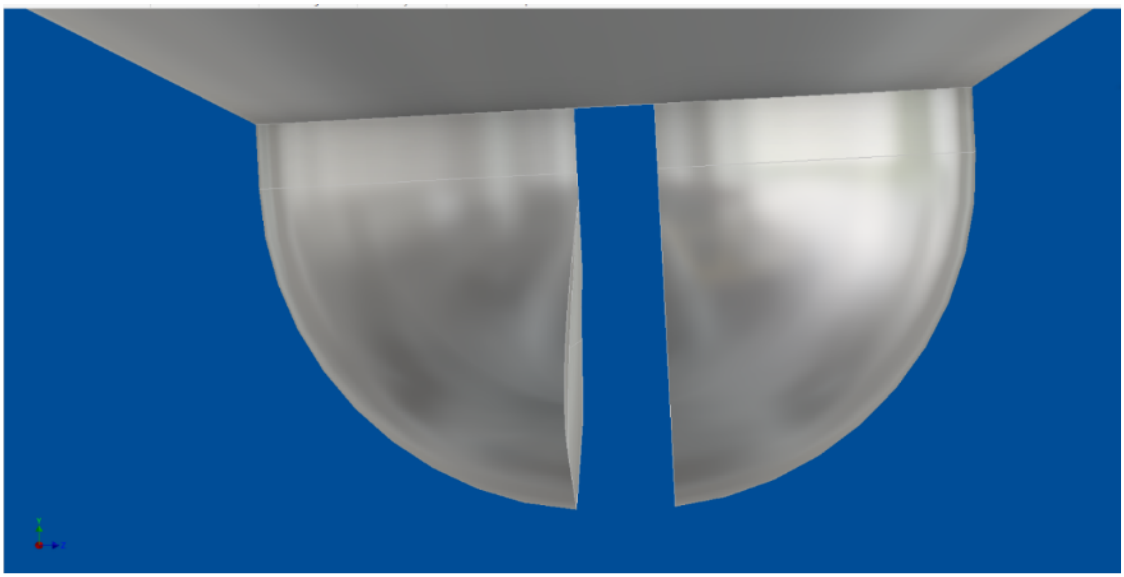

Figure 39: Side view of modified flat fan spray nozzle.

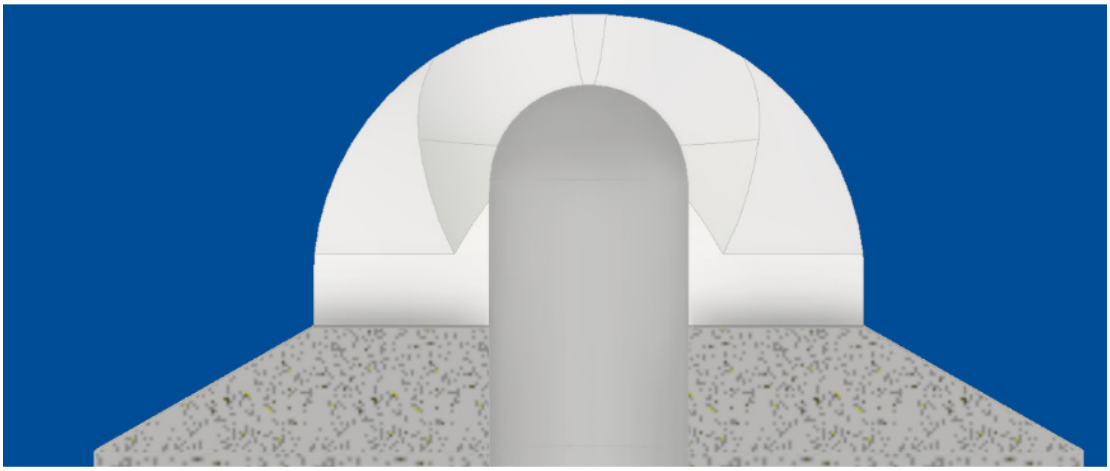

Figure 40: Section view of indentations machined into spray nozzle tip.

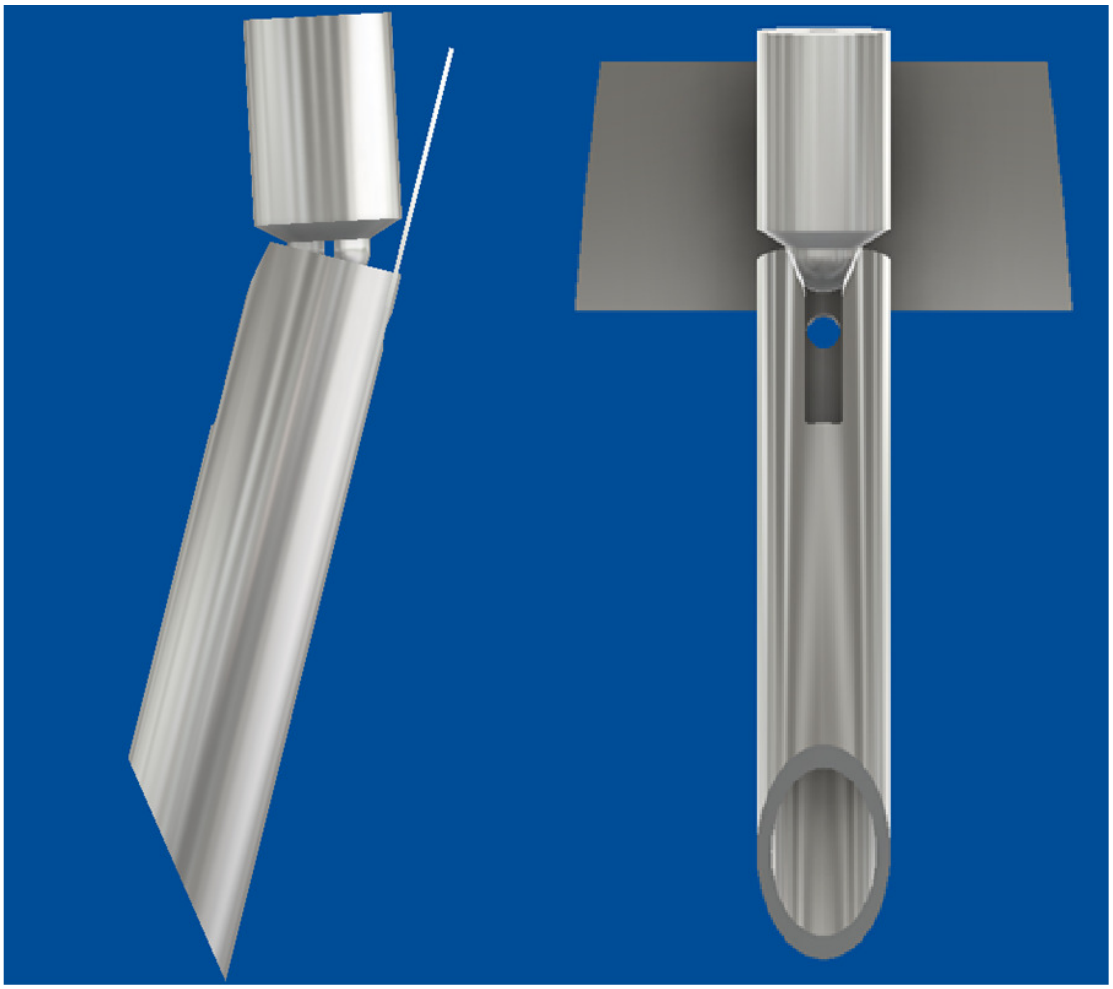

Figure 41: Side and back view of the modeled spray nozzle, collection column, and thermal air deflector.

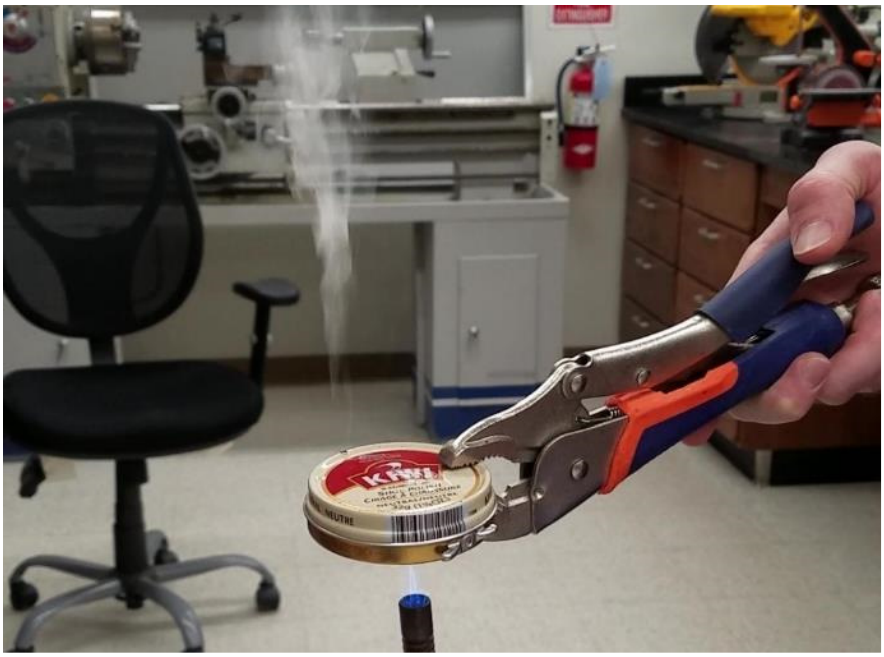

Figure 42: Buoyant aerosols from heated mixture of glycerin and water.

Figure 43: Special effects smoke being drawn into the stainless-steel collection tube. Note the column of smoke being expelled in the background.

Figure 44: Buoyant smoke aerosols being drawn into the stainless-steel collection column via the low-pressure zone facilitated by the atomizer spray nozzle.

inexpensive, fail-fast design philosophy of this experimental work used a small, secondary, floating bottle that rises as feed water is withdrawn from the supply by the spray system.

The buoyancy of the secondary bottle maintains a nearly constant head pressure for the atomizer nozzle because it keeps the feed water level very consistent, even as fluid is withdrawn from the bottle. The small bottle, approximately 95 mL, in this demonstration, is nestled inside a 2.9 L bottle of feed water and is guided by a sleeve to prevent tipping. This secondary bottle is illustrated in Figure 45. The schematics in Figure 46 show the general overview of the 95 mL and 2.9 L bottles and how the respective fluid levels change during operation. Care must be taken that the level of feed water in the secondary container does not drop below a critical level as demonstrated in panel "E" in Figure 46.

As mentioned, this design results in an approximately 3% change in flow rate between when the 95 mL bottle is full to empty, as measured in the experimental data sets. This percent difference is very close to the ratio of the feed water volume in the primary container to that of the secondary container (3.275%). This result implies that minor changes in the feed water pressure head is the dominate source of flow rate variations.

Consequently, it is likely that a larger ratio difference in the volumes of the primary and secondary containers would further reduce the flow rate variations and could be managed to facilitate an arbitrary threshold of constancy in the feed water pressure head. Additional causes of variations in the flow rate of the feed water could arise from variations in the pressures of the compressed air used to supply the atomizer nozzle.

5.7 Importance of Constant Air Pressure Supply

Compressed air is the primary motive force for the Rare Earth Separations Instrument. Early prototypes of the RESI system experienced fluctuations of feed water pass-through rates in excess of 15% that were due to variations of the pressurized air supplied to the atomizer nozzle. The main source of pressure variations in the compressed air supply were determined to stem from the range of air pressure in the air compressor between the pressure the compressor switches on and the pressure at which it turns off during after charging.

The impact of the static pressure range of the compressor on the performance of the RESI system was isolated and identified using a custom-built air manifold. After the source of the problems were identified, a Matheson FM-1050 rotameter was installed in the pressure circuit between the compressor and the atomizer nozzle.

After installation of the rotameter, the range of air pressures supplied to the spray nozzle could be controlled to vary by no more than 0.3 PSIG. Typical operating air pressures for the RESI system as designed are about 60 PSIG. This pressure is further down-regulated to about 25 PSIG by the rotameter before being sent to the atomizer nozzle. To test the resilience of the rotameter in keeping the supplied air pressures stable, the RESI pressure manifold was connected to a 100PSIG nominal air supply. The final pressure output to the atomizer across compressor cycles after adjustment by the rotameter was observed to still fluctuate by within 0.3 PSIG. A schematic of the complete manifold supply and control system as prototyped in this work is shown in Figure 47.

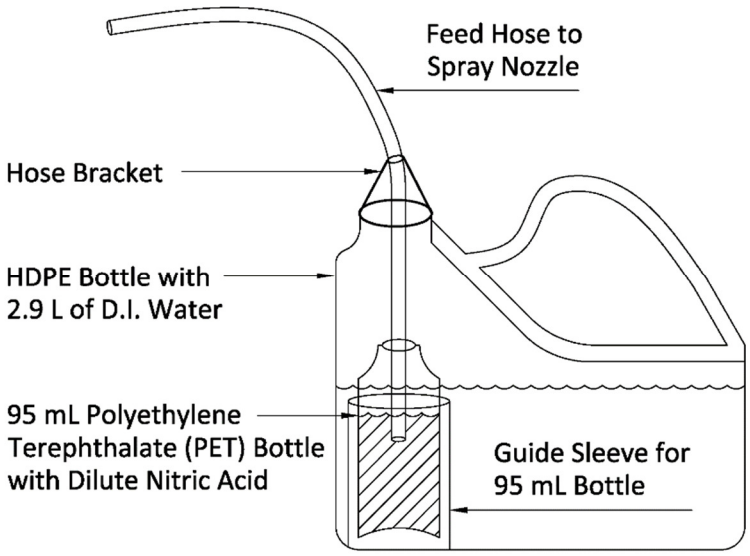

Figure 45: Dilute nitric acid supply bottle with virtually constant pressure head. Note that the hose bracket keeps the feed hose in a fixed position relative to the large storage bottle.

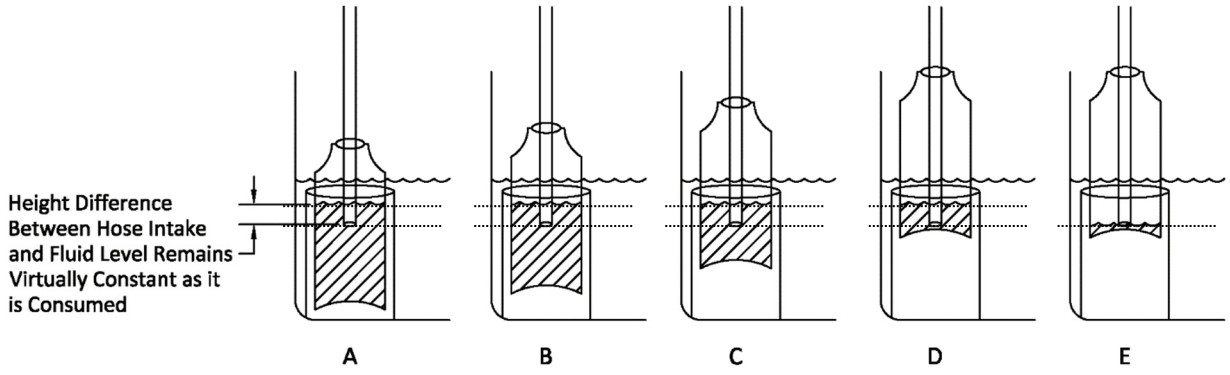

Figure 46: Changing fluid levels in the dilute nitric acid supply system. Panels A through D show how the buoyancy of the small 95 mL generates a nearly constant pressure head on the feed hose. Panel E shows how an experiment running past the intended limits will result in a high variation flow rate and then air ingestion into the feed hose.

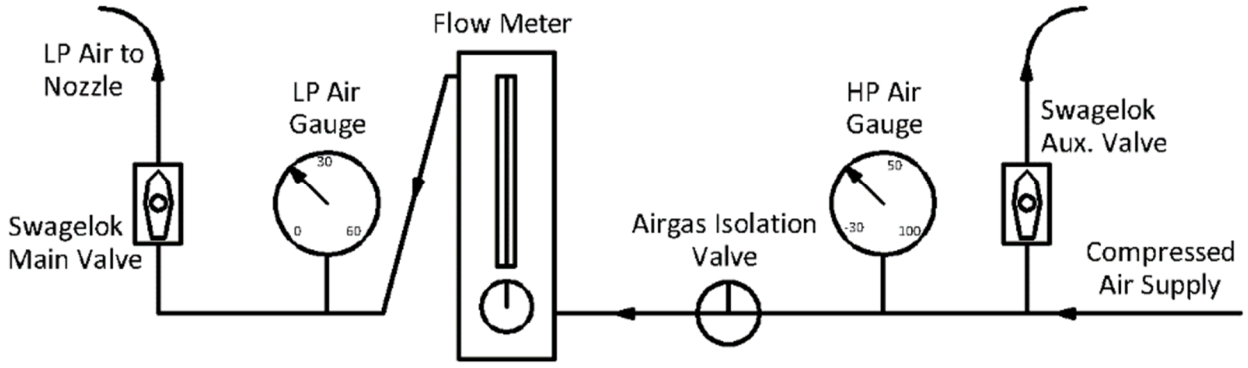

Figure 47: Schematic of the compressed air supply manifold.

The manifold components are a mix of valves and dials with fittings and hoses as needed. The manifold complex was designed and constructed in adherence to the inexpensive fail-fast philosophy implemented throughout this demonstration effort. The manifold base is made from a 19 mm thick Plexiglas base and connected to the top via two half-inch bolts. The top of the manifold stand is 5 mm thick and made from ceramic fiber. A sheet of non-slip shelf liner was placed underneath the base to resist the tendency of the manifold complex to slide across the worktable surface. An added benefit of the non-slip shelf liner was the dampening of transient vibrations occasionally present in the laboratory. Figure 48 shows a photograph of the manifold.

It was noted that the calibration of the Matheson FM-1050 rotameter has a range of 0 to approximately 5.7 liters per minute, which is substantially lower than the minimum rate needed for the Rare Earth Separations Instrument to effectively operate. The minimum volumetric flow rate needed is 8 liters per minute, and optimum system performance occurs near 17 to 22 liters per minute.

Due to the rotameter operating above its calibrated range, a series of volumetric flow rate measurements were performed to ensure that the manifold could produce consistent flow rates from a wide pressure range in the compressed air supply. These measurements were accomplished by repeatedly investigating the time needed to fill a container having a fixed volume with air supplied through the system.

The primary variables to be considered in the measurements are the air pressure supplied to the manifold, the discharge pressure through the spray nozzle, and the time needed to fill a large container. Each combination of the air pressure supply, outlet air pressure through the nozzle, and elapsed time were repeated five times to achieve a limited estimate of uncertainty for determining the effective stability of the flow rates. The maximum recorded variation in the experiment was 3%. A full table of these results are in Appendix A.

5.8 Mass Flow Rate Adjustments

The atomizer spray nozzle is manufactured with a fine threaded needle valve that controls air and liquid flow through the nozzle. It was observed that the needle valve is prone to slightly shifting and is not well suited for reliably reproducing a specific mass flow rate. To solve this problem, a reference disk was designed and fabricated using a 3D printer. This reference disk allows the user to clamp the valve in a fixed position while simultaneously marking the exact location of the partially open valve position.

Implementation of the reference disk virtually eliminated the sensitives of the RESI system to shock and sudden vibrations that had initially been a significant source of unsteady flow. The reference disk was fabricated with 271 groves equally spaced around the top of the disk. Each groove was 0.5 mm in width and aligned radially so that the gap between each increased as the radius from the center of the disk to a point on the groove increases. The selection of 271 as the design number of grooves was based on the resolution capabilities of the printer.

The valve stem of the flat fan spray nozzle is imbedded in the egg-shaped 3D printed upper disk. A small screw is imbedded near the outer edge of the upper disk and can be turned to adjust the

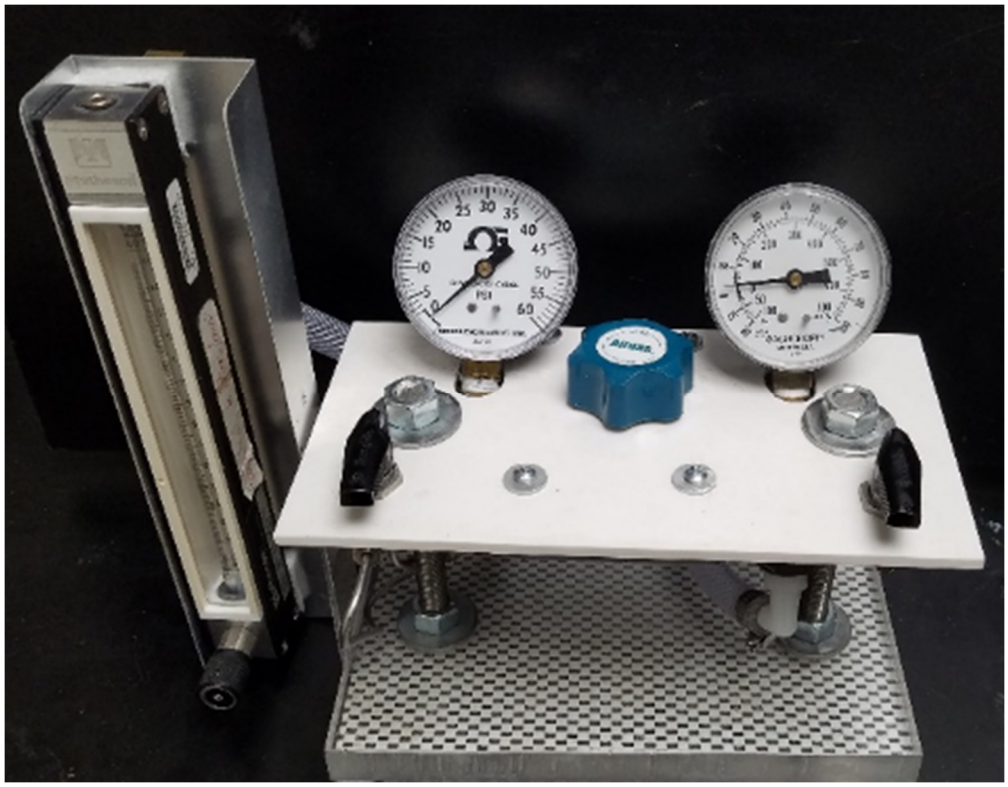

Figure 48: Manifold for Rare Earth Separations Instrument.

height of the screw tip. Adjusting the screw in this fashion allows an operator to either hold the valve stem stationary or allow it to rotate to accommodate opening or closing the spray valve. Figure 49 shows the CAD model of the reference disk, and Figure 50 shows the final configuration.

5.9 Venturi Pumps

Venturi pumping systems are commonly used in hazardous environments due to the absence of moving parts. Pulse jet mixers and reverse flow diverters are two forms of venturi pumping systems widely used in the nuclear industry, particularly with the sampling and transfer of highly radioactive liquids and slurries. Most configurations use a pneumatic jet pump to provide the motive force for both pulse jet mixers and reverse flow diverters.

Pulse jet mixers continually mix storage tanks containing precipitates or slurries whereas reverse flow diverters are used to transfer liquids or slurries from one storage vessel to another. Oscillation in air pressure causes the charge vessel to periodically empty and refill, with the resulting liquid movement producing a mixing action or material transfer within the storage tank. Both systems are widely used in the monitoring and storage of various wastes at the Hanford Site tank farms, Savannah River Site, and other facilities. The general layout for a pneumatic pumping system using a reverse flow diverter is shown in Figure 51 [33][34].

5.10 Reverse Flow Diverters

A reverse flow diverter is a fluid pump with a converging nozzle coaxially aligned with a diverging diffuser separated by a gap as shown in Figure 52. Compressed air is directed through a series of valves and pneumatic jet pumps to alternatingly fill, and then empty, the displacement vessel depicted in Figure 53.

Reverse flow diverters are widely used by British Nuclear Fuel Ltd. at the Sellafield site in Cumbria, England. Their demonstrated reliability in harsh environments, along with no in-cell maintenance, has been the subject of considerable international interest since the 1970s and ultimately led to their introduction at radioactive waste processing facilities in the United States [35][33].

Each pumping cycle begins with a compression pulse and concludes with a suction pulse. The vacuum solenoid opens, allowing pressurized air to enter the vacuum injector and create a low-pressure environment inside the displacement vessel. This draws liquid from the reverse flow diverter nozzle into the displacement vessel and is known as operating in the forward mode as shown in Figure 54.

After reaching the appropriate level, the vacuum solenoid closes while the pressurization solenoid opens. Pressurized air forces liquid out of the displacement vessel and is referred to as operating in reverse flow mode. During which, liquid jets out of the nozzle and into the diffuser. The fluid jet boundary layer undergoes turbulent diffusion, thereby creating a region of low pressure between the two orifices. Creation of this low pressure region is also known as the Venturi effect and is used to draw additional liquid from the storage tank into the diffuser with enough pumping force to create up to 40 feet of pressure head in some applications [35].

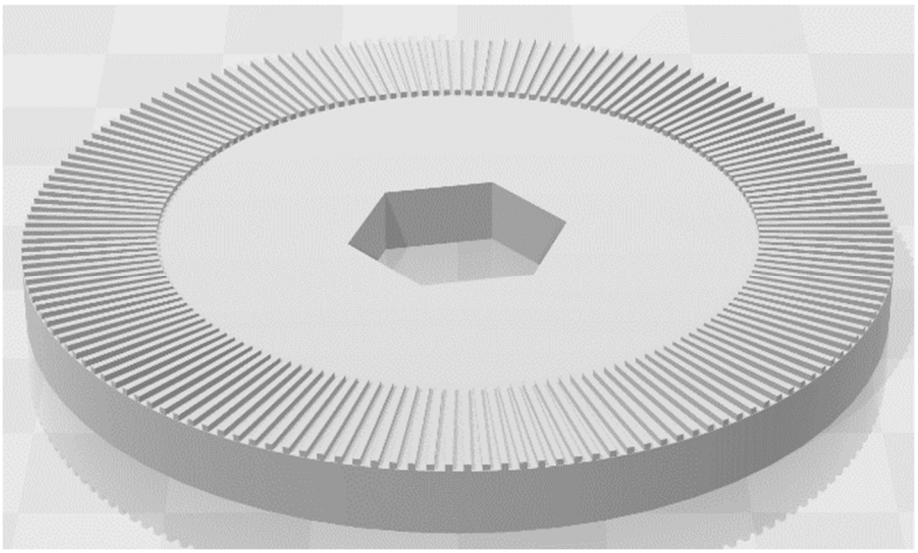

Figure 49: 3D printed base plate with fine grooves to assist with reproducible D.I. water flow control.

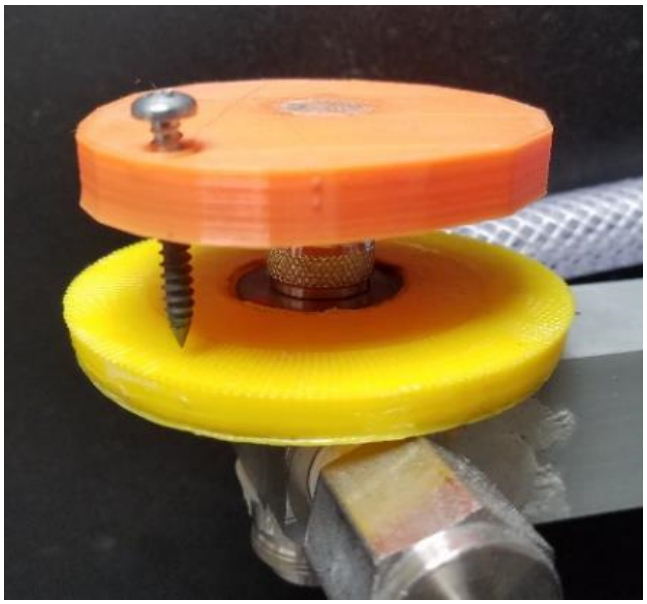

Figure 50: Valve position control for the flat fan spray system.

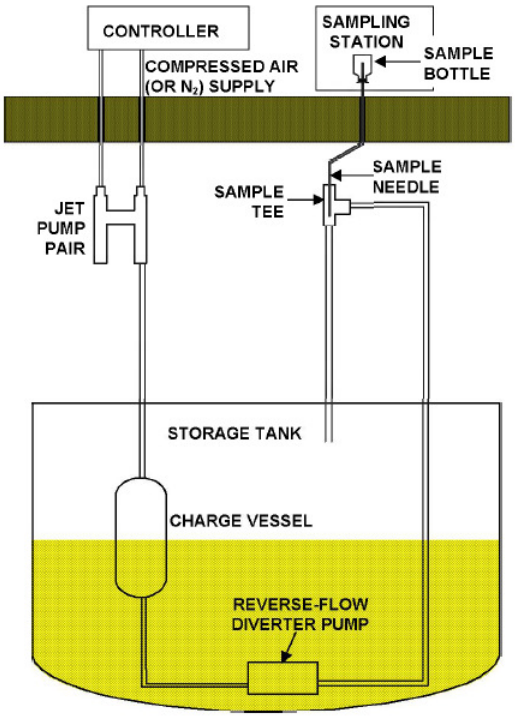

Figure 51: General layout of pneumatically driven flow diverter sampling system[33].

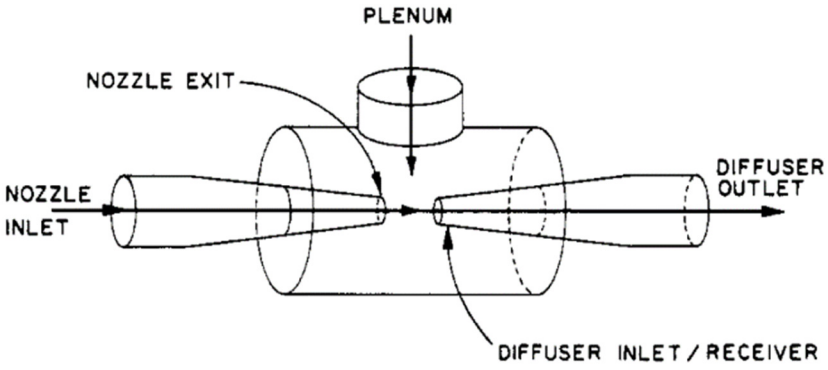

Figure 52: Reverse flow diverter [34].

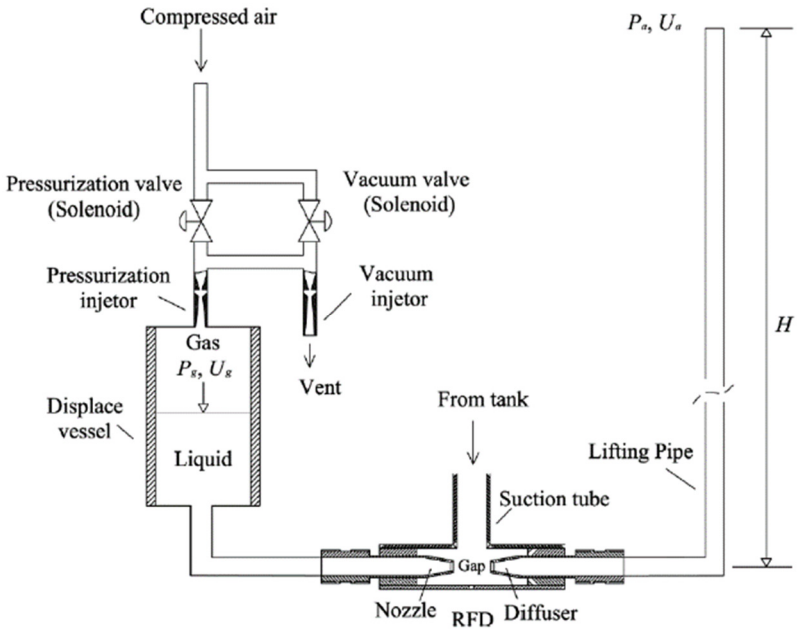

Figure 53: Simplified schematic of a pneumaticly powered reverse flow diverter [36].

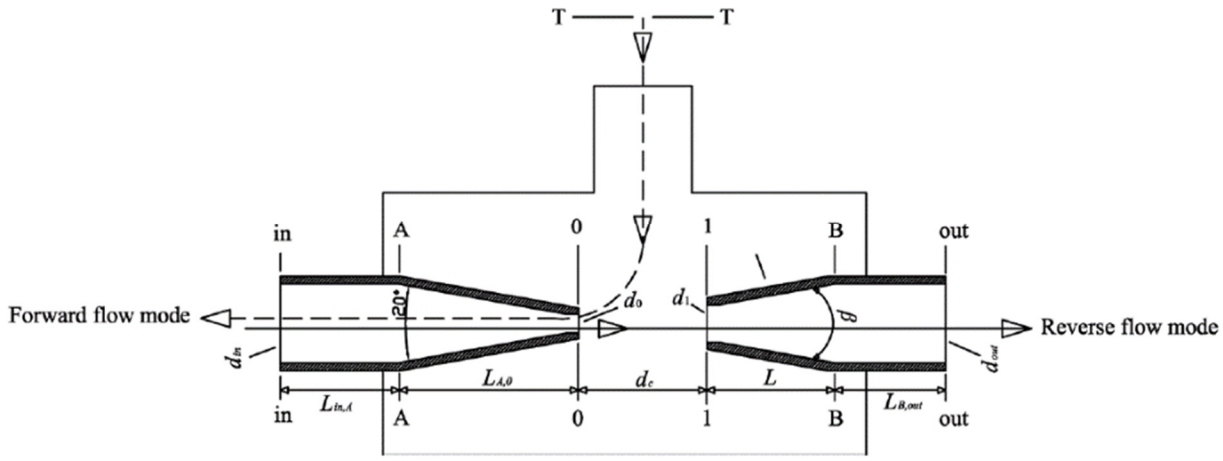

Figure 54: General schematic of a reverse flow diverter [36].

Counce *et al.* and Xu *et al.* noted the importance of the suction gap between the two orifices and ratio of the reverse flow diverter nozzle area to diffuser area [34][36]. Optimizing these design variables as part of the spray system introduced in this chapter proved to be vital.

Chapter 6: Design of Balance of RESI Apparatus

The design of the atomizing spray nozzle modifications and the collection cylinder constituted the majority of the difficult effort for this work. Other aspects of the RESI apparatus such considerations of exhaust gas removal and thermal insulation are also important, but relatively more straight forward. Selected experimentation and feasibility demonstrations of these aspects of the design and testing are given in this chapter.

6.1 Exhaust Gas Removal

To address the possibility of debris from gaseous compounds that exit the bottom of the collection cylinder and become potential sources of subsequent isobaric interferences or radioactive contamination, the Rare Earth Separations Instrument (RESI) was designed to be connected to a fume hood. This connection is facilitated via a snorkel that scrubs any relevant exhaust gases generated by the RESI prior to discharging into the surrounding environment. The vacuum force and exhaust air flow rate provided by the snorkel are sensitive to the number of fittings, length of duct work, and other sources of pressure loss. Vacuum forces can be managed by the capacities and through-puts of a selected vacuum head.

For this work, the vacuum snorkel design and prototype was implemented using the inexpensive, fail-fast philosophy. The vacuum system component of this work was fabricated using glass and PVC fittings. Even with the basic materials used to mockup the prototype vacuum system, experimental testing with the system showed suitability for all tested purposes.

To support the mobile nature of the intended use case of the RESI, attention was given to demonstrating a vacuum system that can be implemented outside a laboratory. For this, a non-fume-hood version of the vacuum system was constructed using a surplus shop vacuum that was adapted to mimic the air flow characteristics of the fume hood snorkel.

Testing of this mobile version of the vacuum system was done in a machine shop. One of the fringe benefits of this implementation was that potential damage to laboratory equipment from fine particulate overspray situations during testing of the spray and rinsing characteristics of the various prototype stages of the collection cylinder could not cause any exposure to sensitive laboratory equipment. Pictures of the adapted shop vacuum and exhaust system are shown below in Figure 56 and Figure 55, respectively. The RESI exhaust duct was designed to fit snuggly into the domed hood of the exhaust snorkel.

6.2 Thermal Insulation

One of the important practical considerations accounted for in this work is the need for the RESI to tolerate the handling of heated materials. The RESI is intended to be used in conjunction with a coated capillary tube as developed in the Hall-Auxier separation method discussed previously.

Prototypes of the RESI system were subjected to thermal testing as described later in this section. To harden the RESI against thermal conditions, thermal insulation was added to enable the PVC and ABS plastic components to withstand elevated temperatures. These material types were

Figure 55: Snorkel exhaust adapter connected to RESI.

Figure 56: Adapted shop vacuum and snorkel exhaust.

selected in this effort in deference to the overall inexpensive fail-fast design philosophy governing the work.

The spray nozzle and apparatus will, in field implementation, be subject to prolonged heating from the intended use case. To demonstrate if the RESI can be appropriately thermally hardened, testing was done using a propane torch. A steel conduit was used to transport heat from the propane torch to the components of interest for testing. Testing with the propane torch was done in excess of the anticipated thermal conditions for the PVC adapter and spray nozzle.

Fiberglass insulation with aluminum backing was used to insulate the PVC components, and a small ceramic tile was fitted to the underside of the spray nozzle. The test continued for approximately 5 minutes, after which the insulation was quickly removed and the PVC examined. The PVC felt slightly warm to the touch but showed no new signs of thermal damage. The spray nozzle was warmer than the PVC components but remained cool enough to touch and handle without the use of gloves. The hose fittings attached to the spray nozzle remained cool to the touch for the duration of the test.

During the thermal testing, compressed air was not supplied to the nozzle, which would be done in normal operation of the RESI. Compressed air moving through the nozzle would serve to cool the nozzle, but the apparatus survived the thermal test even without that cooling effect.

A picture of the thermal test in progress can be seen in Figure 57 and Figure 58. Subsequent designs used mineral wool tiles and Hardie Board instead of fiberglass and ceramic tile to reduce weight and remedy the potential for particulate contamination while still addressing the thermal requirements of the plastic components.

6.3 Practical Mass Flow Rate Measurements

Measurement of the mass flow rate through the spray system was accomplished by magnetically affixing the spray nozzle to the side of a steel box, positioning the aerosol collection column below the spray nozzle at an angle of 80 degrees relative to the worktable surface, then collecting the water as it dripped off the edge of the column. An AWS Gemini series portable milligram scale and timer were used to weigh each water sample. Mass flow rate measurements were conducted in a small room with elevated temperatures and humidity sufficient to reduce the evaporation rate to below detectable levels.

One of the many experiments involved confectioner's sugar injected into the aerosol collection column while the spray nozzle was operating. The water spray removed the airborne particulates and washed them into the sample collection cup while dissolving the sugar crystals. A 5 mL syringe and tubing were used to withdraw samples from the collection cup to simulate the mass spectrometer withdrawing sample liquid. The concentration of dissolved sugar in the withdrawn sample surrogate was analyzed using a refractometer, and the volume of withdrawn liquid was recorded.

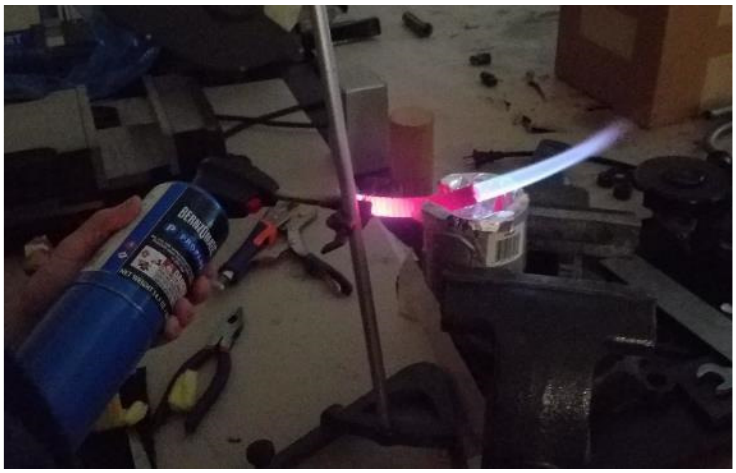

Figure 57: Thermal test of the PVC adapter.

Figure 58: Thermal test of the PVC adapter and spray nozzle.

A series of such samples were withdrawn to estimate the time needed for the sample cup to flush the remaining sugar into the waste stream as shown in Figure 59. The adapted shop vacuum was used to duplicate the exhaust snorkel vacuum system.

6.4 Spray System Proof of Concept Using Sucrose and 0.75mL Reservoir

The spray system efficiency was tested by introducing a sucrose solution sprayed into the collection cylinder using a Freedom 60 subcutaneous infusion pump from CVS Pharmacy, with the output quantified using a Milwaukee MA871 refractometer and Mettler AE163 mass balance. The refractometer was used in this work in lieu of a mass spectrometer because a mass spectrometer was not available.

Consideration was given for impurities in the sucrose, evaporation of the solvent, and measurement uncertainties associated with the available equipment. The experimental configuration utilized a high efficiency spray nozzle and a Matheson rotameter to ensure consistent liquid flow rates.

Two 40 mL sucrose solutions, using food grade sucrose dissolved in deionized water, were prepared with a resulting concentration of 6.0 %w/w. The first was used to flush the sample spray system, which has an internal volume of 5 mL, while the second was used to quantify the overall system performance.

These solutions were tested using the refractometer prior to use. In addition, this initial sucrose concentration was selected to closely correspond to the display accuracy of the refractometer. The initial measurements revealed an error of less than 2% between calculated %w/w values and measured values. A description of the sample preparation process is in Appendix B. This experimental method revealed the need for a substantially larger PVC reservoir, which was subsequently modeled using Autodesk CFD, constructed, and then experimentally tested.

6.5 Spray System Proof of Concept Using Sucrose and 2.0mL Reservoir

Testing the spray system efficiency with the expanded PVC reservoir was accomplished using the same equipment as was used when testing the 0.75 mL reservoir. Sucrose samples were again prepared using the methods described in Appendix B, and continuously sprayed into the sample inlet located on the front face of the collection cylinder.

For this test, sucrose solutions with elevated concentrations of 27.9% w/w were prepared and used. The increased viscosity of the sucrose solutions used here versus those used for the 0.75 mL test, 27.9% versus 6% w/w , reduced the sample spray rate because of the fixed-force operation of the Freedom 60 injection pump and consequently lengthened the experiment duration. Samples of 0.2 mL each were removed from the PVC reservoir at regular intervals using Fisherbrand Sure One micro point pipets. For each sample, the fluid mass was recorded, and the instantaneous sucrose concentration was measured.

The experiment was recorded using an A119 VIOFO camera to provide video documentation of the experiment. The resulting video files were used to identify each time interval between removal of samples from the PVC reservoir. Unless otherwise noted, experimental data recorded was on mass basis and not volumetric basis.

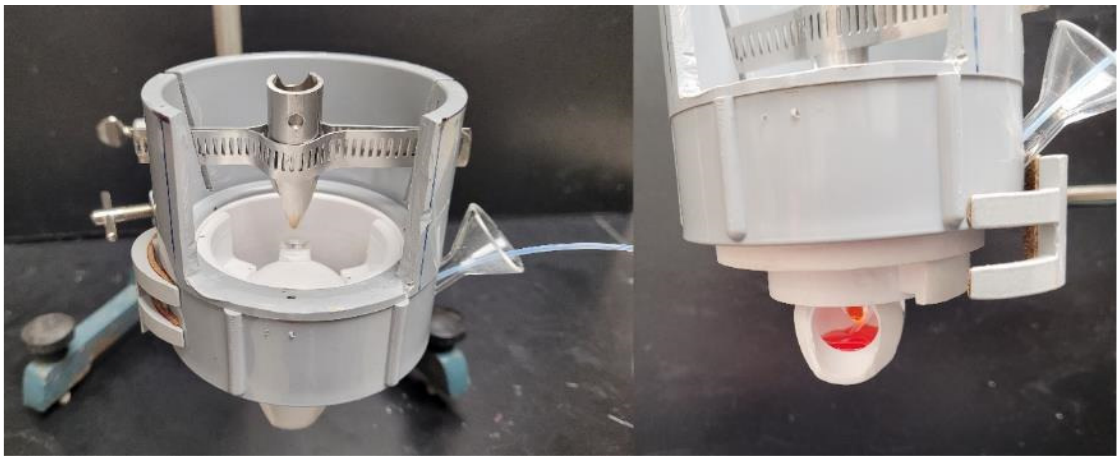

Figure 59: Sample collection apparatus (L), with high contrast surrogate liquid (R). Liquid enters the back of the reservoir and samples are continuously withdrawn via the side port. Reservoir retention capability is slightly more than 0.5 mL of liquid.

Chapter 7: Functional Testing and Characterization of the RESI Apparatus

Early versions of the RESI experienced mass flow rates that had significant variations and inconsistencies that were unexpected. Some variations and inconsistencies were from intuitive causes, while others were not. The most important sources of undesirable variations, in decreasing order of their significance, were:

- Inconsistent air pressure
- Inconsistent water pressure
- Degassing of air in the feed water hose
- Movement of the valve stem seal

These sources of error are identified in the following graphs along with the corrective actions taken. The sequential order of these graphs is newest first and then progressing to the oldest data set.

7.1 Mass Flow Rates for Specific System Configurations

In Figure 60, various features are identified using letters of the alphabet with subsequent descriptions of each feature in the associated paragraphs. The aerosol collection column used for this figure collects approximately two-thirds of the total water consumed and discards the balance as a required limitation of maintaining the chronological sequence of ingested aerosols.

Letter A in Figure 60 shows the steady decline in water flow rate due to the decreasing water level in a common water bottle. As described earlier, decreasing water levels put less head pressure on the hose intake, and results in lower flow rates. This source of error was corrected at letter D in Figure 60 when the system was upgraded to the constant pressure head water bottle previously described.

Letter B in Figure 60 shows the transition from static water pressure to dynamic water pressure when the spray system was directly connected to the building water supply via a utility sink faucet. Static building water pressure is generally at a maximum pressure before the faucet is opened, and steadily drops down to the dynamic water pressure after the faucet is opened. Given that the utility sink was on the ground floor, the severity of this pressure drop was substantial.

Letter C shows a pressure spike and increase in flow rate that occurred when the utility sink valve was first closed. The best theory to explain this is the valve stem moving in the same direction as the initial water flow, thereby adding a pressure transient to the slowly moving downstream flow.

Letter E shows the effects of degassing of dissolved air from water in the feed water hose with the resulting bubbles remaining stationary due to surface tension. Some of these bubbles were dislodged by flicking the feed water hose. This perturbation resulted in free movement of the bubbles out of the hose and removal of the associated pressure loss. The effect result can be seen in the increase in flow rate without any changes to the system settings.

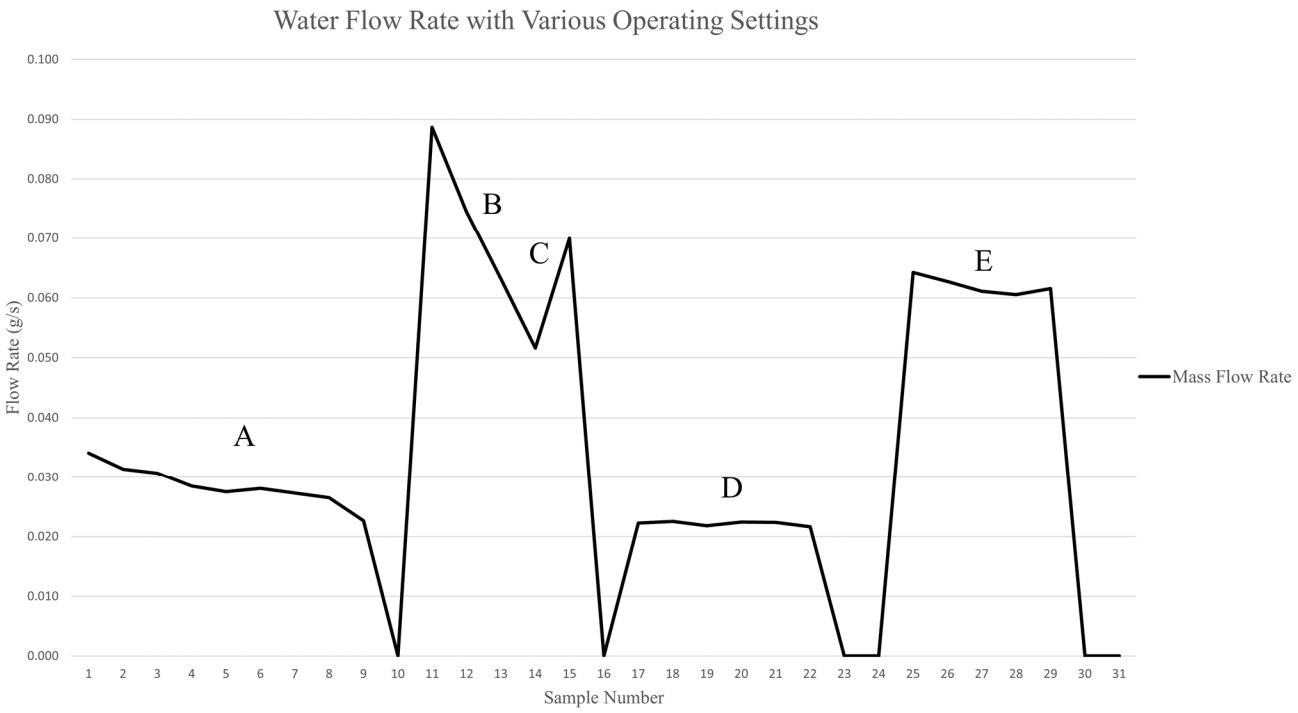

Figure 60: Mass flow rate variations and features.

7.2 Proof of Concept Results with Sucrose

The results show that the spray system efficiency can exceed 85% for samples that are fully dissolved and do not meaningfully change the viscosity of the solvent, in this case deionized water. In the experimental setup, two 40 mL solutions were prepared, each having a concentration of 6.0 %w/w. The first syringe was used to flush in the injection system.

The second experienced a loss of 1 mL due to air entering the injection line while replacing the expended syringe. The injection time for 39 mL of 6 w/w% solution was 97 seconds followed by an additional 30 seconds to allow sufficient time for the spray system to thoroughly rinse the interior of the stainless-steel collection cylinder and PVC recovery sump. The nozzle flow rate was approximately 26 g/minute of deionized water, and the total collection time was 127 seconds. The recovered solution mass was 93.06 g, and repeated Brix measurements indicated 2.3 %w/w of the recovered solution. The recovered mass of sucrose was 93.06 g x 0.023 = 2.14 g. The starting mass of sucrose was 2.34 g, so the recovery efficiency of during the test was 2.14g / 2.34g = 0.91.

A plot of the results is shown in Figure 61, where a 30.1 g solution with 33.1 w/w% was utilized with 0.2 mL of solution removed at each data point and the time stamp recorded after reviewing video of the experiment. With the spray system activated, the steady state concentration in the 2.0 mL PVC reservoir was 27.9 w/w%. The concentration rapidly decreased after the sucrose injection was complete.

The first order of magnitude reduction in concentration required 26 seconds and the second order of magnitude reduction required an additional 27 seconds for a total elapsed time of 53 seconds. The lower detection limit of the refractometer prevented obtaining the time needed for the third order of magnitude reduction in concentration. The time needed for the solution to decrease below detectable levels is 77 seconds.

7.3 Example of Undesirable Sample Retention

A plot of the results is shown in Figure 62, where the injection of 23.9 w/w% sucrose solution was unexpectedly delayed due to a sticky syringe plunger. The full amount of solution was successfully injected at about 6 mL per minute instead of the normal 10 mL per minute and became even slower over the final 40 seconds before completion.

The resulting data plot in Figure 62 shows how a slower injection rate causes the plot shape to broaden while inconsistent release of retained sample material near the end of an experiment can cause the distribution to skew to the right.

7.4 Example of Misaligned Spray Nozzle

A plot of the results is shown in Figure 63, where the injection of 24.6 w/w% sucrose solution was right skewed due to misalignment of the spray nozzle. The misalignment resulted in the back half of the collection cylinder not receiving the needed rinsing action, thereby causing the sucrose solution to remain far longer than intended. The sucrose was eventually rinsed from the back of the collection cylinder. The resulting plot is right skewed and illustrates the importance of the

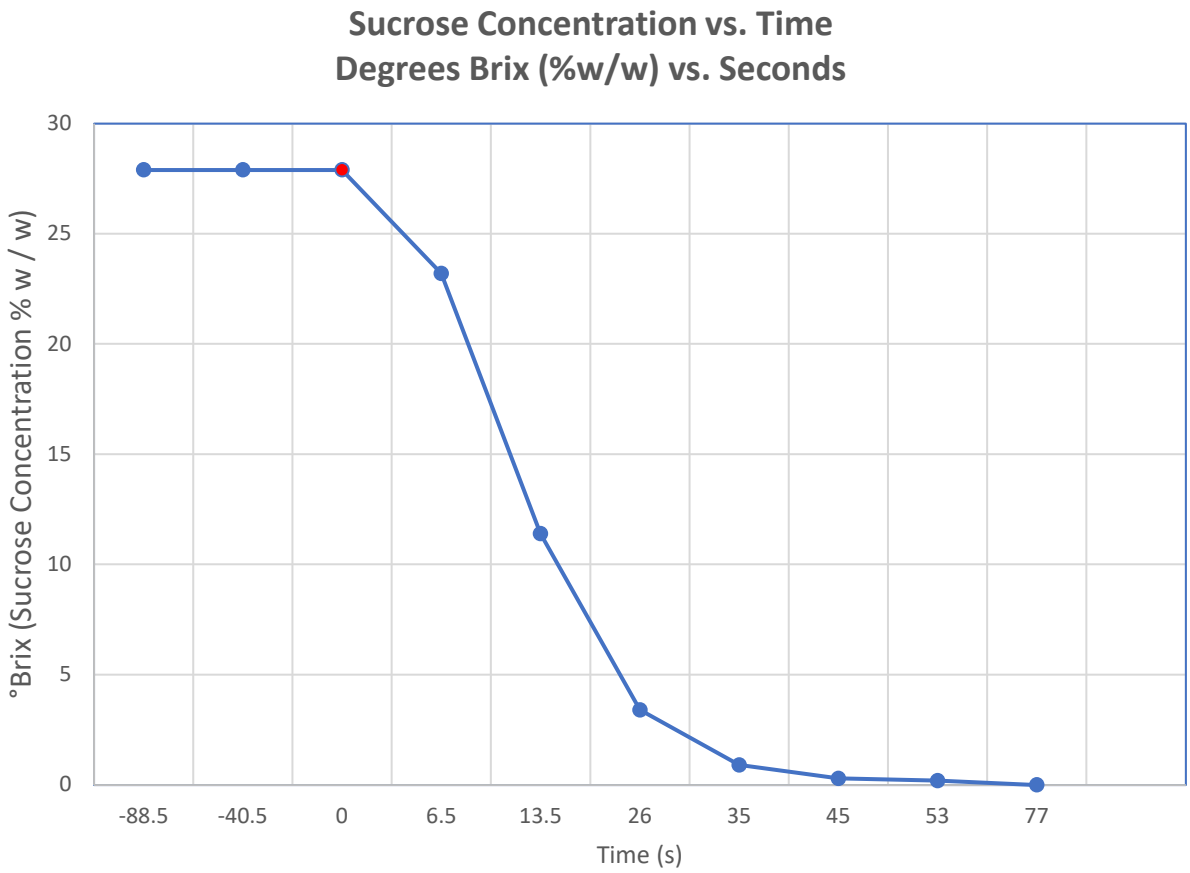

Figure 61: Sucrose concentration in 2 mL reservoir following cessation of injection at Time = 0 seconds.

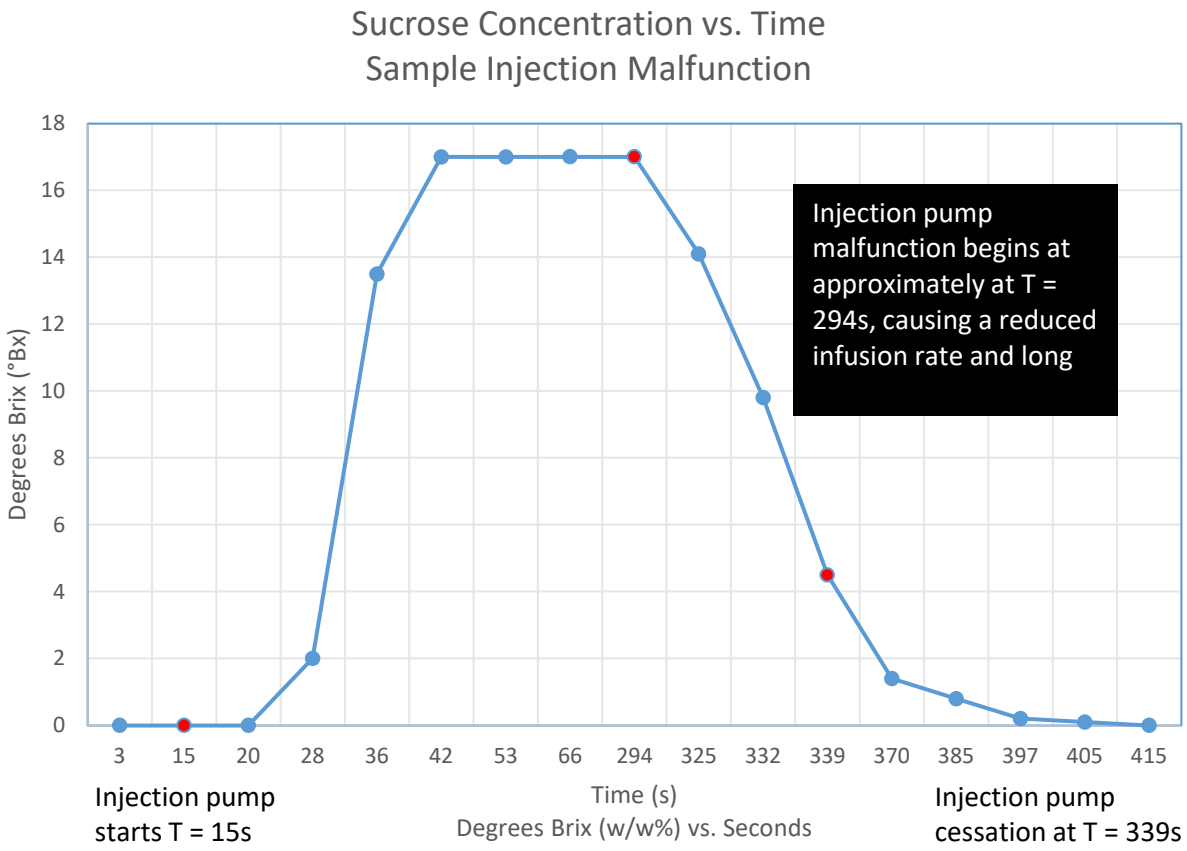

Figure 62: Sucrose injection with reduced output from injection pump beginning at T = 294 seconds with cessation at T = 339 seconds, resulting in the plot being left skewed.

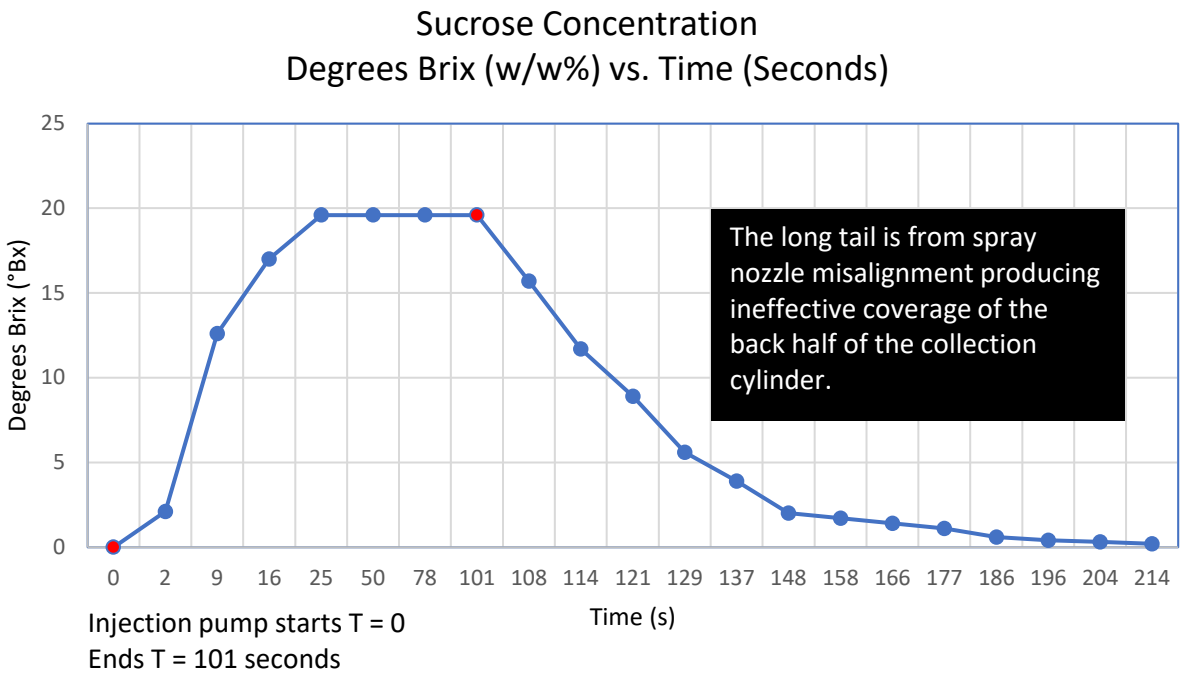

Figure 63: Sucrose injection with misaligned spray nozzle producing ineffective rinsing coverage of the back half of the collection cylinder, resulting in a left skewed plot of concentration versus time.

counter rotating air currents generated by the modified spray nozzle and the rinsing action that they provide.

7.5 RESI Repeatability

Generally, the data shown in the previous datasets in this chapter contain much more information about the concentrations of the surrogate rare earth elements versus time than would be collected by a mass spectrometer. In the intended implementation scenario, the MS would conceptually collect samples withdrawn from the RESI collection pool for some amount of time, for instance 30 seconds, then perform an aggregate analysis on the collected quantity.

To demonstrate the ultimate functionality of the RESI, it is appropriate to measure the percentage of surrogate rare earth elements injected into the device that are ultimately delivered for sampling by the MS. Also, it is appropriate to measure the quality of the rinsing action provided by the atomizer nozzle following each batch of separated rare earth elements delivered to the RESI apparatus in the continuous gaseous stream.

The measurement of these quantities essentially reduces the need for data collection to two main pieces of information rather than the dozen or so shown in the previous characterizations of the RESI apparatus performances.

Several tests were done using the RESI at fixed pressure levels and fixed concentrations of injected sucrose. Aggregate measurements were done on the total amount of dissolved sucrose delivered to the collection pool of the RESI, and a second analysis was done to determine the effectiveness of the rinsing action after each sucrose injection. The results are given next.

7.5.1 Results

A spray rate of 5 mL / minute was used to continuously rinse the collection cylinder. A sucrose solution of 43.5 °Brix was continuously injected into the collection cylinder, which mixed with the rinsing spray. Samples were taken at regular intervals from the mixing reservoir and are shown in Figure 64, where the sucrose injection was terminated at Time = 0. Note that the sucrose concentration in the mixing reservoir was 3.2 °Brix 51 seconds after the sucrose injection was terminated.

The RESI performance criteria calls for a near complete rinsing of sucrose from the collection reservoir between sample runs. In Figure 64, the sucrose concentration was 3.2 at the anticipated start time for a subsequent sample run, which is unacceptably high. To remedy this, a sucrose sample injection was repeated, but with a faster rinsing spray rate.

Figure 65 shows the results from using a 42.9 °Brix sucrose injection and 8 mL / minute rinsing spray rate. Samples were taken from the collection reservoir during the sucrose injection and at regular intervals following the termination of the sucrose injection. The reduction in concentration after 25 seconds of rinsing shows improvement over prior results but still indicates need for additional changes.

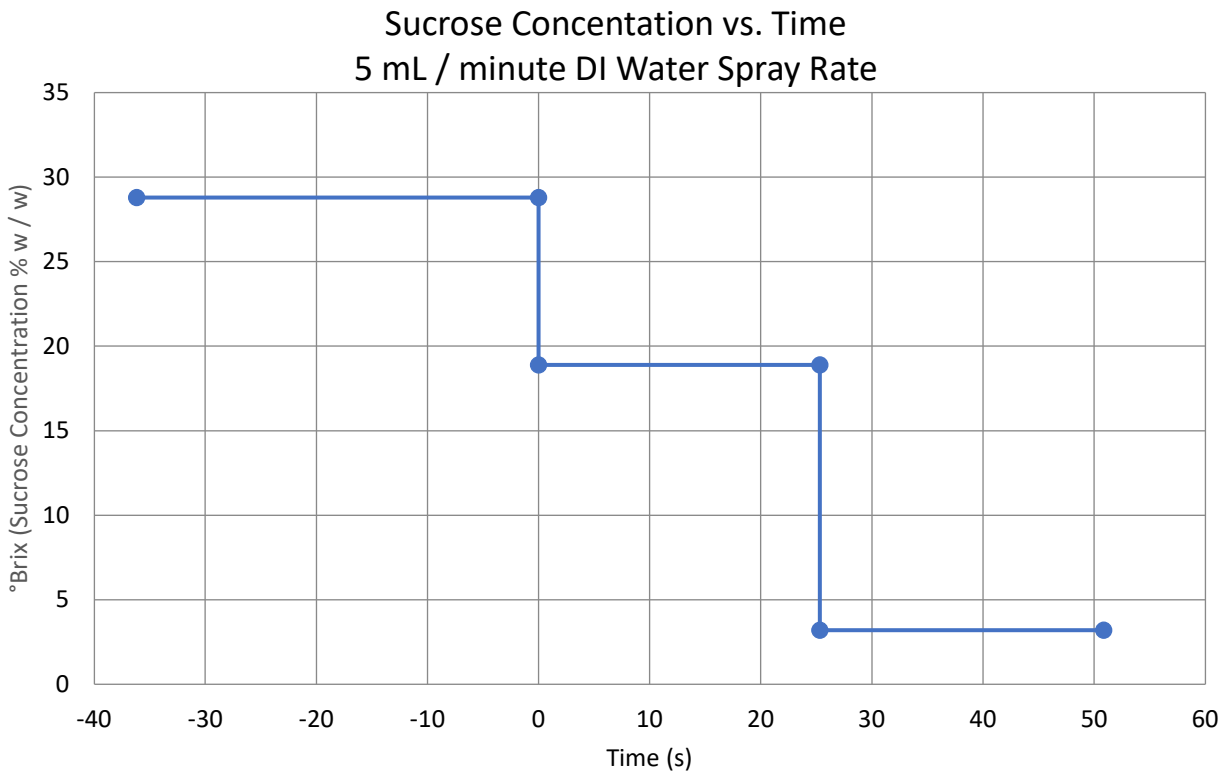

Figure 64: Sucrose injection using 43.5 ˚Brix solution and 5 mL / minute water spray. Sucrose injection ended at Time = 0.

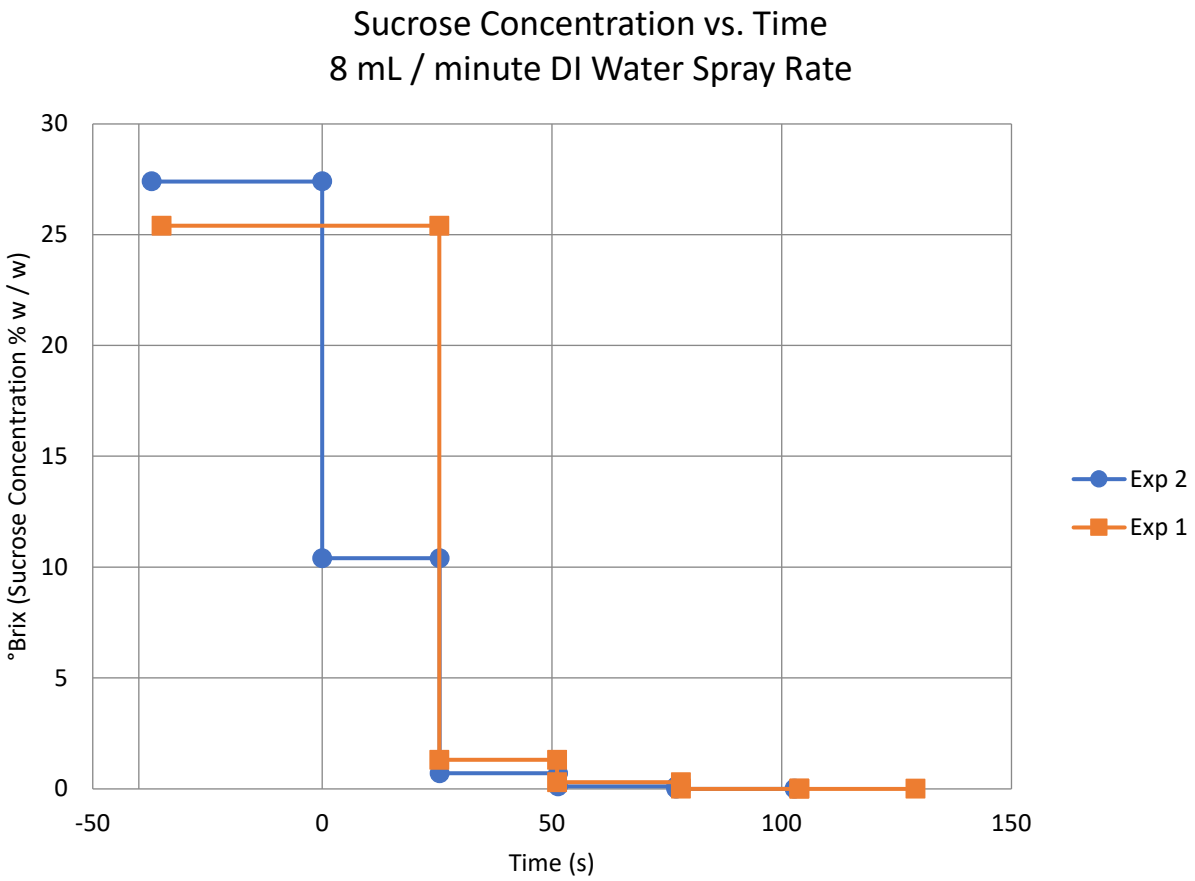

Figure 65: Repeated sucrose injections using 42.9 °Brix solution and 8 mL / minute water spray. Sucrose injection ended at Time = 0

Figure 66 shows the results from using two different DI water flow rates. 8 mL / minute is used during the sucrose injection, followed by a high-speed rinsing action provided by a 32 mL / minute flow rate. This contrasts with the results from using a constant 32 mL / minute DI water spray rate during the sucrose injection and subsequent rinsing stages. The results also show the feasibility of rinsing the collection reservoir within the expected 30 second interval between mass spectrometer runs.

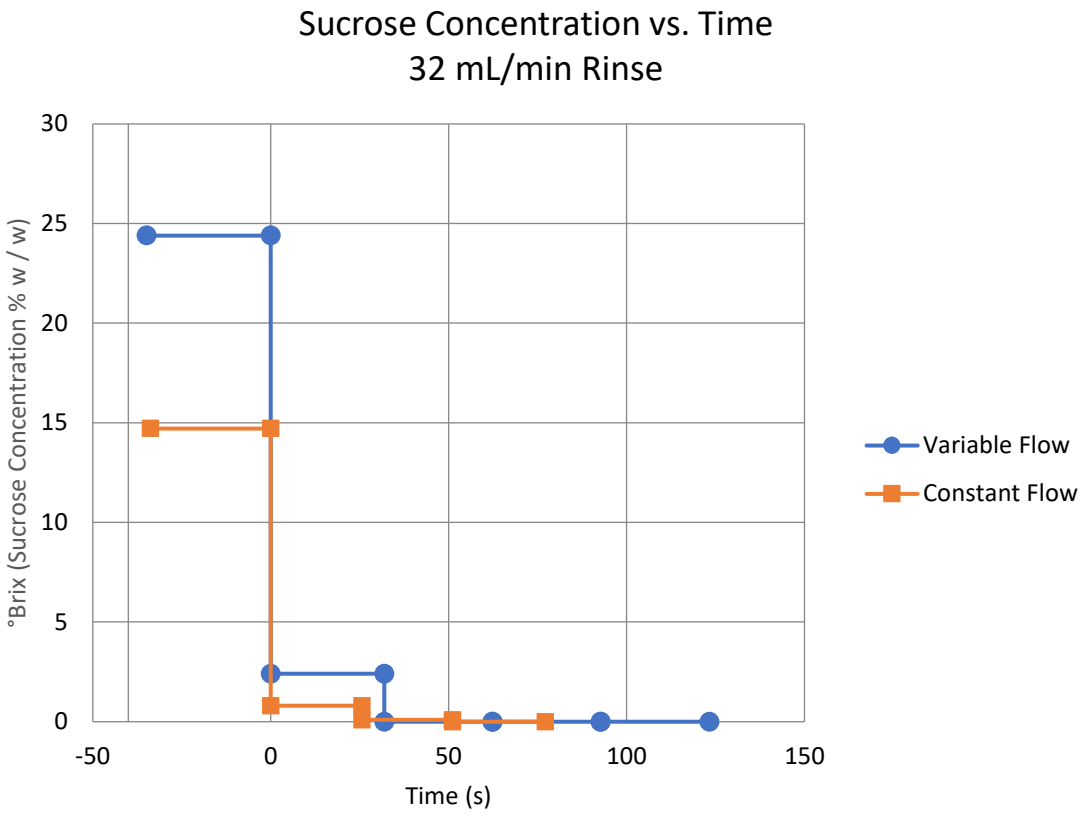

Figure 66: Repeated sucrose injections using 42.9 °Brix solution and variable DI water spray rates. Constant flow of 32 mL / minute DI water spray compared to 8 mL / minute DI water spray during sucrose injection followed by 32 mL / minute rinse rate. Sucrose injection ended at Time = 0

Chapter 8: Research Summary and Next Steps

This work documents the development and demonstration of a prototype collection system intended to continuously collect, dissolve, and discharge rare earth aerosols for isotopic analysis. Notably, this aerosol collection prototype has been optimized for use with gas-phase separation systems to prevent isobaric interferences, thereby shortening the sample preparation time prior to isotopic analysis. This work follows advancements in sample preparation and gas-phase separation methods.

8.1 Research Summary

This effort has demonstrated a key subsystem of an overall concept intended to facilitate improved timeliness of nuclear forensic analyses inspired by developments in gas-phase rare earth element separations methods. In particular, the demonstrated component, called Rare Earth Separations Instrument, or RESI, is designed to accept a continuous stream of rare earth compounds in a gaseous form, dissolve the compounds in dilute nitric acid, and deliver the solute to a mass spectrometer. This replaces time consuming conventional nuclear forensics methods that require liquid-liquid separations methods.

One of the main challenges overcome in this research is the ability to reformat the gaseous stream of separated rare earth compounds into a form suitable for the mass spectrometer without allowing remixing of the rare earth elements. This includes accepting gaseous flow and allowing subsequent separation of carrier gases from dissolved REEs.

Efforts included the basic conceptual design of the RESI, prototypes of each of the RESI sub-components, and functional testing of the assembled apparatus. Throughout the work, prototyping principles of inexpensive, fail-fast methodology were employed. Computational Fluid Dynamics computer modeling was used to inform and otherwise assist the design refinements of the RESI system, and many individual prototype variations were fabricated in the laboratory throughout the design and intermediate testing phases of this work.

The final design of the RESI system was shown to be effective at converting the gaseous form of separated rare earth compound surrogates into a form the mass spectrometer can analyze while keeping separated elements from remixing during the conversion process. The success of the final RESI design suggests that it will be possible to ultimately implement practical equipment that can makes nuclear forensics tasks faster and more efficient.

Beyond the functionality testing of the RESI, practical considerations that demonstrate the ability of the RESI to function in field use have been tested in this work. These tests include tolerance of the RESI to function at high temperature and the ability of the RESI to accommodate the capture and subsequent processing of carrier gases and potential environmental contamination hazards.

In addition to demonstrating a functional practical device relevant to improving nuclear forensics tasks, this work also builds out useful insights into specialized fluid flows supported by modified atomizer nozzles and specialized spray collection devices. Many lessons were learned about essential variables that can contribute to supporting the very specialized flow conditions required by the RESI system.

Many experimental demonstrations of the RESI were done to examine and show the capabilities of the RESI, to characterize the efficiency of the system for delivering the formatted elements of interest to the mass spectrometer, and to demonstrate the ability of the specialized flow patterns facilitated by the RESI to perform continuous rinsing of the internal components.

8.2 Device Summary

As discussed in this dissertation, the RESI uses compressed air and an exhaust removal system as the motive forces of operation. Aerosols injected into the collection cylinder collide with liquid spray droplets provided by a modified atomizing spray nozzle. The droplets readily collect on the interior surface of the collection column before dripping off the tip and into a small reservoir.

The collection system provides continuous spray cleaning of interior surfaces to prevent remixing of separated rare earth compounds prior to downstream isotopic analysis. Thermal insulation protects temperature sensitive components from the coupling oven and capillary column while helping to ensure the gas-phase separations column tip remains hot enough to not clog with condensed deposits. A mass spectrometer or other analysis system withdraws a few mL per minute from the collection pool of the device, while all remaining fluid is continuously flushed out of the pool and into the waste stream. A vacuum system collects and scrubs all waste gases.

8.3 Next Steps

Several next steps are suggested by the results given in this dissertation. These should be undertaken to continue building out infrastructure that can benefit nuclear forensics by adapting new gas-phase separation methods. Some future work should include iterating the RESI design to demonstrate a more robust and precision-engineered prototype.

Items for future work include:

- Perform an engineering design analysis to reduce complexity and variables associated with the demonstrated apparatus

- Iterating the inexpensive, fail-fast prototypes explored in this work toward a more precise system that eliminates some of the engineering variables such as pressure, flow fluctuations, and nozzle alignment that have been shown to be important

- Practical demonstration of the gas-phase separations column suggested in the literature as a feed device for supplying the gaseous stream of separated rare earth element to the RESI

- Demonstration of a complete practical system for implementing the Hall-Auxier methodologies that incorporates a gas-phase separation column, the RESI device, and a mass spectrometer functioning together in real time as a complete solution prototype

- Testing of the RESI, gas-phase separations column, and mass spectrometer system with non-surrogate materials.

Bibliography

[1] D. Hanson, "Synthesis and Thermodynamic Analysis of Volatile Beta-Diketone Complexes of Select Lanthanides via Gas-Phase Separations," University of Tennessee, 2014.

[2] "Public Law 111 - 140." 111th Congress, Washington, DC, pp. 1–6, 2010.

[3] *Daubert et ux., individually and as guardians ad litem for Daubert, et al. v. Merrell Dow Pharmaceuticals, Inc.* 1993, pp. 585–589.

[4] B. Cole, *Federal rules of evidence research*, vol. 8, no. 3–4. 1988, pp. 219–232.

[5] C. Venchiarutti *et al.*, "IRMM-1000a and IRMM-1000b: uranium reference materials certified for the production date based on the 230Th/234U radiochronometer. Part II: certification," *J. Radioanal. Nucl. Chem.*, vol. 308, no. 1, pp. 105–111, 2016.

[6] J. A. Gill, "Rapid Dissolution for Destructive Assay of Nuclear Melt Glass," University of Tennessee, Knoxville, 2015.

[7] A. Vahle, S. Hubener, R. Dressler, and M. Grantz, "Development of an apparatus for seaborgium studies by high temperature gas chromatography," *Nucl. Instruments Methods Phys. Res. A*, vol. 481, pp. 637–645, 2002.

[8] A. Türler *et al.*, "Evidence for relativistic effects in the chemistry of element 104," *J. Alloys Compd.*, vol. 271–273, pp. 287–291, 1998.

[9] D. Makinson, K.R.; Tabor, "© 1964 Nature Publishing Group," *Nature*, vol. 201, pp. 464–466, 1964.

[10] "Thermo Scientific TGA-MS Product Specification Brochure," 2017. [Online]. Available: http://www.equipar.com.mx/web2012/wp-content/uploads/2012/09/TGA-Versatherm.pdf.

[11] "Thermo Scientific TGA-FTIR," 2017. [Online]. Available: https://assets.thermofisher.com/TFS-Assets/CAD/Specification-Sheets/specsheet_TGA-IR_web_2.pdf. [Accessed: 12-May-2017].

[12] I. Langmuir, "The Vapor Pressure of Metallic Tungsten," *Phys. Rev.*, vol. 2, no. 5, pp. 42–45, 1913.

[13] D. M. Price and M. Hawkins, "Calorimetry of two disperse dyes using thermogravimetry," *Thermochim Acta*, vol. 315, pp. 19–24, 1998.

[14] S. Shahbazi, S. A. Stratz, J. D. Auxier, D. E. Hanson, M. L. Marsh, and H. L. Hall, "Characterization and thermogravimetric analysis of lanthanide hexafluoroacetylacetone chelates," *J. Radioanal. Nucl. Chem.*, 2016.

[15] E. B, T. A, and G. HW, "Thermochemical characterization of seaborgium compounds in gas adsorption chromatography," *J Phys Chem A*, vol. 103, pp. 9296 – 9306, 1999.

[16] S. Shahbazi, S. A. Stratz, J. D. Auxier, D. E. Hanson, M. L. Marsh, and H. L. Hall, "Characterization and thermogravimetric analysis of lanthanide hexafluoroacetylacetone chelates," *J. Radioanal. Nucl. Chem.*, vol. 311, no. 1, p. 618, 2017.

[17] B. Gäggeler, H., Dornhöfer, H., Schmidt-Ott, W.D., Greulich, N., Eichler, "Determination of adsorption enthalpies for polonium on surfaces of copper, silver, gold, palladium and platinum," *Radiochim. Acta*, vol. 38, no. 103, 1985.

[18] H. W. Gaggeler *et al.*, "OLGA II, an on-line gas chemistry apparatus for applications in heavy element research," *Nucl. Inst. Methods Phys. Res.*, vol. A309, no. 1–2, pp. 201–208, 1991.

[19] D. C. Hoffman, D. Lee, A. Ghiorso, and M. J. Nurmia, "Fission properties of the 1.5-s spontaneous fission activity produced in bombardment of 248Cm with 18O," *Phys. Rev. C - Nucl. Phys.*, vol. 24, no. 2, 1981.

[20] K. Sümmerer *et al.*, "ROMA—A Rotating Wheel Multidetector Apparatus used in experiments with 254Es as a target," Darmstadt, 1983.

[21] M. Schädel, E. Jäger, E. Schimpf, and W. Brüchle, "Modeling a nielsbohrium (element-107) online gas-phase separation procedure with rhenium," *Radiochim. Acta*, vol. 68, pp. 1–6, 1995.

[22] R. Eichler *et al.*, "Chemical characterization of bohrium (element 107)," *Nature*, vol. 407, no. September, pp. 63–5, 2000.

[23] M. Schadel *et al.*, "Chemical properties of element 106 (seaborgium)," *Nature*, vol. 388, no. 6637, pp. 55–57, 1997.

[24] A. Türler *et al.*, "First measurement of a thermochemical property of a seaborgium compound," *Angew. Chemie - Int. Ed.*, vol. 38, no. 15, pp. 2212–2213, 1999.

[25] A. Türler *et al.*, "On-line gas phase chromatography with chlorides of niobium and hahnium (element 105)," *Radiochim. Acta*, vol. 73, pp. 55–66, 1996.

[26] A. Türler, "Gas phase chemistry experiments with transactinide elements," *Radiochim. Acta*, vol. 72, pp. 7–17, 1996.

[27] Hamamatsu, "Si PIN photodiode." pp. 5971–5974, 2014.

[28] H. Haba *et al.*, "Performance of the gas-jet transport system coupled to the RIKEN gas-filled recoil ion separator GARIS for the 238U (22Ne , 5n) 255No Reaction," *Sci. York*, vol. 9, no. 1, pp. 27–31, 2008.

[29] H. Haba *et al.*, "RIKEN Gas-filled Recoil Ion Separator (GARIS) as a Promising Interface for Superheavy Element Chemistry — Production of Element 104 , 261 Rf , Using the GARIS / Gas-jet System —," *Chem. Soc. Japan*, vol. 38, no. 5, pp. 426–427, 2009.

[30] I. Zvara, "Simulation of thermochromatographic processes by the Monte Carlo method," *Radiochim. Acta*, vol. 38, pp. 95–101, 1985.

[31] S. A. Stratz, "Thermodynamic Characterization and Isothermal Separability of Heavy Fission Product Organometallics for Post-Detonation Nuclear Forensic Analysis," University of Tennessee, 2017.

[32] J. R. Garrison, D. E. Hanson, and H. L. Hall, "Monte Carlo analysis of thermochromatography as a fast separation method for nuclear forensics," *J. Radioanal. Nucl. Chem.*, vol. 291, no. 3, pp. 885–894, 2012.

[33] U.S. Department of Energy, "Innovative Technology Summary Report: Fluidic Sampler," Aiken, SC, 1999.

[34] S. M. Robinson, R. M. Counce, and G. V. Smith, “Performance Characteristics of a Continuous-Flow Fluidic Pump,” *Ind. Eng. Chem. Res.*, vol. 26, no. 8, pp. 1698–1704, 1987.

[35] J. R. Bontha, G. R. Gokar, N. Hannigan, and P. N. Division, “Demonstration and Optimization of BNFL ’ s Pulsed Jet Mixing and RFD Sampling Systems Using NCAW Simulant,” 2000.

[36] C. Xu and S. Jing, “Dimensionless performance and design guidelines for reverse-flow diverters during reverse-flow mode,” *Chem. Eng. Commun.*, vol. 199, no. 7, pp. 912–924, 2012.

[37] Y. A. N. Chunhua, J. I. A. Jiangtao, and L. Chunsheng, “Rare Earth Separation in China,” *Tsinghua Sci. Technol.*, vol. 11, no. 2, pp. 241–247, 2006.

[38] J. Auxier II *et al.*, “Thermodynamic analysis of volatile organometallic fission products,” *J. Radioanal. Nucl. Chem.*, vol. 307, no. 3, pp. 1621–1627, 2015.

[39] B. J. Mincher *et al.*, “The Radiation Chemistry of CMPO: Part 2. Alpha Radiolysis,” *Solvent Extr. Ion Exch.*, vol. 32, no. 2, pp. 167–178, 2014.

[40] M. Nilsson and K. L. Nash, “TALSPEAK Chemistry in Advanced Nuclear Fuel Cycles,” 2008.

[41] S. A. Ansari, P. N. Pathak, V. K. Manchanda, M. Husain, A. K. Prasad, and V. S. Parmar, “N,N,N′,N′-Tetraoctyl Diglycolamide (TODGA): A Promising Extractant for Actinide-Partitioning from High-Level Waste (HLW),” *Solvent Extr. Ion Exch.*, vol. 23, no. 4, pp. 463–479, 2005.

[42] P. Horwitz, “The Science of Radiochemical Separations,” in *Radiobioassay & Radiochemical Measurements*, 2011.

[43] B. J. Mincher, G. Modolo, and S. P. Mezyk, “Review article: The effects of radiation chemistry on solvent extraction 3: A review of actinide and lanthanide extraction,” *Solvent Extr. Ion Exch.*, vol. 27, no. 5–6, pp. 579–606, 2009.

[44] E. P. Horwitz and W. W. Schulz, “The Truex process: A Vital Tool for Disposal of US Defense Nuclear Waste,” *Chem. Tech. Radioact. Waste*, no. Iii, pp. 21–29, 1991.

[45] J. J. Katz and G. T. Seaborg, *The Chemistry of the Actinides and Transactinide Elements*, 4th ed. Springer Science & Business Media, 2010.

[46] J. D. Anderson, *Computational Fluid Dynamics*, 3rd ed. Springer-Verlag Berlin Heidelberg, 2009.

[47] P. Kelly, “Solid Mechanics Part I: An Introduction to Solid Mechanics Lecture Notes,” 2013. [Online]. Available: http://homepages.engineering.auckland.ac.nz/~pkel015/SolidMechanicsBooks/FEM/index.html. [Accessed: 10-Apr-2021].

[48] I. Autodesk, “Finite Element vs. Finite Volume,” 2018. [Online]. Available: https://knowledge.autodesk.com/support/cfd/learn-explore/caas/CloudHelp/cloudhelp/2019/ENU/SimCFD-Learning/files/GUID-12A9AED8-2047-4D3A-BC80-82BE9CF47517-htm.html. [Accessed: 10-Apr-2021].

[49] W. S. Janna, *Introduction to Fluid Mechanics*, 3rd ed. International Thompson Publishing, 1993.

Appendices

Appendix A: Manifold Air Flow

Table 1: Manifold volumetric air flow measurements

Wall Regulator Pressure (PSIG)	Manifold Inlet Pressure (PSIG)	Manifold Outlet Pressure (PSIG)	Measured Time per Run (s)	Air Flow Rates		
				CFM	LPM	GPM
60	60	20	54	0.749	21.22	5.61
60	60	20	54	0.749	21.22	5.61
60	60	20	54	0.749	21.22	5.61
60	60	20	55	0.736	20.84	5.50
60	60	20	54	0.749	21.22	5.61
70	70	20	55	0.736	20.84	5.50
70	70	20	55	0.736	20.84	5.50
70	70	20	54	0.749	21.22	5.61
70	70	20	54	0.749	21.22	5.61
70	70	20	55	0.736	20.84	5.50
50	50	25	46	0.880	24.91	6.58
50	50	25	47	0.861	24.38	6.44
50	50	25	47	0.861	24.38	6.44
50	50	25	47	0.861	24.38	6.44
50	50	25	46	0.880	24.91	6.58
70	70	25	45	0.899	25.47	6.73
70	70	25	46	0.880	24.91	6.58
70	70	25	46	0.880	24.91	6.58
70	70	25	46	0.880	24.91	6.58
70	70	25	45	0.899	25.47	6.73

Appendix B: Sucrose Solution Preparation

Each 40 mL sucrose solution was prepared using food grade sucrose and deionized water. Mass measurements of sucrose and deionized water were recorded using a Mettler AE163 mass balance, which was calibrated a few minutes before the first measurement. The deionized water had an initial resistivity of 1.1 M Ohms, measured using Omega CDH-93 resistivity meter. The purity of sucrose was not tested, but solutions with known concentrations were tested with a Milwaukee MA871 refractometer to quantify deviations between the calculated %w/w of the solutions and measured degrees Brix, or %w/w, caused by impurities in the sucrose.

Prior to use the refractometer was calibrated using steam distilled water provided by the manufacturer. Also, initial sucrose concentrations were identified that would best coincide with the display accuracy of the refractometer. These initial measurements revealed an error of less than 2% between calculated %w/w values and measured values caused by sucrose impurities.

Mixing of the sucrose and deionized water was accomplished using a small PTFE coated stir bar placed in the respective mixing beakers and agitated for 240 seconds using a Thermolyne Stir-Light, model SL-7225 shown below in Figure 67. The weight of each borosilicate beaker was recorded prior to the introduction of sucrose and deionized water, and then again immediately after mixing. Each solution was then immediately placed in a BD (Becton, Dickson, and Company) 60mL syringe with a Luer-Lok™ tip to minimize evaporation of the solvent. The remaining mass of solution in the 50mL borosilicate beaker was also recorded.

Figure 67: Thermolyne Stir-Light, model SL-7225.

Appendix C: Liquid Phase Separations

The purification and separation processes used to handle elements relevant to nuclear forensics often involve the use of liquid phase chemistry, which is inefficient and expensive compared to potential gas phase separation methods. One of the formerly common liquid phase separation methods used for large scale applications is counter-current extraction[37], where a sample is dissolved in an acidic solution and processed through a series of columns counter to the flow of an immiscible organic solvent.

The composition of the organic solvent and precise control of the aqueous solution pH determines which of the dissolved constituents transfer from the aqueous solution to the organic solvent. A series of columns is often used to maximize the transfer between fluids, hereafter referred to as phases. To maximize economic return on investment, the used organic phase is reconditioned by scrubbing unwanted solutes from the solution, stripping the analytes of interest, and then purification via ionic adsorption. Traditionally, counter-current solvent extraction is utilized on an automated continuous basis with the frequent use of organic phase modifiers tailored for specific applications. Counter-current extraction is further discussed in section C.1.

At laboratory scales, several liquid separation methods have been successfully examined and applied Non-volatile samples have been traditionally processed using solid-liquid exchange columns or liquid-liquid extraction methods. Separation of rare earth elements from actinides is often done via cation exchange columns, which take advantage of chemical differences between the elements present. In general, separations for nuclear forensic applications occur in the liquid phase due to the low volatility and elevated temperatures associated with gas chromatographs. Liquid phase separations require additional time to complete compared to gas phase separations, but traditionally achieve excellent resolution [38].

C.1 Solvent Extraction

Liquid – Liquid extraction, more commonly known as solvent extraction, was first used on a wide basis by the petroleum industry during the 1930's. Other applications include hydrometallurgical, nuclear, and pharmaceutical industries. This separation method combines two immiscible liquids where one or more solutes transfer from one phase to the other before the two liquids separate. One phase is often an aqueous solution containing the analyte while the other is an organic solvent having a significant affinity for the analyte. The process can be reversed, also known as stripping or back-extraction, by combining the loaded organic solvent with a third immiscible liquid that has a greater affinity for the analyte. In this context, immiscible fluids must be able to rapidly separate after being combined, and greater differences in the densities of the fluids used accelerate the separation process. An important advantage of solvent extraction method is the capability of operating continuously in counter-current mode. In this mode, multiple stages are utilized, resulting in high separation factors and potentially high process rates. The counter-current name is derived from the opposite flow direction between the aqueous solution and the organic solvent. This is depicted in Figure 68.

In Figure 68, the solute(s) awaiting extraction enter the flow diagram at A_{N+1} while the organic solvent enters at O_0. When the respective streams reach the last stage, the solvent is loaded with the analyte(s) of interest at O_N while the raffinate exits at A_1. As a result, the greatest analyte concentration occurs in stage N while the concentration gradient remains relatively stable across

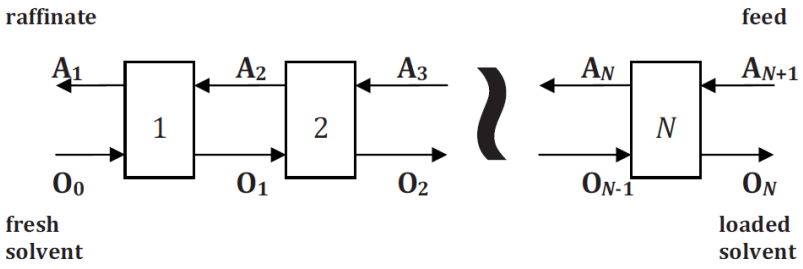

Figure 68: Multistage counter-current flow diagram[32].

the stages. This configuration presumes the solvent will be recycled and reused to improve economic return on investment.

Various reagent groups can be used in solvent extraction of rare earth elements. Some of these include organophosphorus, malonamides, and diglycolamides. Important organophosphorus reagents include octylphenyl-*N,N*-di-isobutylcarbamoylmethylphosphine oxide (CMPO) and di-2-ethyl-hexyl phosphoric acid (HDEHP) [39], which are used in the TRansUranium Extraction (TRUEX) and Trivalent Actinide – Lanthanide Separation by Phosphorus reagent Extraction from Aqueous Komplexes (TALSPEAK) processes, respectively[40]. Other options include malonamides likes dimethyl-dioctyl-hexylethoxymalonamide (DMDOHEMA) and diglycolamides like N,N,N',N'-tetraethyl diglycolamide (TODGA) [41]. Due to repeated use of the solvent, degradation from radiation is a concern.

Other potential causes of degradation include acid hydrolysis and radiolysis, and substantial changes in the solvent composition due to evaporation or solubility in the aqueous phase [42]. Further potential problems include organic solvent and aqueous phase emulsions, which causes reduced efficiency, and buildup of solid deposits at the phase interface, often referred to as crud.

Of these potential problems, radiolysis is perhaps the most significant due to the potential for damaged phases to suddenly (and catastrophically) destabilize. Mincher *et al.* [15] examined the radiolytic yields, commonly denoted with the letter "G" and used to describe the number of ion pairs produced per 100 eV of deposited energy, from CMPO in various solvents and noted that CMPO in octylphenylphosphinic acid achieved the preferred lowest yield, as shown in Table 2 [43]. Solubility of analytes in the organic phase can be increased substantially by the addition of phase modifiers like dodecane and trichloroethylene (TCE).

Generally, alpha and beta radiation from sources at or below 10^{-3}mCi/mL result in negligible effects. From 10^{-3} to 1 mCi/mL the long-term effects of these radiation types are limited to discoloration, and from 1 to 10^{3}mCi/mL, in the radiation effects include decomposition of organics. Above 10^{3}mCi/mL, the radiation causes profound effects in liquid phases [39]. It should be noted that these generalities are based on observations noted during TRUEX work where the numerous isotopes present in solution would have made correlating physical effects to energy deposited per unit volume prohibitive. One of the indicators of radiolysis is the gradual discoloration of liquids. Notwithstanding these disadvantages, solvent extraction provides high selectivity, rapid chemical equilibrium, and is well suited for large scale applications [44].

C.2 Liquid – Solid Ion Exchange

Ion exchange is a process where ions and polar molecules are separated based on their affinity for a stationary resin or phase and is commonly used for organic and inorganic applications. In radiochemistry, one of the most common forms is ion exchange chromatography, where a column is packed with inert beads or granules saturated with a stationary resin. As a liquid phase flows over the resin, analytes are retained on the resin surface while other dissolved substances traverse and exit the column. Subsequent washing of the column bed with a strong acid, often HNO_3, causes

Table 2: Radiolytic yields (No. ion pairs per eV deposited) of CMPO degradation products in various solvents. Table reproduced from Mincher *et al.* [43].

Product	CMPO/TCE	TRUEX / TCE	TRUEX/ dodecane
Octylphenylphosphinic acid	0.013	0.017	0.022
Octylphenylphosphinylacetic acid	not detected	0.029	0.017
Monoisobutyl-CMPO	0.064	0.054	0.061
HDBP	N/A	0.204	0.081

the analytes to elute. One such example is the separation of ^{225}Ac and ^{223}Ra from the parent ^{229}Th. Elution from the column as a function of time is shown in Figure 69 [45].

HCl solution is used to wash any of the initial solution from the column prior to the introduction of HNO_3. After separation is complete, the ^{229}Th is stripped from the column bed by washing with diluted HNO_3. The rapid separations possible in ion-exchange chromatography allow for its use in the search for some of the new transactinide elements with the added benefit that the short duration substantially reduces the potential for radiolysis damage to the resin or column.

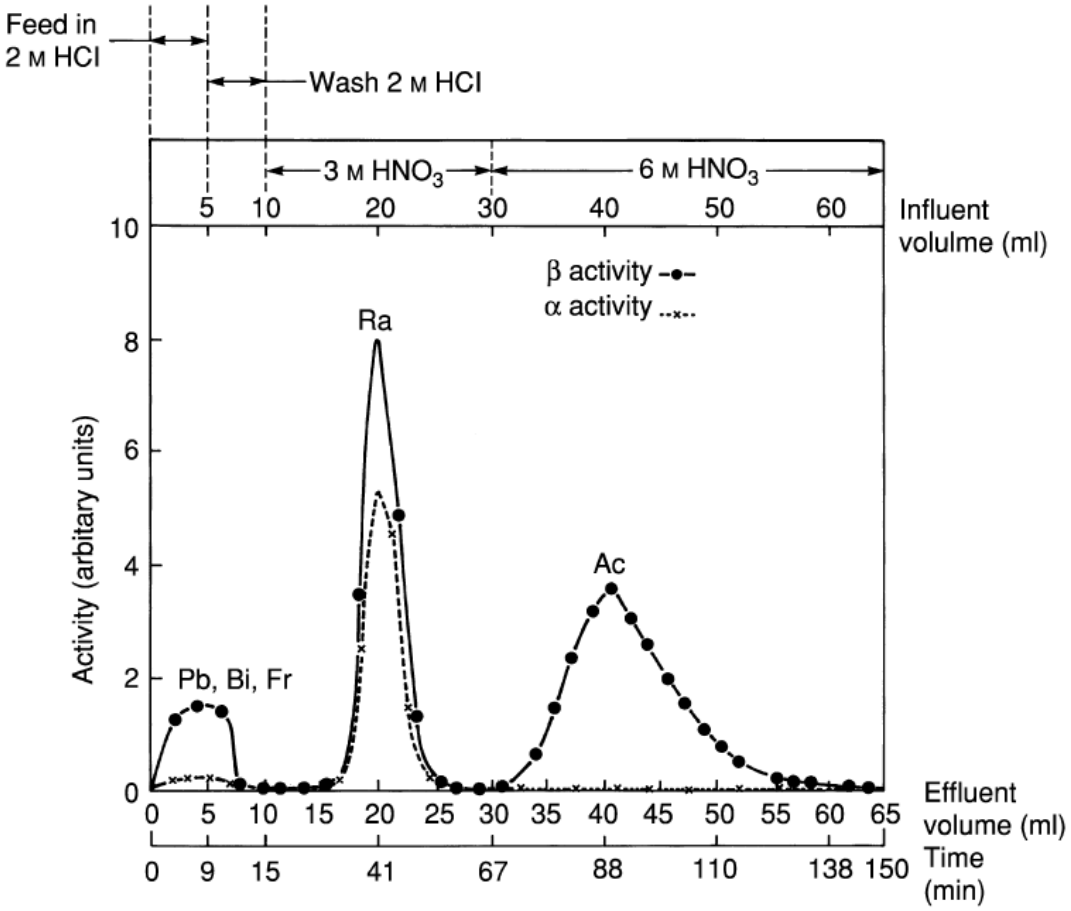

Figure 69: Separation of decay products via ion exchange chromatography [45].

Appendix D: Introduction to Computational Fluid Dynamics (CFD)

Computational fluid dynamics, abbreviated CFD, mathematically divides a fluid flow into small, discretized, domains and solves a series of equations for each domain. The selected equations provide a description of the physical environment. CFD is commonly applied in modern contexts to assist and accelerate development processes.

Fluid flow and heat transfer are described by partial differential equations, including Navier-Stokes equations, continuity equation, and continuity of energy equations. They are closely coupled and non-linear, which precludes general analytic solutions in most situations. Most problems of interest must be solved using approximate methodologies.

D.1 Governing Equations

The governing CFD equations address the conservation of mass, conservation of energy, and the momentum of fluid within the context of a CFD environment where each finite volume element is the respective frame of reference for the governing equations. The governing equations can be described in conservative and non-conservative forms. The conservative forms allow for surface integration over finite volumes, whereas non-conservative mathematical forms are better suited for finite element analysis methods. Given the use of finite element analysis methods within the CFD solver, the following governing equations are described in non-conserved form.

The terms within the partial differential equation continuity equation are change in density with respect to time, $\frac{D\rho}{Dt}$, (material derivative) coupled with the divergence of velocity for the motion of an infinitesimal fluid element, $\vec{V}$. The mass within the fluid element is fixed, but the volume needed to contain the mass as it flows is not constant, and will often become unwieldy in size, hence the use of the term 'divergence' to describe it. This equation is highly effective on the limited time scales needed for CFD iterations and given in the non-conserved form in Equation D.1.

$$\frac{D\rho}{Dt} + \rho\nabla \cdot \vec{V} = 0$$

Equation D.1

The momentum equation accounts for viscosity, density, and pressure terms, also known as the Navier – Stokes equations. When written in non-conservation form and simplified for a specific axis, they can be expressed as Equation D.2, where acceleration in the x direction is given by $\frac{Du}{Dt}$, the density is ρ, pressure is p, and viscosity is given by τ.

$$\rho\frac{Du}{Dt} = -\frac{\delta p}{\delta x} + \frac{\delta\tau_{xx}}{\delta x} + \frac{\delta\tau_{yx}}{\delta y} + \frac{\delta\tau_{zx}}{\delta z} + \rho f_x$$
$$\rho\frac{Dv}{Dt} = -\frac{\delta p}{\delta y} + \frac{\delta\tau_{xy}}{\delta x} + \frac{\delta\tau_{yy}}{\delta y} + \frac{\delta\tau_{zy}}{\delta z} + \rho f_y$$
$$\rho\frac{Dw}{Dt} = -\frac{\delta p}{\delta z} + \frac{\delta\tau_{xz}}{\delta x} + \frac{\delta\tau_{yz}}{\delta y} + \frac{\delta\tau_{zz}}{\delta z} + \rho f_z$$

Equation D.2

The energy equation describes a relationship between rate of work, heat flux, and the resulting rate of energy change within a finite volume or element. Those three components can be described using the simple format shown in Figure 70.

In non-conserved mathematical form, the energy equation can be more precisely written as Equation D.3, where temperature, viscosity, density, velocity, pressure, sheer, and normal stresses contribute to the rate at which the energy within a finite volume or element change [46].

$$\rho\frac{D}{Dt}\left(e+\frac{V^2}{2}\right) = \rho\dot{q}+\frac{\delta}{\delta x}\left(k\frac{\delta T}{\delta x}\right)+\frac{\delta}{\delta y}\left(k\frac{\delta T}{\delta y}\right)+\frac{\delta}{\delta z}\left(k\frac{\delta T}{\delta z}\right)-\frac{\delta(up)}{\delta x}-\frac{\delta(vp)}{\delta y}-\frac{\delta(wp)}{\delta z} + \frac{\delta(u\tau_{xx})}{\delta x}+\frac{\delta(u\tau_{yx})}{\delta y}+\frac{\delta(u\tau_{zx})}{\delta z}+\frac{\delta(v\tau_{xy})}{\delta x}+\frac{\delta(v\tau_{yy})}{\delta y}+\frac{\delta(v\tau_{zy})}{\delta z}+\frac{\delta(w\tau_{xz})}{\delta x} + \frac{\delta(w\tau_{yz})}{\delta y}+\frac{\delta(w\tau_{zz})}{\delta z}+\rho\vec{f}\cdot\vec{V}$$

Equation D.3

D.2 Discretization Method

After being adjusted to reflect conditions describing the desired model, the governing equations must then be transformed into an algebraic set to be solved, also known as discretization. The most common methods of implementing this are known as finite difference, finite element, and finite volume. Finite difference method uses a series expansion to replace each of the partial derivatives. This is often accomplished with a Taylor series expansion as shown in Equation D.4 where $f^n(a)$ is the nth derivative of the equation f(x), evaluated at point (a).

$$f(x) = \sum_{n=0}^{\infty}\frac{f^n_{(a)}}{n!}(x-a)^n$$

Equation D.4

For relatively straightforward geometries, this method is effective for generating results with high precision, but quickly becomes untenable for complex geometries due to the partial differential equations requiring complex transformations before being solved with series expansion. These complex transformations often generate problems from cross-coupled equations and poor convergence of the solution.

The finite volume method is used by many CFD programs, including ANSYS Fluent, to convert volume integrals in the governing equations into surface fluxes and then solve for the conditions

Figure 70: Summary of the Energy Equation.

where all surface fluxes within the environment balance. Two significant advantages of this method are that it quickly adapts to complex geometries and generates physically relevant results as it progresses through the iterative process. However, some CFD problems require the use of irregular shaped cell volumes, which generates a vast number of fluxes that must be tracked and solved, placing significant demands on the flux solver. This is a disadvantage not shared with the other two discretization methods.

The finite element method, used by Autodesk CFD, integrates the governing equations over a small element or volume and assigns shape functions to nodes along the respective boundaries. Solutions are calculated for specific nodes and then the shape functions are used to interpolate between the nodes to produce an approximate solution for the element. These shape functions are often low order polynomials [47]. A pictorial description of a linear shape function is shown in Figure 71.

This method accommodates complex geometries, abrupt changes in element resolution, efficient parallel processing, and material property customizations on a sub-element scale that would not be well suited for the other two methods. The disadvantage is considerable mathematical complexity compared to the other two methods [48].

D.3 Mesh Refinement

Some CFD software suites have mesh refinement features that assist by automatically applying a finer mesh to surface regions with small radii or sharp angles along with boundary layer flow regions, and coarsening the mesh in other areas that are free of these features. The overall effect is to reduce the computational demands of a model versus creating a small mesh everywhere while maintaining or improving the accuracy of the results versus creating a coarse mesh everywhere.

An important example of where mesh needs to be relatively fine is in immediate proximity to the surface of a pipe or other physical boundary, also known as boundary layer flow. These are regions of extreme gradients and abrupt changes to fluid properties. However, the relatively fine mesh is generally not required for free stream regions that are further away from the nearest physical boundary and the various gradients are relatively small. An example of automatic mesh refinement is shown in Figure 72, which depicts a cross sectional view of a compressed air line located within a hollow steel cylinder. The compressed air is backlit in yellow while ambient air is shown in blue.

D.4 Adiabatic Compressible Fluid Flow

Subsonic fluid flow without heat transfer can be treated as adiabatic, where total energy is conserved. The sum of thermal energy and kinetic energy is constant and can be expressed as

$$h_{total} = \frac{1}{2}V^2 + h_{static}$$

Equation D.5

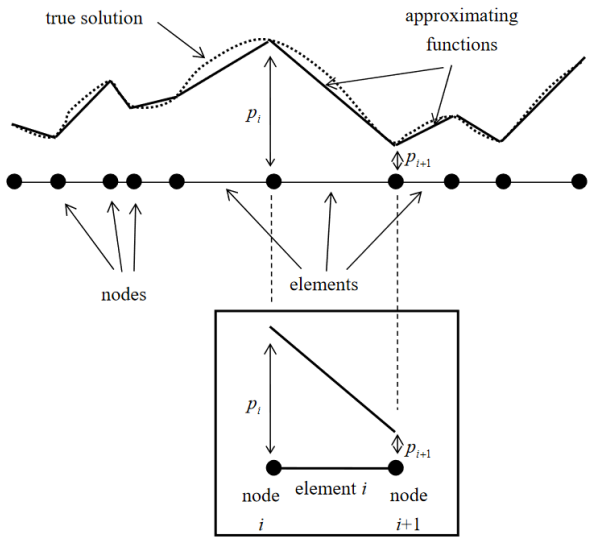

Figure 71: Conceptual example of a one-dimensional mesh and linear shape function [47].

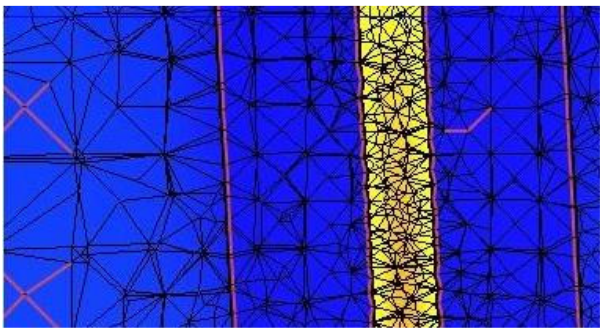

Figure 72: Mesh autosizing applied to crossectional view of a compressed air line, backlit in yellow with ambient air backlit in blue.

where V is velocity, h is volumetric enthalpy. If we presume the fluid is well approximated as an ideal gas, Equation D.5 can be rewritten using temperature and specific heat capacity at constant pressure:

$$T_{total} = \frac{1}{2}\frac{V^2}{c_p} + T_{static}$$

Equation D.6

where the stagnation temperature, also known as the total temperature and shown as T_{total}, equals the dynamic temperature plus the static temperature. The specific heat capacity at constant pressure can be calculated using:

$$c_p = \frac{\gamma R_{gas}}{\gamma - 1}$$

Equation D.7

Where γ is specific heat at constant pressure over specific heat at constant volume and R_{gas} is the gas constant.

D.5 Absolute, Total, Static and Dynamic Values

The pressure equation combines pressure contributions from the momentum equation, p=mv, with reference, rotational, and gravitational pressure heads. The absolute pressure at a position X is calculated as follows:

$$P_{absolute} = P_{rel} + P_{ref} + \rho_{ref} \sum_i g_i X_i + \rho_{ref} \sum_i \omega_i^2 X_i^2$$

Equation D.8

where P_{ref} is calculated from fluid specific reference values, ω is the rotational velocity, P_{rel} is the relative pressure, and g is gravitational acceleration. The gravitational and rotational terms take into account all three coordinate axes, and the reference density, ρ_{ref}, is calculated from the initial temperature and pressure. If the density of the fluid remains constant, then ρ_{ref} remains constant. The relative pressure equals the gauge pressure in cases where the fluid has no appreciable gravitational or pressure heads. In most cases, the terms dynamic and static are associated with compressible fluids and high velocity flows. The dynamic temperature and pressure can be calculated as follows and incorporates Equation D.9.

$$T_{dynamic} = \frac{1}{2}\frac{V^2}{c_p}$$

$$P_{dynamic} = \frac{1}{2}\rho V^2$$

Equation D.9

D.6 Laminar and Turbulent Fluid Flow

Fluids have two major flow regimes: laminar and turbulent. These are described as either having smooth layers, called laminae, in the case of the former, or, in the case of the latter, having erratic eddies and vortices that cause the fluid layers to rapidly mix. A transition region exists between the slower moving laminar flows and the high velocity turbulent flows. Flows are classified as laminar or turbulent based on the Reynolds number, a dimensionless quantity. Reynalds number can be calculated for flow in pipes using the following equation:

$$Re = \frac{\rho V D}{\mu}$$

Equation D.10

where μ is the viscosity, the density is ρ, V the velocity, and D is the interior diameter of the pipe. For flows not inside a pipe, the interior diameter, D, is replaced with the hydraulic diameter, Dh, which can be calculated using:

$$Dh = \frac{4A}{P}$$

Equation D.11

where the cross-sectional area is A and the wetted perimeter is P. Laminar flows occur below a Reynold's number of 2,300 and turbulent flows begin above 2,900 for fully developed flow conditions. The transition region between laminar and turbulent is not a fixed range and includes modest variations due to surface roughness and distance from the entrance to the pipe or channel. Transitional fluid flows are highly unstable and often oscillate between laminar and turbulent, making for a difficult flow regime to model.

D.7 Boundary Layer Flow

Fluid flowing past a rigid surface, such as the interior of a pipe, has a depth infinitesimally close to the surface where fluid molecules are virtually stationary relative to the direction of bulk fluid flow. Due to the action of shear forces, the fluid forms thin layers between a rigid surface and region of bulk fluid flow. The fluid viscosity has a significant influence on the depth of these boundary layers, which are laminar even when the bulk flow is turbulent. An example flow profile is shown in Figure 73 [49].

D.8 Inviscid and Viscous Flow

The number of fluids that are truly inviscid, having a viscosity of zero, is exceptionally small. Inviscid fluids are solved using Euler equations, which are categorically part of the Navier-Stokes

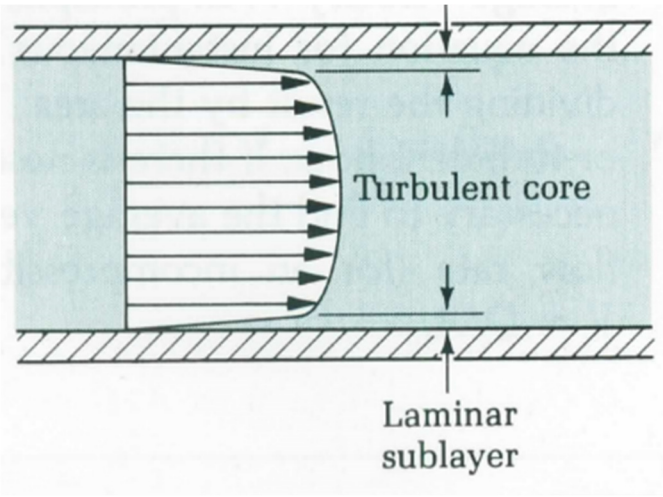

Figure 73: Turbulent flow profile with laminar boundary layers [49].

equations. It is numerically much easier to solve Euler equations than the expanded Navier-Stokes system, and for flow regimes with small viscosities, many models will make this simplification. If an inviscid flow is without rotational effects, then the velocity potential function can be used to describe the flow. This further simplifies the solution set because only a single equation is required for all the parameters. These two simplifications are not applicable for many engineering problems, but they do allow for a rapid estimate of system performance.

D.9 Fluid Flow Description: Newtonian and Non-Newtonian Fluids

Common Newtonian fluids include air, water, steam, and numerous hydrocarbons. Common non-Newtonian fluids include slurries, paper pulp, plastics, blood, and rubber compounds. Newtonian fluids exhibit a linear relationship between strain and shear forces where viscosity is a constant or temperature dependent. For Newtonian fluids, the shear stress, τ, equals the velocity gradient multiplied by the viscosity coefficient μ as shown in Equation D.12.

$$\tau_{xy} = \mu \frac{\delta u}{\delta y}$$

Equation D.12

Non-Newtonian fluids have a non-linear strain rate, where the shear stress is a multi-order equation and written as:

$$\tau_{xy} = m \frac{\delta u^n}{\delta y}$$

Equation D.13

where the consistency index is m and the power law index is n. In the oil and gas industry, drilling mud is commonly described using the Herschel-Buckley fluid model which uses the following mathematical description:

$$\tau_{xy} = \tau_0 + k \frac{\delta u^n}{\delta y}$$

Equation D.14

D.10 Heat Transfer: Conduction, Convection, and Radiation

Heat transfer occurs through three modes: conduction, convection, and radiation. Conductive heat transfer occurs from molecular motion and is dependent on thermal conductivity as shown in the following simplified equation:

$$\dot{Q} = -kA \frac{dT}{dx}$$

Equation D.15

where Q is the heat transfer rate, k is the conductivity of the material, the total area is A, and dT/dx is the temperature gradient. Convection is from fluid motion and can be described by the following

equation where the convective heat transfer coefficient, h, is a function of the fluid properties and the geometry.

$$\dot{Q} = Ah\,\Delta T$$

Equation D.16

Radiative heat transfer is from electromagnetic waves transferring energy and encompasses a wide range of energies. For most conditions encountered within CFD problems, radiative heat transfer can be approximated by the following equation:

$$\dot{Q} = \varepsilon\sigma A T_s^4$$

Equation D.17

where T_s is the surface temperature, σ is the Stefan-Boltzmann constant, emissivity is ε, and A is the surface area. The most common event where fluids emit or absorb substantial quantities of radiative energy is during a combustion process or when passing through a furnace. Radiant interchanges between surface and fluids involves adding the following heat flux term to the governing equations:

$$q_{ri} = A_i(G_i - J_i)$$

Equation D.18

where q_{ri} is heat flux for the ith fluid element. The incident radiation is G_i for the element i, while the radiosity of the ith element is J_i. Radiosity can be described as:

$$J_i = (1 - \varepsilon_i - \tau_i)G_i + \varepsilon_i\sigma T_i^4$$

Equation D.19

Where the emissivity is ε_i, the transmissivity of surface i is τ_i, and σ is the Stefan-Boltzman constant. The incident radiation G_i is calculated by using the view factors between the applicable surfaces:

$$G_i = \sum_{j=1}^{N} J_j F_{i-j}$$

Equation D.20

View factors are calculated in most CFD programs either by using a hybrid ray-tracing discrete ordinate model or by projecting an element face image onto a sphere encompassing the element face of interest. This later method is conducive for solar radiation contributions.

D.11 Natural, Mixed, and Forced Convection

Buoyant driven fluid flow is a topic of significance for several engineering disciplines. These fluid flows arise from temperature driven changes to fluid density and are assisted by secondary changes to other physical properties including viscosity. In contrast, forced convection is dominated by the

bulk movement of the fluid and the effects of buoyancy are small by comparison. Mixed convection is the combination of these two fluid movement forms and is frequently utilized to achieve improved system performance. The Grashof number is the ratio of buoyant to viscous forces present on a fluid and used for natural convection problems. Likewise, the Reynolds number is used for mixed convection and forced convection fluid flow to identify the flow regime. The Grashof number can be calculated using the equation:

$$Gr = \frac{\beta g L^3 \Delta T}{\nu^2}$$

Equation D.21

Where the acceleration of gravity is g, β is a volumetric expansion coefficient, characteristic length is L, ν is the kinematic viscosity, and ΔT is the change in temperature between the start and end points.

The Reynolds and Grashof numbers have geometric dependence, but the Prandtl number does not because it uses a ratio of the diffusion of momentum to the diffusion of mass, also known as the ratio of kinematic viscosity to thermal diffusivity. It can be calculated using the following equation:

$$Pr = \frac{C_p \mu}{k}$$

Equation D.22

where C_p is the constant pressure specific heat, the viscosity of the fluid is μ, and k is the thermal conductivity of the fluid.

D.12 Practical Application

Traditionally, proposed designs are digitally created in a 3D environment, imported into a CFD program, discretized, and paired with the desired fluid conditions and applicable governing equations. Creating discretized geometry produces a wire framed object and is commonly referred to as a mesh within the CFD community. The finer the mesh, the more precisely the geometry is mathematically described with a proportional increase in time needed to solve the applicable governing equations. As a result, it is vital to balance the mesh spacing with the available time and computing resources so that the CFD results are both useful and available within a reasonable time frame.

Vita

David Schappel was born in Dallas, Texas to Dave and Ruth Schappel. He has a sister, Bekah, and brother, Danny, who graduated from the University of Tennessee Knoxville with a PhD in Nuclear Engineering. Schappel was home educated by his parents and graduated from Circle Christian School in Orlando, Florida. He was fascinated by the historical account of Richard Rhodes in the book, The Making of the Atomic Bomb, from childhood, and decided to pursue Nuclear Engineering with his Florida Bright Futures Scholarship. He graduated from Seminole State College with his Associates degree, then earned his Bachelor's degree and Master's degree in Nuclear Engineering from The University of Florida. David then started his PhD work at the University of Tennessee, Knoxville with an interest in nuclear forensics and safeguards. He served as a Graduate Teaching Assistant for several years in the Nuclear Engineering Department and completed his PhD in 2023.